The increase of dike stability due to unsaturated soil strength

A study of the spatially and temporally varying presence of matric suction

Marjolijn Mascini

TU Delft ARCADIS

The increase of dike stability due to unsaturated soil strength

by

Marjolijn Mascini

to obtain the degree of Master of Science
at the Delft University of Technology, Faculty of Civil Engineering and Geosciences
to be defended publicly on September 30th, 2022

Student number:	4494644	
Project duration:	January 9, 2022 – September 30, 2022	
Thesis committee:	Dr. A. P. Van den Eijnden,	TU Delft (Chair)
	Dr. ir. R.C. Lanzafame,	TU Delft
	Ing. R. Koopmans,	Arcadis
	Dr. S. Huizer,	Arcadis

Cover image: Picture of a the IJssel at Derxen during a high water in February 2021 (de Kleine, 2021).

TU Delft Delft University of Technology

ARCADIS

Preface

This thesis report was written as the final part of the master Hydraulic Engineering at the faculty of Civil Engineering and Geosciences of the TU Delft. The research has been conducted on behalf of Arcadis, where I have been writing this thesis as a graduation intern from January to September 2022.
During the past 9 months, I have learned a great deal about a topic that I previously had very little knowledge about: unsaturated groundwater flow and its effect on macro-stability. I have found this to be a challenging topic, and I have said more than once that I did not fully understand my own thesis topic for the first 7 months of writing it. Nonetheless, it has been a great time and it has taught me a lot about the theory, as well as what this theory can mean in engineering practice.

I would like to thank Rimmer Koopmans from Arcadis for creating this challenging thesis subject, the personal guidance and for the detailed feedback you have given me on the versions of this thesis. I have greatly enjoyed our weekly meetings. Furthermore, I would like to thank dr. ir. Robert Lanzafame for his guidance and for challenging me to dive extra deep into the subject. I would like to thank dr. ir. Bram van den Eijnden and dr. Sebastian Huizer for participating in my committee and for their sharp comments during our meetings. Finally, I would like to thank my family, Floris and my friends for supporting me throughout my studies and for the unforgettable years as a student.

I sincerely hope you enjoy reading this thesis report about suction in the unsaturated zone of dikes.

Marjolijn Mascini
Rotterdam, September 2022

Abstract

River dikes in the eastern part of the Netherlands are characterized by a relatively low daily water table. In the unsaturated zone above the water table, a negative pore pressure (matric suction) is present that binds the soil particles together. Suction can be especially large in soils with small grains, such as clay, and increases the strength of a soil due to higher effective stress. High suction in soils has been proven to significantly increase the stability of dikes. However, due to water level variations and other climatic influences such as precipitation and evapotranspiration, suction in a dike will vary over the year and throughout the cross section. The research described in this report aims at evaluating whether there are parts of a cross-section of a dike where soil suction remains throughout a high water event in a river such that an increase in the strength of the soil can be used in stability analyses. The analysis is centered around a case study of an existing dike in the east of the Netherlands and uses time-dependent unsaturated groundwater flow models to simulate the spatially and temporally varying suction for a number of different initial conditions and climatic influences defined by scenarios. The results show that it is very unlikely that suction in the dike will be lost during the summer months. Due to high evapotranspiration, the water content in the dike is low, which results in a lower water table during a high water event and less infiltration in the dike occurs during precipitation. During winter, the probability that suction is lost throughout the dike cross-section is larger and will occur after heavy precipitation with a long duration where the return period is $1 - 10$ years. Although in most scenarios some suction will remain present, the amount of suction during the winter is generally low, between 0.5 and 1 meter, which results in an apparent cohesion of $2 - 4$ kPa. A simple stability calculation illustrates that the increase in strength in the dike due to suction does not result in a significant increase in the stability of the dike during high water conditions.

Contents

List of Tables v

List of Figures vii

1 Introduction 1

2 Theory and background: how water flows through a dike 5
2.1 The subsurface based on the water regime . . . 5
2.2 Groundwater flow . . . 7
2.3 Processes in a clay dike . . . 11
2.4 Suction and the unsaturated shear strength . . . 12
2.5 Modelling transient saturated/unsaturated groundwater flow . . . 14

3 Suction in the case study dike: the factors of influence 21
3.1 Methods . . . 21
3.2 The water table and initial conditions . . . 22
3.3 The high water wave . . . 25
3.4 Soil-specific parameters and variability . . . 28
3.5 Infiltration in a 1D soil column . . . 32
3.6 The influence of precipitation . . . 37
3.7 Conclusions after the sensitivity analysis . . . 42

4 Suction in the case study dike: return periods and the influence on slope stability 44
4.1 Probability of saturation based on the time series . . . 44
4.2 Scenario Analysis: set-up . . . 45
4.3 Scenario Analysis: Results . . . 50
4.4 The strength increase due to matric suction . . . 52
4.5 The influence on the probability of failure . . . 56

5 Discussion 61

6 Conclusion 64
6.1 Recommendations . . . 64

References 66

Appendices 68

A Analysis of the soil data 68

B The effect of averaging precipitation and evapotranspiration 71

C Simulating evapotranspiration with SWAP 73

D Statistics of discharges and river levels 75

E The influence of the clay type on the height of the phreatic surface: Hydrostatic conditions 76

F Results 36 year analysis 78

G IDF curves: comparing empirical and fitted distributions 83

H Results of the scenario analysis 85

I Results of the Monte Carlo analysis to the variation of the Safety Factor 87

List of Tables

2.1 Variables and distributions to determine the apparent cohesion for clay soils. 14
2.2 x-coordinates of the sections S0-S5 in the cross-section. 16
3.1 Parameters used for the soil layers in the analysis. 22
3.2 Discharges at Lobith and river levels at the Lathumsedijk with their return periods 27
3.3 Unsaturated parameters for sandy clay soils in the Staring series 29
3.4 Unsaturated parameters for clay soils in the Staring series 30
3.5 Statistics of the precipitation in De Bilt between 1980 and 2016 39
3.6 Summary of precipitation events that led to saturation of the soil 40
3.7 Summary of the conditions previous to the events that led to saturation of the entire soil columns. 40
4.1 Initial and boundary conditions used in the scenarios 49
4.2 Summary of the median pressure head and probability of full saturation 52
4.3 Shear strength properties and soil characteristics for the different layers in the stability model. . 53
4.4 Safety factors for undrained and drained soil behaviour 56
4.5 Slopes of the linear relation between apparent cohesion and relative safety factor 59
A.1 Available data of the Lathumsedijk, Duiven. 68
A.2 Variation of the (unsaturated) soil parameters used in the research in this report. 69
C.1 Variables used to calculate potential evaporation and transpiration. 74
D.1 Discharges at Lobith and river levels at the Lathumsedijk with their return periods 75
E.1 Parameter ranges in the Staring series (Heinen et al., 2020) 76
F.1 Summary of the events that led to complete saturation of the soil at a depth of -2m+GS. 78

List of Figures

1.1 Zones in a cross section of a dike based on the presence of matric suction . . . 2
1.2 The location of the case study dike . . . 3
2.1 Vertical profile of the subsurface with zones based on the water regime . . . 5
2.2 Example of a water retention curve . . . 7
2.3 Example of a water retention curve and a hydraulic conductivity curve . . . 9
2.4 Water content, pressure head and total head profile for a 1D soil column after infiltration . . . 10
2.5 Relationship between fitting parameter κ and apparent the plasticity index . . . 13
2.6 Relationship between matric suction and apparent cohesion . . . 14
2.7 Positions of the sections in the cross-section . . . 16
2.8 Comparison of the pressure head calculated with Seep/W and SWAP . . . 17
2.9 Comparison of the pressure head obtained with 2D model Seep/W and quasi 2D model SWAP . 18
2.10 Comparison of the pressure head calculated with Seep/W and SWAP during a high water . . . 19
2.11 Comparison of the pressure head obtained with 2D model Seep/W and quasi 2D model SWAP . 19
3.1 Schematization of the case study dike . . . 21
3.2 Height of the water table along vertical sections for varying initial river levels . . . 23
3.3 Duration before the water table is 95% of the steady state elevation for varying initial river levels 23
3.4 Height of the water table along vertical sections for a varying initial infiltration . . . 24
3.5 Duration before the water table is 95% of the steady state elevation for varying initial infiltration 25
3.6 Shape of the discharge wave in the Rhine as calculated by GRADE (after Chbab (2017)). . . . 26
3.7 The varying shapes of the high water waves used in the analyses . . . 26
3.8 Height of the water table for varying shapes of the high water wave . . . 27
3.9 Schematized shapes of the flood wave at the case study dike with varying return periods. . . . 28
3.10 Water tables along the sections during high water waves in the river with varying return periods 28
3.11 Water retention curves for sandy clay soils . . . 29
3.12 Height of the water table along vertical sections for varying characteristics of the cracked clay layer 30
3.13 Water retention curve and hydraulic conductivity curves for varying clay soils . . . 31
3.14 Height of the water table along vertical sections for varying characteristics of the clay core . . . 31
3.15 Initial pressure head along section 1 at t=0 for the five calculations with a varying clay core. . . 32
3.16 Set up of the analyses of the cracked layer including the boundary- and initial conditions. . . . 33
3.17 Precipitation over time used as the top boundary condition. . . . 33
3.18 Maximum pressure head after infiltration for varying characteristics of the cracked clay layer . . 34
3.19 Set up of the analyses of the clay core layer including the boundary- and initial conditions. . . . 35
3.20 Maximum pressure head after infiltration for varying characteristics of the clay core . . . 36
3.21 Set-up and results of the influence of the height of the water table on infiltration . . . 37
3.22 Schematization of the boundary and initial conditions used in the analyses 1 and 2. . . . 38
3.23 Average precipitation statistics recorded at the meteorological station De Bilt (1980-2016) . . . 39
3.24 Daily precipitation at De Bilt with an intensity $\geq$ 20mm/day . . . 41
3.25 Measured and averaged daily precipitation in De Bilt. . . . 41
3.26 Modelled and schematized pressure head on December 31st 1997. . . . 41
3.27 The difference in pressure head between real time and averaged precipitation. . . . 42
4.1 Median pressure heads in the cross section based on the 37 year analysis during winter and summer 44
4.2 Probability of saturation per year during winter and summer based on the 37 year time-series. . 45
4.3 Median pressure head with confidence intervals in January and July for varying clay core properties 46
4.4 Comparison of the median pressure head in SWAP and the initial pressure head used in Seep/W 47
4.5 Discharge statistics for the year 2020 (after Rijkswaterstaat (2020)) . . . 47
4.6 High discharges per month recorded in the Rhine at Lobith . . . 48
4.7 Return period plot for the precipitation depth over a varying duration. . . . 49
4.8 Maximum pressure head after 10 combinations of precipitation events for scenarios 1.1-1.4. . . . 50
4.9 Maximum pressure head in the dike after both a high water (T=2 years) and heavy precipitation 51
4.10 Maximum pressure head in the dike after both a high water (T=1250 years) and heavy precipitation 51
4.11 Original cross-section of the case study dike in D-stability . . . 53
4.12 results of scenario analysis in January with soil properties B10 . . . 54
4.13 Absolute safety factor for macro stability as a function of apparent cohesion . . . 55
4.14 Relative safety factor for macro stability as a function of apparent cohesion . . . 55
4.15 Average daily suction during 11m river level in January, February and March. . . . 58
4.16 Relationship between suction and cohesion . . . 58

4.17 Safety factor for macro stability as a function of apparent cohesion 59
4.18 Histogram of the apparent cohesion and the safety factor for a high water of 11m+NAP. 60
A.1 Schematization of the case study dike 68
A.2 Plasticity index of the samples taken in the dike 70
A.3 Histogram of the plasticity index and a fitted Lognormal distribution 70
B.1 Comparison of analyses with hourly and daily precipitation data for a relatively wet year 71
B.2 Comparison of analyses with hourly and daily precipitation data for a relatively dry year 72
D.1 Stage-relation curve for the discharge at Lobith and the water level at the case study dike 75
E.1 Height of the water table along vertical sections for varying clay properties and no infiltration . . 76
F.1 Pressure head in a 1D column before and after saturation of the soil 81
F.2 Daily precipitation at De Bilt with intensity $\geq$ 20mm/day 82
H.1 Governing slip plane for the scnenario in January with soil properties B10 85
H.2 Results of scenario analysis in July with soil properties B10 85
H.3 Results of scenario analysis in January with soil properties B12 86
H.4 Results of scenario analysis in July with soil properties B12 86
I.1 Results of Monte Carlo analysis to the relative safety factor for a river stage of 11m+NAP 87
I.2 Results of Monte Carlo analysis to the relative safety factor for a river stage of 12m+NAP 88
I.3 Results of Monte Carlo analysis to the relative safety factor for a river stage of 13m+NAP 89
I.4 Results of Monte Carlo analysis to the relative safety factor for a river stage of 13.64m+NAP . . 90

1 Introduction

The Netherlands is protected by many kilometers of dikes, which keep 60% of the country from flooding. In the coming years, hundreds of kilometers will have to be reinforced and heightened to comply with the Dutch safety standards (Rijkswaterstaat, 2021). When a flood defence is designed or assessed, it has to be checked for multiple failure mechanisms, one of which is the stability of a dike, for which the height of the water table is an important factor. Since data regarding the height of the water table in the dike during a high river stage is generally not available, the water table in a dike is schematized. This is generally very simplistic and conservative as it cannot take into account factors that have a large influence on the phreatic surface. For stability calculations, a steady state phreatic line for a high water event in the river is assumed within the dike body. Since a saturated soil has a lower effective stress, a high phreatic line results in a conservative assessment with respect to the actual stability of a dike.

Below the water table, the soil can be assumed to be fully saturated with water, while above the water table the pores are partially filled with air and water and the soil is considered unsaturated. This zone is commonly referred to as the vadose zone and can be characterized by the presence of a negative pore water pressure that can bind soil particles together. This is also called matric suction, and the suction is equal to the difference between the atmospheric pressure and the and the pore water pressure water in the soil. Due to increasing effective stress, suction in the vadose zone results in higher shear strength of a soil. As a result, suction can positively influence the stability of a dike against sliding. Previous research by Walrave (2021) has led to the conclusion that soil suction in a clay river dike can have a significant positive influence on the factor of safety (FoS) of the macro stability of that dike.

In the vadose zone the pore pressures are (generally) negative and the magnitude of the pressure head depends on the water content in the soil (volume of water per volume of soil) or the degree of saturation (fraction of pore space filled with water). A lower water content results in a lower pressure head (more negative), such that there is higher suction. The relation between the water content and the suction is soil-specific and can be described by a water retention curve. Since a dike is subjected to varying external weather conditions, suction in a dike-body varies throughout the cross section and over time. Generally speaking, the water content is high near the water table and decreases over the height up until the ground surface. In the core of a clay dike, the representative suction will vary between 0 and 5 meters depending on the season. During summer, high suction can be present in the top layer of dikes due to evaporation from the ground surface and transpiration of grass. As a result, the upper layer of dikes is known to crack, which makes the top layer of a dike easily influenced by the weather. During precipitation events water can infiltrate relatively easily through the cracks and suction in that layer is easily lost. During winter, when high water events in rivers are more likely and there are more rainy days, the water content in the dike will increase and suction will decrease.

During a high water event, the position of the water table will increase and the soil below the water table will be saturated. Above the water table, there might be suction present, depending on the season and previous climatic conditions. The top 1 meter of the dike is the cracked layer. These three areas are depicted in figure 1.1. Zone 1 represents the area below the phreatic surface (the phreatic surface in the figure is a schematized situation during a high water), where the soil is saturated and there will be no suction present during that high water. Zone 2 is above the phreatic surface, where the soil is unsaturated and suction might be present. The magnitude of suction in this part of the cross section is influenced by factors such as the weather during the time prior to the situation and moment that is schematized. Zone 3 represents the cracked top layer, which in practice is generally assumed to have a thickness of 1 meter. While there might be (very) high suction in that area during the summer, the suction will also be easily lost during precipitation or a high water event and a strength increase of the soil in that area should not be relied upon.

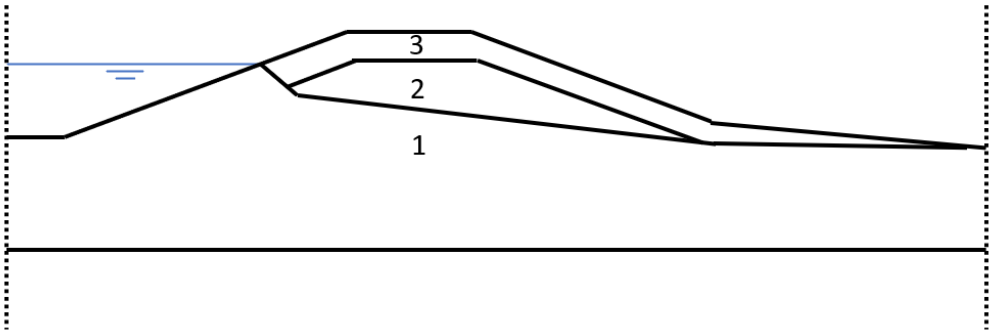

Figure 1.1: Schematization of zones in a cross section of a dike based on if suction will be present for a situation with a simplified position of the water table during a high water event. Zone 1 is fully saturated and no suction will be present. Zone 2 is partially saturated and suction might be present. Zone 3 is the cracked top layer where suction might be present but one can not account for a strength increase.

The figure presented above presents a schematization of a situation during a high river stage. The shapes and sizes of zones 1 and 2 will change over the year, together with the magnitude of suction. It is thus unclear if there is part of a dike in which we can be significantly sure that suction will remain, such that it can be included in stability analyses. The problem can be summarised as follows:

Soil suction increases the strength of a soil and has a positive influence on the macro-stability of a dike. However, it is unclear if there are parts of a cross-section of a dike where soil suction remains throughout a high water event in a river such that it can be used in a stability analysis.

The subject of the work presented in this report is to determine the presence of suction over time and throughout the cross section in dikes, and to see what the expected strength increase is, to include this in the assessment of the stability of a dike.

Scope

Since water flow through the unsaturated zone is influenced by many external and internal processes, which can not all be considered, the scope of the research should clearly be defined.

Ideally, the spatially and temporally presence of suction in different types and geometries of dikes is considered, as the geometry, varying soil types and layers are expected to have a significant influence on the development of suction in the vadose zone. However, due to time limitations, the analysis presented in this report considers a specific cross section of an existing dike in the eastern part of the Netherlands called the Lathumsedijk. The Lathumsedijk (the case study dike) is a dike on the southern part of the river IJssel, of which the location is included in figure 1.2.

Figure 1.2: The location of the Lathumsedijk, Duiven (in red) (GoogleEarth, 2021).

This specific cross-section was chosen for three main reasons. The first reason is that the case study should ideally be a clay river dike. Generally speaking the capillary rise is higher and suction is larger in soils with small grains. The other reason why this dike is chosen as the case study dike is that data about the soil layers were available through numerous borings and cone penetration tests (CPTs). Finally, the cross section can be considered as a typical cross section for a clay river dike in the Netherlands, which makes it easy to put the results from this study in context for other, similar dikes.

The work presented in this report includes processes and models with varying sources of uncertainties. Since dikes are largely influenced by processes with a natural variability, such as the weather, these uncertainties are considered in this report. They are included with the help of historic weather data and statistics. Throughout the world, more extreme weather has been recorded, such as very dry summers and higher intensity rain, due to climate change. Although these extremes can influence suction in a dike, changes in climatic conditions due to climate change are outside of the scope of this research and only statistics based on historic data are used.

The subject of the research in this report is the strength increase of dikes due to suction and where and when this strength increase may be present. To determine this, transient unsaturated numerical models are used to calculate the pressure heads over time and space to see which part of a cross section remains unsaturated. An increase in the strength of soil that are initially unsaturated during daily conditions, but below the water table during a high water in the river, is not considered.

As stated before, the pores between the soil grains are partially filled with air and partially filled with water in the vadose zone of a soil. In reality, all three of these phases (the soil particles, air and water) can move. However, in this modelling study, the soil skeleton is assumed to be rigid such that the soil particles can not move and the permeability of a soil (at full saturation) remains constant. Moreover, flow of air is not included in the analyses and the pore air pressure in the soil is assumed to remain constant and equal to 0 kPa. As a result of these two assumptions, suction in the soil is determined as the negative of the pressure head in the soil. Another assumption with respect to modelling is that only 1D and 2D models are used in the presented research. Although dikes are 3D objects that can vary along the cross section, they are normally considered as 2D cross sections for a dike section where similar properties and layers are expected. Since this assumption is generally valid, the research presented in this report consists only of 1D and 2D modelling. Variations along the section and smaller 3D variations such as burrows are outside of the scope of this research.

Objective

The objective of the research is to determine where in a dike cross section an increase in soil strength due to suction can safely be included in a stability analysis, and under what conditions this is reasonable.
To reach the objective, time-dependent and unsaturated groundwater flow numerical models will be used to evaluate the case study dike to answer the following sub-questions:

1. Which factors have a large influence on the development and reduction of soil suction?

2. When does suction result in a significant increase in the factor of safety of the macro stability?

3. What is the probability that a significant soil suction will remain present throughout a high water event in location (x_i, y_i) for unsaturated zones in the cross section?

4. What is the return period of full saturation of the cross section of the dike?

While these questions can generally be answered using principles of soil mechanics and groundwater flow, this research will focus specifically on the case study dike. The first sub-question will be answered with a sensitivity analysis performed with the models. The second and third sub-question will be answered by modelling scenarios for which the return periods can be estimated in combination with a simple stability analysis to observe the increase in the factor of safety.

2 Theory and background: how water flows through a dike

Flow of water through a dike is a complex process due to variability in the subsurface, interaction between air and water in soil pore space and the time-dependent (transient) development of forces and water movement. Fundamental concepts used in this study are introduced in this chapter, including an overview of water regimes in the subsurface (Section 2.1), principles of groundwater flow through porous media (Section 2.2) and processes that may influence suction in a clay dike body (Section 2.3). Moreover, relationship between suction and strength increase is elaborated in Section 2.4 and a framework is presented that shows how transient groundwater flow can efficiently be modelled (Section 2.5).

2.1 The subsurface based on the water regime

The subsurface consists of a mixture of soil, air and water particles. The pores in between the soil skeleton can be either fully saturated with water, fully saturated with air, or a mixture of water and air. A distinction can be made between zones in the subsurface based on the water regime that is present in the soil. The water saturation of a soil, S_w, is the fraction of the pore space that is filled by water and is directly related to the water content of the soil by the porosity of the soil (saturation is water content divided by the porosity). The volumetric water content (θ [m^3m^{-3}]) is the volume of water per unit volume of soil. When all the pores in a soil are saturated with water, S_w is 1 and the water content is equal to the saturated water content θ_S [m^3m^{-3}]. The zone below the Ground Water Table (GWT) (the theoretical height where the pore pressure is zero), is called the saturated zone and the pores of the soil are fully saturated with water. The GWT is generally considered to be the upper boundary of saturated groundwater flow (Gillham, 1984). The area above the GWT is called the vadose zone, where the soil is partially saturated with water and partially with air. The partial saturation of water is due to capillary forces. The area above the GWT where water is present in the pores is called the capillary fringe. Throughout literature the definition of the capillary fringe is not uniform. Some use the term to describe only the part just above the water table, where the water content is equal to the saturated water content. However, in this report the definition as proposed by (Ronen et al., 2000) will be used, where the capillary fringe is defined as the interface region between the water table and the unsaturated zone where the unsaturated zone is defined as the zone where the saturation is equal to the residual water content θ_r [m^3m^{-3}]. A schematization of the subsurface based on the water regime is given in Figure 2.1.

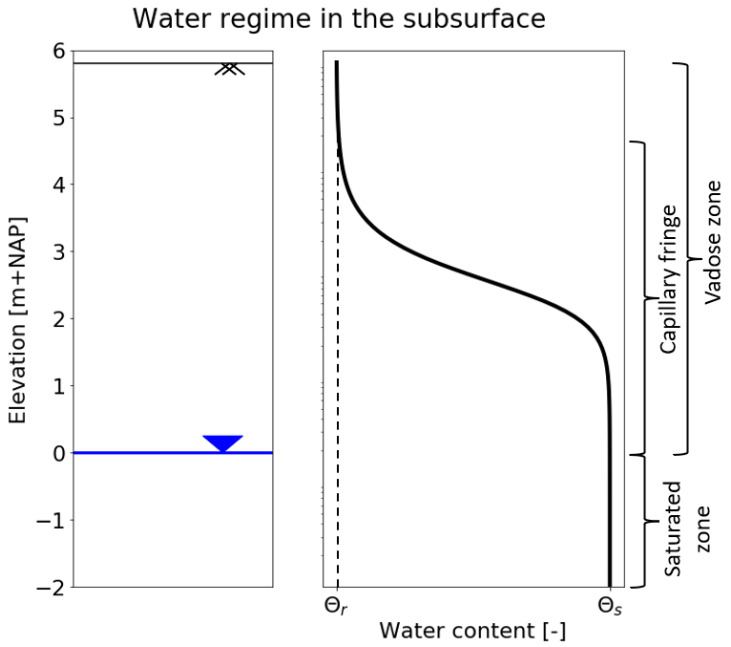

Figure 2.1: Vertical profile of the subsurface with zones based on the water regime with the water table at 0 m+NAP.

The thickness of the capillary fringe is dependent on the type of soil, of which the size and uniformity of the particles both have an effect. Since the pores of a soil in the vadose zone are partially filled with water and

partially filled with air, the flow of these two fluids can be described with a two-phase model, where the two phases are air and water. In reality, the movement of the soil particles can also be represented by a phase, resulting in a three-phase model. However, in most modelling studies of flow through a soil skeleton, the soil skeleton is assumed to not move. The surface of the soil particles attracts the water particles due to surface tension, which results in the capillary rise (Szymkiewicz, 2013). A similar process can be observed when a small tube is put in water: the water molecules are attracted by the wall which results in the rising of water and a curved water surface. A smaller diameter of the tube will result in a higher rise of the water. This is also what happens in the unsaturated zone above the water table. The pressure drop across the interface is called the capillary pressure (p_c) [kPa] or matric suction (ψ) [kPa] and is equal to the difference of the pressure potential of air and water and is a function of the water content in the soil (equation 1). If the air in the pores has an atmospheric pressure and the atmospheric pressure is zero, the capillary pressure is equal to the atmospheric pressure minus the water pressure.

$$p_{\mathrm{a}} - p_{\mathrm{w}} = p_{\mathrm{c}}\left(\theta\right) \tag{1}$$

Where p_a is the pressure of air [kPa], p_w is the pressure of the water [kPa] and p_c is the capillary pressure [kPa].

Water retention curve

The relationship between the capillary pressure and the water content or the matric suction and the water content can be described by a water retention curve (also called a soil water characteristics curve). An example of a water retention curve is given in Figure 2.2. When a soil is fully saturated, the water content is equal to θ_s and S_w is 1. The pressure in the soil is 0, which means that there is no tension that tries to pull the water out of the soil. When the pressure exceeds the air entry pressure p_e^{drain} [kPa], air can enter the soil and the largest pores will release their water. The air entry pressure is the capillary pressure above which air flow is possible. With an increasing pressure, the pores of the soil will fill with air and the water will be released. The water content will decrease until the residual water content, θ_r is reached, when no more water can be pulled out of the soil but there is still some water left (the residual water). This process is described by the primary drainage curve in Figure 2.2, of which the steepness of the curve is determined by the uniformity of the pore sizes. When the sizes of the pores are very uniform, the curve will be steep because the pores will release their water for a similar capillary pressure (Szymkiewicz, 2013).

When a soil is completely dry (oven-dry) and the pressure drops, water can enter the pores again. However, the curve will not follow the same path as the drainage curve due to hysteresis: for the same pressure in the soil, the saturation of the soil will be less during wetting as compared to drying. The main reason for this is that during drying, the large pores will release their water first while during wetting, the small pores will fill first. It is generally not possible for a soil to become fully saturated again outside a lab setting, due to the trapping of air bubbles. The maximum water content that can be reached is equal to 1 minus the residual air content $\theta_{r,a}$ [m^3m^{-3}]. In Figure 2.2, the main drainage curve and the main wetting curve represent the path that is followed when the initial water content is somewhere in between $\theta_{r,w}$ and $1 - \theta_{r,a}$.

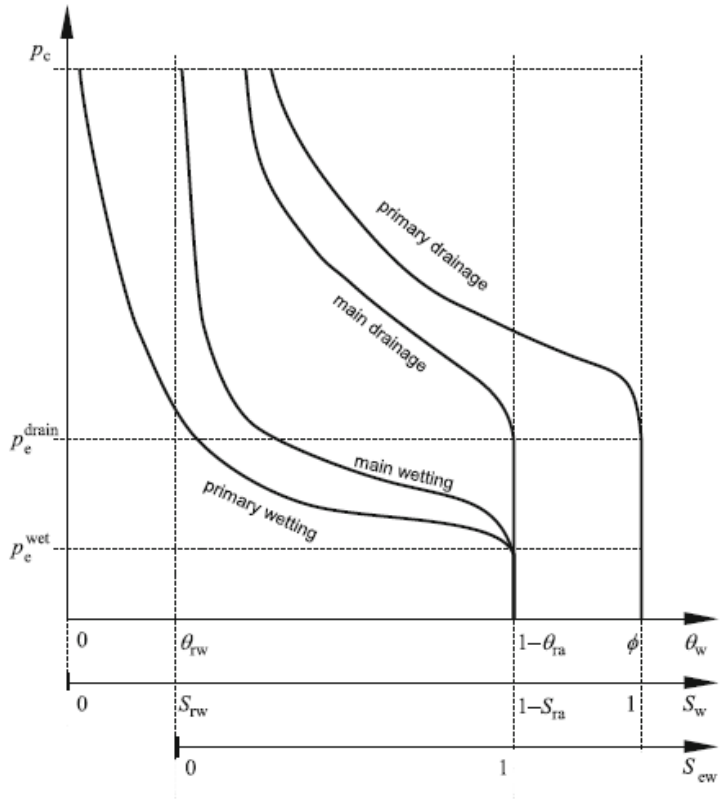

Figure 2.2: Example of a water retention curve (after Szymkiewicz (2013)).

A water retention curve is soil-specific and can be described by mathematical equations. One well-known model to describe such a curve is with the Van Genuchten-Mualem curve, given in equation 2.

$$S_e = \frac{\theta - \theta_r}{\theta_s - \theta_r} = \frac{1}{[1 + (\alpha p_c)^n]^m} \tag{2}$$

In which S_e is the effective water saturation, α [1/m or 1/kPa] is a parameter that is related to the size of the pores and m [–] and n [–] are parameters related to the distribution of the pore sizes where $m = 1 - 1/n$. The equation can also be written in terms of matric suction (ψ) instead of the capillary pressure.
Another analytical model to describe the relationship between the water content and the capillary pressure is the model by Brooks and Corey. The expressions are given in equation 3 and 4.

$$S_{\mathrm{e}} = \begin{cases} (p_{\mathrm{c}}/p_{\mathrm{e}})^N & \text{if} \quad p_{\mathrm{c}} > p_{\mathrm{e}} \\ 1 & \text{if} \quad p_{\mathrm{c}} \leq p_{\mathrm{e}} \end{cases} \tag{3}$$

$$p_{\mathrm{c}} = p_{\mathrm{e}} \left(S_{\mathrm{ew}}\right)^{-N} \tag{4}$$

In which p_{e} is the air entry pressure [kPa] and the parameter N is an empirical parameter related to the distribution in pore-sizes that generally ranges from 0.2 - 5 [–] (Szymkiewicz, 2013). A smaller N results in a steeper curve which means that the distribution of the pore sizes is more uniform.

2.2 Groundwater flow

The total hydraulic head of a liquid is composed of a pressure head, an elevation head and a kinetic head according to Bernoulli's equation (equation 5).

$$h = \frac{p_w}{\rho_w g} + z + \frac{v^2}{2g} \tag{5}$$

In this equation the first term is called the pressure head, the second term the elevation head and the third term the velocity head. Where h is the total head [m], ρ is the density of water [kg/m^3], g is the gravitational

acceleration [m/s^2], z is the elevation [m] and v is the velocity of the water [m/s]. Since v in groundwater flow problems is generally very small, the velocity head $v^2/(2g)$ is negligible when compared to the pressure head and the elevation head. When describing the total head in groundwater flow problems, equation 5 reduces to the following equation.

$$h = h_e + h_p \tag{6}$$

Where h_e is the elevation head [m], representing the gravitational potential energy due to elevation and h_p is the pressure head [m], which is the energy due to the pore fluid pressure. When there is a difference in hydraulic head within a soil there is a hydraulic gradient and flow of water will occur from a high hydraulic head to a low hydraulic head. The flow of water through a soil can be described by equations and (soil dependent) parameters. Groundwater flow in both the saturated zone and the vadose zone can be described by Darcy's equations.

Groundwater flow in the saturated zone

Darcy found with experiments that the flow through a saturated porous medium can be described by a linear relation between flow velocity and the hydraulic gradient. The Darcy equation for water flow through porous media in its simplest form is presented in equation 7.

$$\begin{aligned} q_x &= -K\frac{\partial h}{\partial x} \\ q_y &= -K\frac{\partial h}{\partial y} \\ q_z &= -K\frac{\partial h}{\partial z} \end{aligned} \tag{7}$$

In which q_n is the specific discharge [m/d] in direction n and K is the hydraulic conductivity (or permeability coefficient) [m/d]. The hydraulic conductivity is a soil dependent parameter. For stationary flow, the flow in a control volume should be the same as the flow out of the control volume (assuming a constant density), which can be described by the continuity equation (equation 8).

$$\frac{\partial q_x}{\partial x} + \frac{\partial q_y}{\partial y} + \frac{\partial q_z}{\partial z} = 0 \tag{8}$$

When there are transient flow conditions of water through a control volume, water is stored in the soil, otherwise there would be no continuity of mass. In the subsurface, water can be stored by filling the pores above the ground water table, and therefore increasing the water table. This is called phreatic storage and it is determined by the specific yield S_y [m^{3}m^{-3}]. The most important factor that determines specific yield of a soil (and thus the phreatic storage) is the porosity of the soil. (Van der Meer et al., 2004).

Water can also be stored in a soil when the soil is already fully saturated. This happens when the pore pressures in a soil increases which will lead to the expansion of the soil skeleton. This phenomenon is called elastic storage. Due to the expansion of the soil skeleton, there is more space for water to be stored (Chowdhury, 2020). Elastic storage is especially important for clay and peat layers. For sand layers, the elastic storage is most of the time negligible when compared to the phreatic storage (Van der Meer et al., 2004). How much water can be stored in a soil due to elastic storage is determined by the specific storage (S_s [m^{-1}]). The specific storage depends mainly on the compressibility of the soil and water and the porosity of the soil.

Groundwater flow in the vadose zone

While for a saturated soil a linear relation can be used to describe the flow of water as a function of the hydraulic gradient, this is not the case for flow through an unsaturated soil. In an unsaturated soil, the hydraulic conductivity depends on the water content in a soil. The reason for this is that the water will flow through the pores where water films are present. When the water content is higher, the water can flow more easily through the soil. The part through which the water can flow, is called the relative permeability (k_r [–]). The relation between hydraulic conductivity in an unsaturated soil and the matric suction is given by the hydraulic conductivity curve. The unsaturated hydraulic conductivity is calculated with the saturated hydraulic conductivity K_s and the relative permeability. For the Van Genuchten and Mualem model the relative permeability as a function of the effective saturation is given by the following expression (van Genuchten, 1980; Mualem, 1976).

$$k_{\mathrm{r}}\left(S_{\mathrm{e}}\right)=S_{\mathrm{e}}^{\lambda}\left[1-\left(1-\left(S_{\mathrm{e}}\right)^{1/m}\right)^{m}\right]^{2} \tag{9}$$

In which λ is a shape parameter [–] that determines the tail of the curve for high matric suction and low water content and is most of the time assumed at 0.5. The unsaturated hydraulic conductivity is the product of the saturated hydraulic conductivity and the relative permeability.

$$K(\theta)=K_s\left(\frac{\theta-\theta_r}{\theta_s-\theta_r}\right)\left[1-\left(1-\left(\frac{\theta-\theta_r}{\theta_s-\theta_r}\right)^{1/m}\right)^{m}\right]^{2} \tag{10}$$

In which $K(\theta)$ [m/d] is the hydraulic conductivity in the unsaturated soil with water content (θ) and K_s is the saturated hydraulic conductivity. The hydraulic conductivity is maximum at the saturated water content and equal to the saturated hydraulic conductivity K_s. When the water content is equal to the residual water content, the films of water in the pores are not connected to each other and the hydraulic conductivity will be 0.

The Brooks and Corey model calculates the unsaturated hydraulic conductivity from the saturated hydraulic conductivity with equation 11 (Morel-Seytoux et al., 1996). In this equation, the term after the saturated hydraulic conductivity represents the relative permeability, k_r [-].

$$K(\theta)=K_{\mathrm{s}}\left[\frac{\theta-\theta_{\mathrm{r}}}{\theta_{\mathrm{s}}-\theta_{\mathrm{r}}}\right]^{\varepsilon} \tag{11}$$

The parameter ε is the Brooks-Corey exponent [-]. To reduce the number of parameters, a relation between N and ε was developed by Corey (1977).

$$\varepsilon=\frac{2+3\cdot N}{N} \tag{12}$$

An example of a water retention curve and a hydraulic conductivity curve following the Genuchten and Mualem model for a clay is given in Figure 2.3. The figure shows that the hydraulic conductivity reduces orders of magnitude for a relatively small increase in matric suction (or a small decrease in water content).

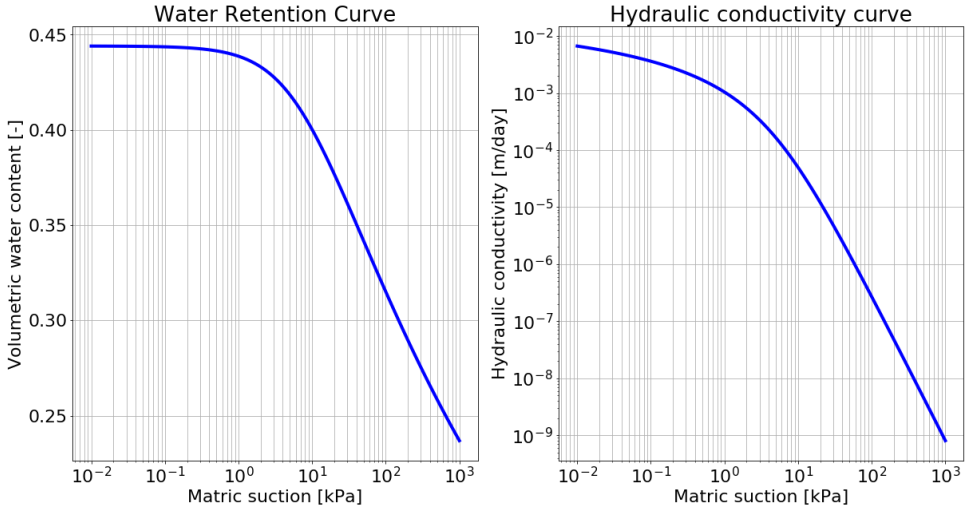

Figure 2.3: A water retention curve and a hydraulic conductivity curve following the van Genuchten and Mualem model with: θ_r=0 [m^3m^{-3}], θ_s=0.444 [m^3m^{-3}], α=0.146 [1/kPa], n=1.126 [–] , K_s=0.0212 [m/d].

Transient water flow through an unsaturated porous medium is often described by Richards equation (Richards, 1931). Equation 13 describes the transient water flow in an unsaturated soil and is called the mixed form of the Richards equation for unsaturated conditions (Szymkiewicz, 2013).

$$\frac{\partial\theta\left(\psi\right)}{\partial t}-\nabla\left[\mathrm{K}\left(\psi\right)\nabla\left(\psi+z\right)\right]=0 \tag{13}$$

In the Richards equation it is assumed that when the water enters pores where initially air was present the air does not impede the advance of the water. When comparing this with expressions for transient flow in saturated porous media, it shows that 1) the hydraulic conductivity is a function of the matric suction (and thus of the pressure head) and 2) the storage term is written as the change in the volumetric water content over time. While compaction or expansion of the soil can still result in an additional storage of water, as is the case in storage in a saturated soil, this amount is insignificant when compared to storage due to water content change. It is therefore most of the time ignored in unsaturated flow.

Infiltration in the vadose zone

It is clear that flow through the vadose zone is not as straightforward as flow through a saturated soil. When water evaporates or infiltrates, there will be a change in water content which will result in a change in pore pressure. As a result, the total head will also change (following equation 5). Moreover, due to the varying water content, also the hydraulic conductivity will change. As mentioned before, Darcy's equation remains valid in an unsaturated soil. The only change is that the hydraulic conductivity (and the total head), are now a function of the water content.

$$q = -K(\theta)\nabla h \tag{14}$$

To understand what the effect is of infiltration and evaporation on the water content profile and the pressure head, a 1D model is used. The 1D model considers a soil column of 10 meters high with soil characteristic parameters of a clay soil type and with the water table at 5 m+NAP. A sketch of the initial situation is displayed in Figure 2.4. Initially, hydrostatic conditions are considered, meaning that there is no gradient in total head and the water content profile follows the water retention curve. After t_0, infiltration starts from the top of the soil column. The water content increases (in this case all the way to the saturated water content) and the pressure head increases to 0 m. In a subsequent time step ($t > t_0$) the so-called wetting front propagates downward. Over the area where the water content is equal to the saturated water content the pressure head is 0 m. As a result, the total head is equal to the elevation head and there is a hydraulic gradient which results in the flow of water from a high total head to a low total head.

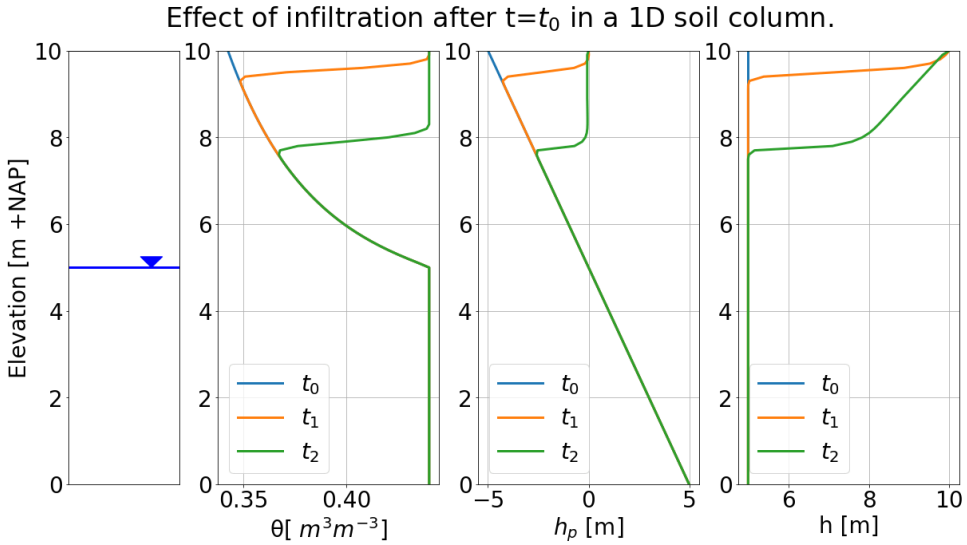

Figure 2.4: Water content, pressure head and total head profile for a 1D soil column where water starts infiltrating from the top after t_0 ($t_0 < t_1 < t_2$).

It depends on the soil characteristics and the rate and duration of infiltration what the shape and depth of the wetting front is. Rehman et al. (2015) researched what the effect of the soil type is on the shape and depth of the wetting front during a single low-intensity rainfall event. They also determined what the effect was on the matric suction in the soil. Five soil types were included in the analysis, ranging from sandy soil to clayey soil. Their research showed that a combination of a low saturated hydraulic conductivity and a high saturated water content will result in a situation where the wetting front will increase the water content to the saturated water content, meaning a matric suction of 0 in the soil. Soils with a low hydraulic conductivity but a lower

saturated water content, did not result in complete saturation over the infiltration depth.

Duong et al. (2019) did research to the influence of the intensity of the rainfall with respect to the saturated hydraulic conductivity of the soil on the transient seepage through a soil. Three cases were analyzed: one where the rainfall intensity was lower than the soil hydraulic conductivity, one where the rainfall intensity was slightly higher than the hydraulic conductivity and one where the rainfall intensity was much higher than the hydraulic conductivity. They found that for the first case, the rainwater would infiltrate in the soil and (for a high hydraulic conductivity), this will result in a rapid rise of the water table. When the rainfall intensity was slightly higher than the hydraulic conductivity and a pond could form on the ground surface, a wetting front would form and also the water table would rise after some time. Finally, they found that for a low hydraulic conductivity with respect to the rainfall intensity, a pond would form quick and a wetting front would descend slowly. In the case where no pond could form, the wetting front will descend very slow and the water table does not rise quickly.

2.3 Processes in a clay dike

The processes described above, form the basis for water flow through porous media. The objective of this research report is to see how the flow of water proceeds through a dike body and how it affects the matric suction. This is eminently a situation of transient saturated / unsaturated flow and therefore a complex problem. In this section a brief overview is presented of the possible effects of different external processes and internal variations on the matric suction in a dike body. The previous sections have showed that suction can be lost due to the progression of the water table and due to the increase in the water content through infiltrating water. It is noted that infiltrating water itself, can also result in the rise of the water table.

Average water levels and saturation

The average water level in the river and the average water level in the polder determine for a large part the course of the water table during normal conditions. The average conditions in a dike fluctuate with the seasons, resulting in a lower water table in summer and a higher water table in the winter. Also during the seasons itself, the water level might show some fluctuations. The water table during 'normal' conditions is thus not really stationary (Van der Meer et al., 2004).

The high water wave

When a dike is designed, a high water situation is chosen for the load situation related to the safety standard. A high water situation will result in higher pore pressures and thus a lower effective stress of the soil (see equation 15 and 16). In a standard stability analysis, generally the steady state phreatic surface is used, since this is the worst case scenario. In reality, the pore pressures will increase during a high water and the phreatic surface will rise. This rise will be fast at first but will decrease over time. Whether the steady state condition is really reached, depends on the soil type and the duration of the high river stage. Water will flow relatively slow through a dike with a clay core, due to the low hydraulic conductivity. As a result, a steady state condition will most of the time not be reached during a high water event in the river. Another reason for this is that the duration of the peak of the high water will only remain for a very short amount of time (in the order of one day). The shape of a high water wave in the river Rhine has been extensively researched, with the latest research presented in Chbab (2017). In this reports, standard shapes of the high water wave are included that can be used to schematize the course of a high water in (numerical) seepage analyses.

Precipitation

When rainfall occurs, a part of the precipitation will run off of the dike where it will infiltrate in the ground adjacent to the dike or flow in the river. A part of the rainfall will infiltrate in the dike and flow through the unsaturated zone, which was described in the previous section. The infiltrating water has an effect on the water content in the dike body, and this affects the suction in a direct way and in an indirect way. The infiltrating water affects the suction directly by the progression of the wetting front. It depends on the soil type and duration and rate of the infiltration how much suction will remain during infiltration. Only a part of the infiltrated water will reach the core of the dike and will increase the height of the water table, most of the water will evaporate through evapotranspiration (Van der Meer et al., 2004). Some of the infiltrated water will still be in the soil, increasing the water content locally, when follow up rain will infiltrate or when a high water event happens. This is the indirect effect: because the water content is already higher than in hydrostatic conditions, the hydraulic conductivity will also be higher and water will flow faster.

Overtopping and overflow

Overtopping has a similar effect as precipitation, as it will result in some infiltration in the dike body. However, when considering river dikes, infiltration due to precipitation will be larger than due to overtopping since wave heights are generally small. Therefore, infiltration due to overtopping will not be included further in this research. On the other hand, during overflow there might be a significant flux of water on the dike which can influence suction in the dike body. However, this (load) condition will more likely result in the failure of the dike due to other failure mechanisms, making the presence and magnitude of suction trivial during such a situation. It is therefore not included in this study.

Evapotranspiration and cracks

The evaporation of water from the top layer of the soil, together with the transpiration of water through plants is called evapotranspiration. It decreases the water content in the vadose zone and thus results in an increase in suction. During summer, when evapotranspiration is high, the suction in soils can get so high that the soil will start to crack. During winter, when the water content in the dike increases, some of these cracks might close up again. However, some of the larger cracks will remain, resulting in a weaker soil structure. Through these cracks, which can have lengths up to 1 meter, water can infiltrate more easily in the soil (Van der Meer et al., 2004; Jamalinia et al., 2020). As a result, the extra shear strength that is gained from suction will reduce quickly during infiltration and it should therefore be assumed that there is no increase in strength of the soil in the top layer (the first 1 meter) of a dike. Both the influence of evapotranspiration as the more permeable top layer of the dike are considered in this study.

Internal variations of a dike

Generally, a clay dike body is assumed to be made up of one material with homogeneous properties. However, in reality there is always some heterogeneity, both spatially and temporally. After construction of a dike, the soils will gradually deform and other variations, such as the previous mentioned cracks due to high suction, will start to form.

Historical dike reinforcements have resulted in irregularities in dike profiles. In the Netherlands, there is a long history in building and reinforcing dikes. Every new layer that has been applied to a dike might have a slightly varying soil properties (van Woerkom, 2021). It is also possible that there is a sand layer or an old road present somewhere in the dike cross section, as it is often not entirely clear how the dike is built up. Moreover, traffic and other loads on top of dikes can result in compaction of the soil which will alter the properties of the soil. Due to time constraints, heterogeneity of the soil properties within soil layers are not included in the presented research.

Besides the formation of cracks due to high suction in the top layer of the dike, irregularities and open spaces will also form due to biological activity. These open spaces are mostly present in the top layer of the dike but can also extend deeper in the dike body. In this presented research, the combined effect of cracks and fractures due to biological activity is included by modelling the top 1 meter of the dike with a higher permeability and by not accounting on additional shear strength in that layer.

2.4 Suction and the unsaturated shear strength

The strength of a soil is given by the effective stress which is generally described by Terzaghi's effective stress equation given in equation 15

$$\sigma' = \sigma - p_{\mathrm{w}} \tag{15}$$

In which σ is the total stress in the soil, σ' is the effective stress and p_w is the pore water pressure. However, in this formulation of the effective stress, extra strength due to suction in a soil is not included. Bishop proposed a modified form for the effective stress in an unsaturated soil, where the contribution of matric suction is also included (equation 16)(Bishop, 1959).

$$\sigma' = \sigma - p_{\mathrm{a}} + \chi \left(p_{\mathrm{a}} - p_{\mathrm{w}}\right) \tag{16}$$

In this formulation χ is the effective stress parameter (ranging from 0 to 1 and dependent on the effective saturation) and the term (p_a - p_w) is the matric suction in a soil. With this equation, the effective stress of

a soil can be calculated while including the increase of strength due to suction. With help of equation 16 the following equation for the shear strength of an unsaturated soil was determined.

$$\tau = c' + (\sigma - p_a) \tan \varphi' + \chi \, (\mathrm{p_a} - \mathrm{p_w}) \tan \varphi' \tag{17}$$

In which τ is the shear strength, c' is the effective cohesion [kPa] and φ' is the internal friction angle [°]. In this formulation the first two terms are related to the saturated strength of the soil and the third term is due to the unsaturated strength. This third term, the apparent cohesion, varies with the matric suction in the soil. Vanapalli et al. (1996) found the following empirical relation to determine the apparent cohesion (c_{app}) of a soil.

$$c_{app} = (p_\mathrm{a} - \mathrm{p_w}) \, (\Theta^\kappa) \tan \varphi' \tag{18}$$

Where Θ is the normalized water content, which can be assumed equal to the degree of saturation S_e and κ is a fitting parameter that depends on the plasticity index of the soil. The relationship between the plasticity index and the fitting parameter κ in Figure 2.5 was found by Vanapalli et al. (2000) and Vanapalli (2001). The figure shows that the fitting parameter κ is larger for soils with a higher clay content, characterized by a higher plasticity index. As a result, the expected apparent cohesion is less for clay soils than for sandy soils, since $S_e \leq 1$.

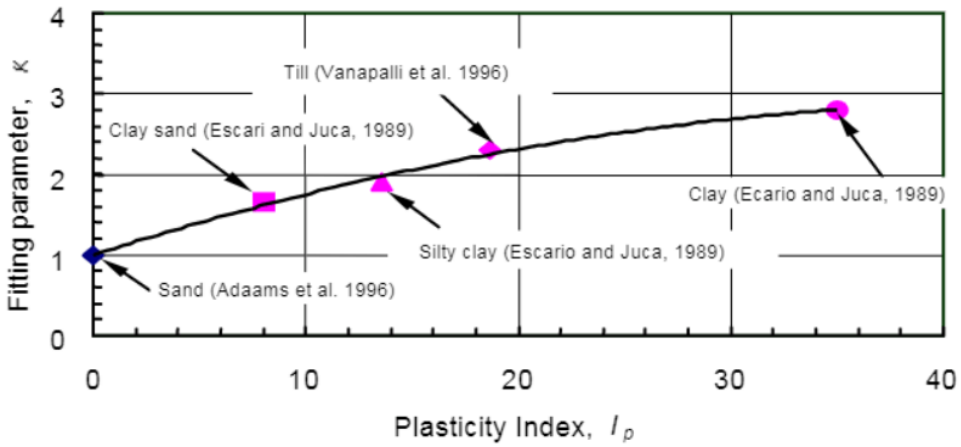

Figure 2.5: The relationship between the fitting parameter, κ, and the plasticity index, I_p. (from (Vanapalli et al., 2000)).

The unsaturated soil strength can be included in stability analyses by adding an apparent cohesion to soil layers where an increase in shear strength is present. Equation 18 and Figure 2.5 show that the amount of apparent cohesion that can be expected for a given suction, depends on the effective saturation (and thus on the water retention curve) and the plasticity index. Using the formulation of van Genuchten and Mualem (equation 2), equation 18 can be rewritten as follows:

$$c_{app} = (p_\mathrm{a} - \mathrm{p_w}) \left(\frac{1}{[1 + (\alpha p_c)^n]^m} \right)^\kappa \tan \varphi' \tag{19}$$

With estimates for the parameters θ_r, θ_s, n, α, I_p and φ', the expected apparent cohesion for a soil can be determined. Since the focus of the research in this thesis is on river dikes with a clay core (specifically, the case study dike), distributions were determined for clay soils and included in Table 2.1. Data from the case study dike showed that the plasticity index in the core of the dike varies between 14 and 43 %, and that it can best be described by a lognormal distribution (see Appendix A). To obtain an estimate for κ, a linear relation was assumed with I_p, which seems like a valid assumption for I_p ranging from 14–36% according to figure 2.5. It is assumed that this relation is also valid above 36%. The linear regression line in equation 20 was fitted to the upper three data points in figure 2.5. The uncertainty related to the slope and intercept of this linear line are not included.

$$\kappa = 0.045 \cdot I_p + 1.25 \tag{20}$$

Table 2.1: Variables and distributions to determine the apparent cohesion for clay soils.

Variable	Unit	Distribution	Parameters	Notes
θ_r	[m^3m^{-3}]	Deterministic	0.01	Based on Heinen et al. (2020)
θ_s	[m^3m^{-3}]	Normal	μ=0.50, σ=0.05	Based on Heinen et al. (2020)
n	[–]	Lognormal	s=0.3, loc=1.05, scale=0.05	Based on Heinen et al. (2020) [1]
α	[1/kPa]	Normal	μ=0.012, σ=0.001	Based on Heinen et al. (2020)
I_p	[%]	Lognormal	s=0.39, loc=0.0024, scale=26.7	see Appendix A
φ'	[°]	Normal	μ=30, σ=3	Based on Cheng & He (2020)

With the distributions in Table 2.1 the expected relationship between the matric suction and apparent cohesion could be determined for a clay soil by performing a Monte Carlo simulation. The median and the 95% confidence interval is given in figure 2.6.

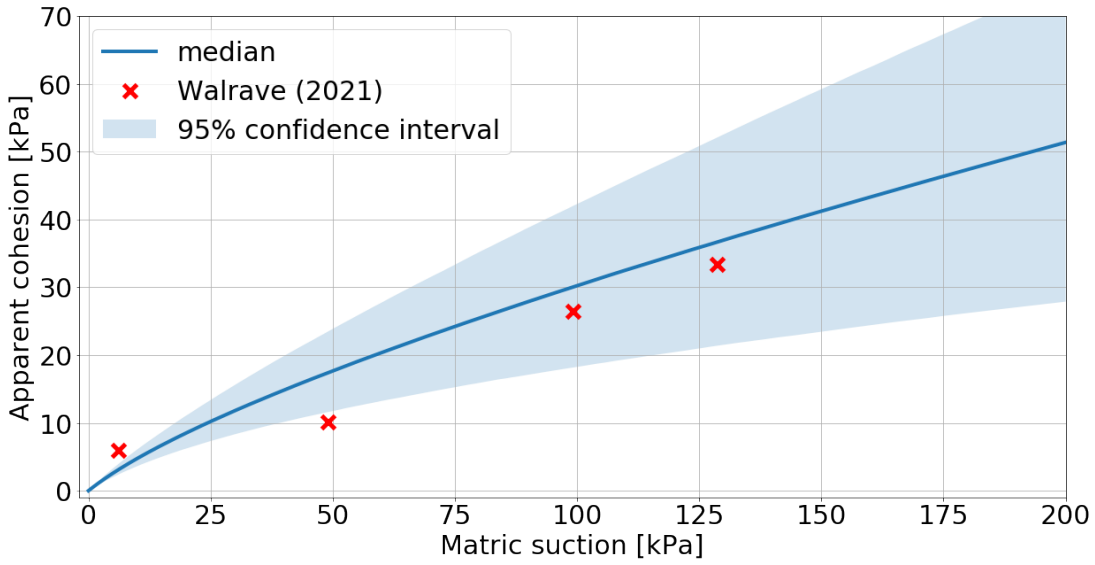

Figure 2.6: Expected relationship between matric suction and apparent cohesion and the 95% confidence interval, together with the measurements of Walrave (2021)

Walrave (2021) performed measurements in the laboratory with clay samples from a river dike in the Netherlands along the Maas to determine the unsaturated soil characteristics of that soil and to find the strength increase due to matric suction. The results of the measurements are included in figure 2.6, and show a variation from the expected apparent cohesion, especially for low suction. The plasticity index of this clay from the Maas dike has a mean of 22.7% and a standard deviation of 6.45 [%], which is less than the plasticity index of the clay at the case study dike. Since a lower I_p means a lower κ, the curve will be steeper for the Maas clay, resulting in a larger deviation from the results. The figure can be used in further analyses, but it should be used with caution. This variation from the results can be due to measurement inaccuracies or because the empirical relation in equation 18 does not hold for low suction or for clay in dikes.

2.5 Modelling transient saturated/unsaturated groundwater flow

Due to the non-linear relations in unsaturated soils and the transient processes that dikes are subjected to, modelling these problems is not straightforward and generally takes a lot of computational time. The research presented in this report was done using two models: a 2D model Seep/W and 1D model SWAP. the 2D model

[1] A lognormal distribution was chosen because n has a lower limit of 1

Seep/W was mainly used to determine the progression of the water table over time and the 1D model SWAP was mainly used to observe how infiltration and evaporation affect matric suction in a soil column. This can be schematized to a 1D problem since the flow through the unsaturated zone is mainly 1D. First a brief introduction to the two models is given after which the quasi 2D modelling approach for the schematization of infiltration is validated.

Seep/W

Seep/W is a finite element seepage model of Geostudio. It can take into account the unsaturated zone and the unsaturated properties can be defined by using the Van Genuchten parameters. While Seep/W also contains other models to determine the unsaturated region, they are not used and thus not included in this report. The parameters that have to be defined are θ_r, θ_s, n, α^{-1} and K_s. The parameter λ is not included as a parameter in Seep/W and is fixed at 0.5 [-] as in the traditional approach. Time steps can be defined in different units and a time step of one day was used in the research.

SWAP

The model SWAP (Soil Water Atmosphere and Plant) is a 1D model created by Wageningen university that can simulate the transport of water, solutes and heat in unsaturated/saturated soil. In this research only the transport of water through unsaturated/saturated soil is used. SWAP takes as input parameters for the unsaturated characteristics of soils the Van Genuchten parameters, the parameter λ (which defines the tail of the hydraulic conductivity curve) and the air entry pressure, p_e^{drain}. The air entry pressure is not included in the original Mualem and van Genuchten functions. However, when there is no air entry pressure, the water retention curve can become discontinuous at h_p=0, resulting in a sharp drop in hydraulic conductivity for h_p=0. This is especially the case for low values of n (near its lower limit of 1.0) (Vogel et al., 2000). Since this discontinuity can cause numerical instabilities, a modification was proposed by Vogel et al. (1985) and Vogel et al. (2000) that introduces a minimal height, h_s, over which the water content is equal to the saturated water content and a slight alteration of θ_s, for h>h_s. The modification is included in equations 21 and 22. For h_s, a value of -0.01 or -0.02 m was proposed and a value of -0.01 m is used in the model.

$$\theta(h) = \begin{cases} \theta_\mathrm{r} + \frac{\theta_\mathrm{m} - \theta_\mathrm{r}}{(1+|\alpha h|^n)^m} & h < h_\mathrm{s} \\ \theta_\mathrm{s} & h \geq h_\mathrm{s} \end{cases} \tag{21}$$

$$\theta_\mathrm{m} = \theta_\mathrm{r} + (\theta_\mathrm{s} - \theta_\mathrm{r})\,(1 + |\alpha h_\mathrm{s}|^n)^m \tag{22}$$

SWAP takes as input a file with meteorological data, including rain intensities, temperatures, radiation and humidity. This makes it easy to subject the soil to real weather data, while the possibility to insert synthetic data also remains. Since weather data is generally available as daily data, a time step of 1 day is common. However, there is also the possibility to use smaller time steps, up to 1 hour. Since rain falls in a random pattern over the day, averaging rain events over a day (or over longer periods) can have a large implication. Suppose there is a high intensity rain event with a duration of an hour during a day where no other rain falls. When the rain falls on the grass, and the intensity is higher than the conductivity the rain will run-off (especially of a sloping dike). If this rainfall event is schematized as an average precipitation per 24 hours, the intensity is less, which might result in that all precipitation will infiltrate in the soil. On the other hand, an averaged peak will result in a smaller wetting front, which can be in turn underestimate the influence of the precipitation. Naturally, this might also be true for evaporation and transpiration. This effect is elaborated on in appendix B. Transpiration of plants can be included by specifying a file with data regarding the crop. In the case of river dikes, suction is the result of evaporation and transpiration of grass. An elaboration about modelling evaporation and transpiration with SWAP is presented in appendix C. To correctly model evaporation and infiltration near the surface, a compartment thickness of 0.01 m was chosen (Kroes et al., 2017). In all analyses it was assumed that ponding could not occur, since water that can not infiltrate in the dike will run off the dike.

Validation of quasi 2D model

To reduce computational time and to be able to use real weather data as a boundary condition, the 1D model was used to observe the effect of infiltration and evaporation. The rate and direction of flow is determined by the gradient of the total head. If the gradient of the total head in the y-direction (in a 2D x,y-plane) is much larger than the gradient in the x-direction, the flow will be mostly vertical. If this is the case, a quasi 2D model is a valid alternative for a 2D calculation. In the quasi 2D model, the cross section is divided into columns with a width of 0.25 meter and by performing a 1D calculation for every column. When water infiltrates a soil from

the ground surface, the water content will increase and the pressure head increases as well. As a result the total head increases and a large vertical gradient occurs (see again Figure 2.4). When the position of the water table can assumed to be fixed, horizontal gradients (in total head) can exist in a dike due to a difference in water level in the river and in the polder (meaning that there is a sloping water table). Moreover, in the part where the dike has a slope there will be a gradient in the horizontal direction when infiltration takes place. This gradient will be similar, but opposite to the gradient of the slope of the dike.

To validate the presented approach, two scenario calculations were made with both the 2D model and the quasi 2D model for the cross-section in Figure 2.7. The first scenario is characterized by an initial river level of 10.00 m+NAP, resulting in an almost horizontal water table (the polder level is 9.50m+NAP), and hydrostatic conditions. After day 0 it starts raining for 10 days with an intensity of 5 mm/day. To compare the results of the two calculation, a contour plot was made of the pressure heads on an arbitrary day (day 5) with the two models (Figure 2.8a and 2.8b). The figure shows very similar results, however to be able to compare the results even better, the pressure head along 5 sections were plotted for three arbitrary days (see Figure 2.9). The x-coordinates of the sections are included in Table 2.2 and a figure with the cross section and the sections that were made is included in Figure 2.7.

Table 2.2: x-coordinates of the sections S0-S5 in the cross-section.

Section number	**Description**	**x-coordinate [m]**
S0	Left corner of the crest	29.2
S1	Middle of the crest	30.7
S2	Right corner of the crest	32.2
S3	Mid-slope	37.45
S4	Start of berm	42.7

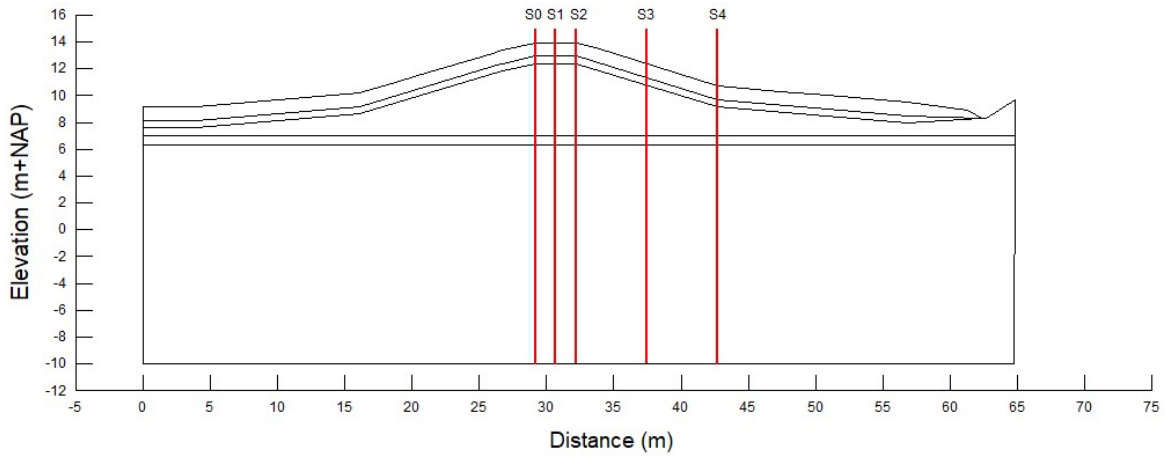

Figure 2.7: Cross section with the position of the 5 sections along which data was retrieved.

The graphs show that the results of the two models are very similar along sections S0–S4, where variations in pressure head are smaller than 0.1m. The wetting front progresses at an approximately similar rate. Especially the results along S1 are similar, which is as expected since S1 is a section through the middle of the crest of the dike (where no gradients due to a sloping surface exist). However, also the results along sections S0, S2 and S3 are very similar, and S3 is situated in the middle of the slope. Only along S4, the results vary. The reason for this is that the water table is situated very close to the ground surface and that the pressure head at the bottom of the soil column is fixed in the quasi 2D calculation. However, since our main focus is in the upper part of the core of the dike and there is little to no suction expected in the inner toe of the dike, the results match well enough for the quasi 2D model to be used.

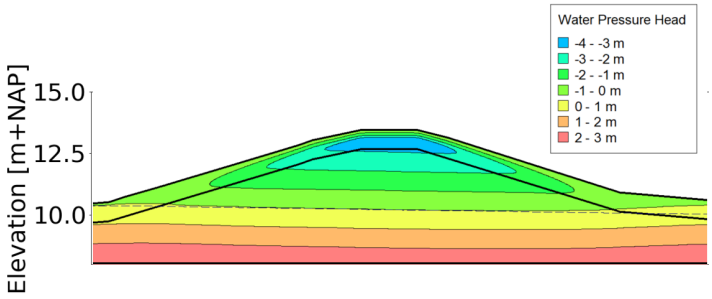

(a)

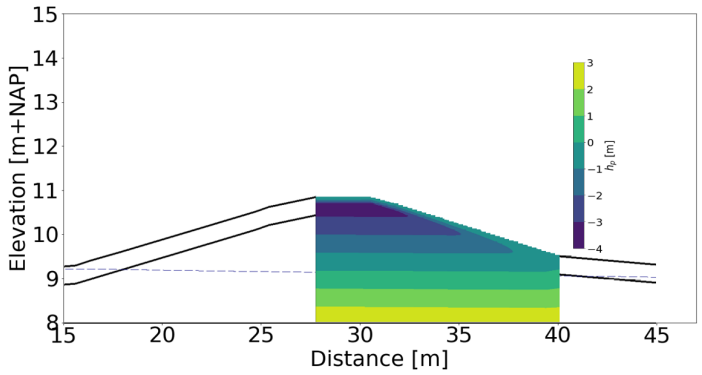

(b)

Figure 2.8: Pressure head in meters on day 5 of infiltration calculated with the 2D model SEEP/W (2.8a) and quasi 2D model SWAP (2.8b)

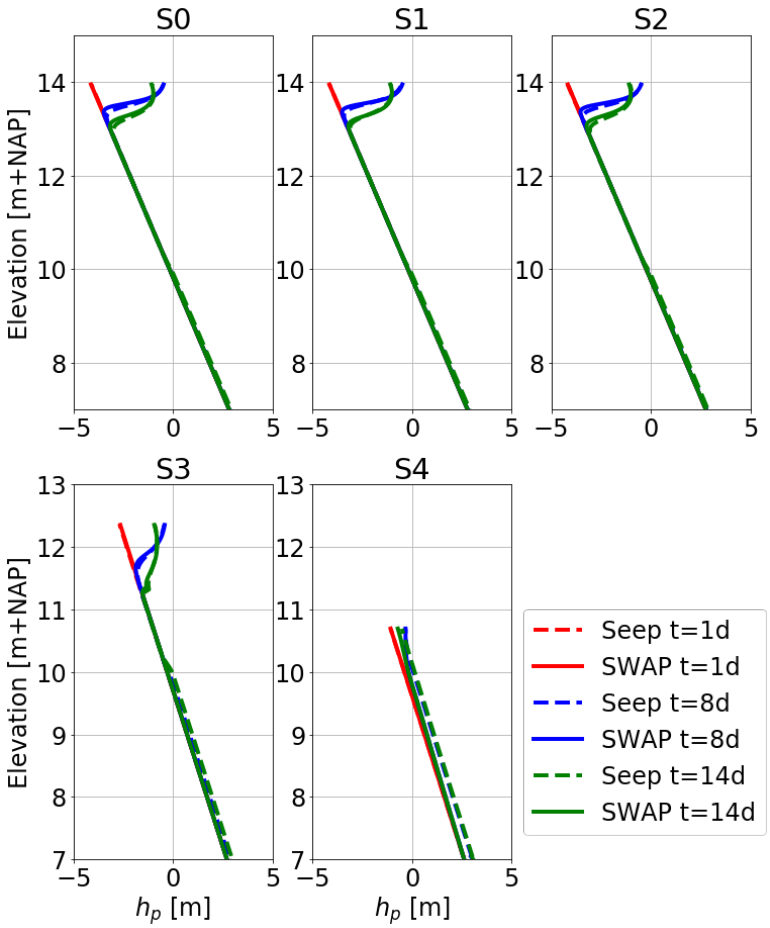

Figure 2.9: Comparison of the pressure head along sections S0-S4 obtained with 2D model Seep/W and quasi 2D model SWAP

The other validation calculation that was made was with a (larger) sloping water table for a river stage of 12.00 m+NAP (included in Figure 2.10a and 2.10a). The figures still show similar results, although the effect of the schematization can now more clearly be seen in the upper part of the inner slope. To see how large the variation is, the shapes of the wetting fronts were plotted again for three days (see Figure 2.11). This variation is due to the combined horizontal gradient due to the slope of the dike and the slope of the water table. The graphs show that along the sections, the difference in the pressure head is in the order of 0.1–0.2 meter. These results suggest that the approach is less valid when the water table is expected to be dynamic (for example during a high water event) and that the quasi 2D approach should be used with caution, or not be used (depending on the expected variations), in such cases.

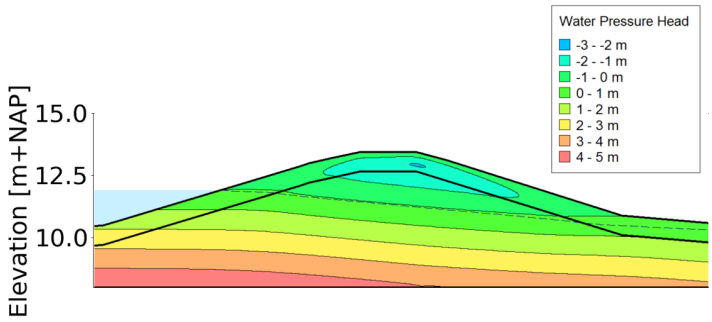

(a)

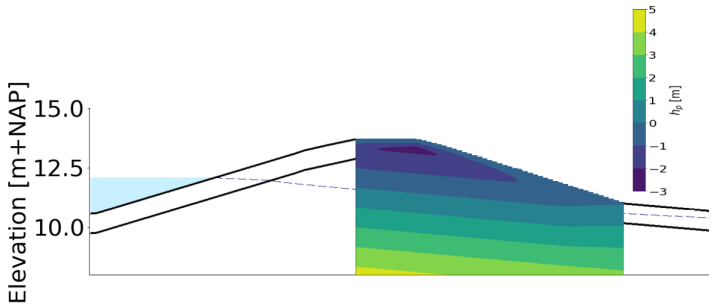

(b)

Figure 2.10: Pressure head in meters on day 5 of infiltration calculated with 2D model SEEP/W (2.10a) and quasi 2D model SWAP (2.10b) for a river level of 12.00 m+NAP

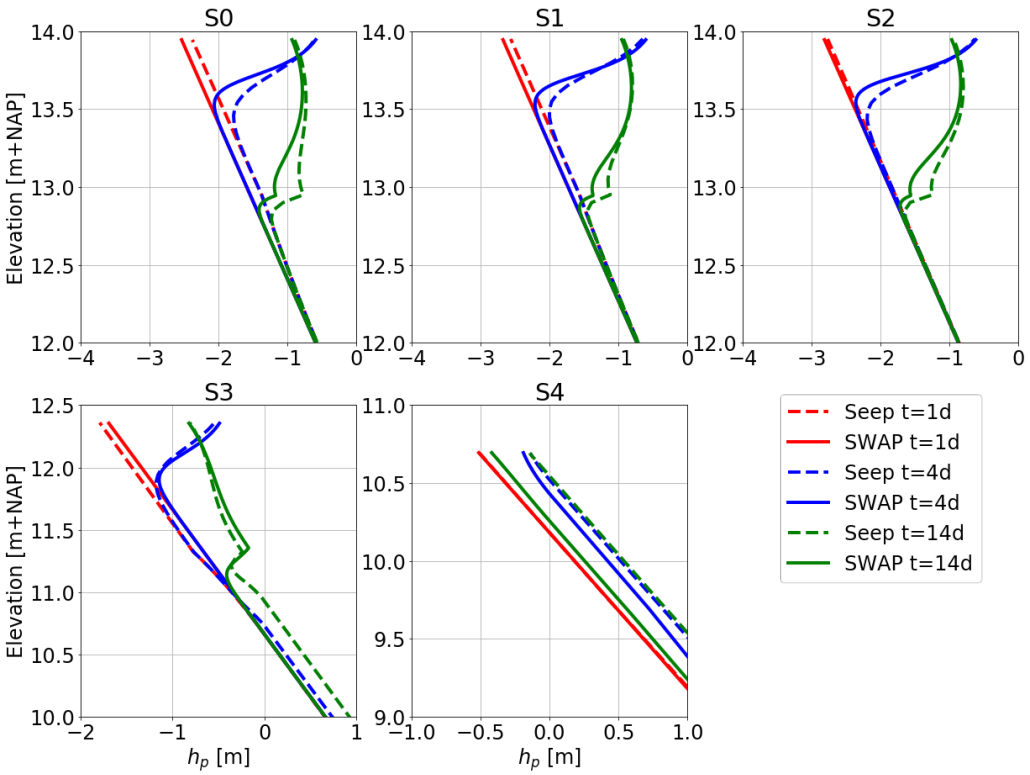

Figure 2.11: Comparison of the pressure head along sections S0-S4 obtained with 2D model Seep/W and quasi 2D model SWAP for a river level of 12.00 m+NAP

Characteristics of soil layers

To be able to use the information about the soil layers in (numerical) seepage analyses, characteristic values had to be determined to define a water retention curve and a hydraulic conductivity curve for each soil layer. This was done with help of the Staring series (Heinen et al., 2020). The Staring series describes the average retention capacities and the average permeability of 36 subsoil types. They are classified based on if they are an upper layer or a lower layer of the subsurface, where the upper layer of the subsurface is defined as the layer where the roots of plants reach (Wösten et al., 2001). The series are further subdivided in sand, sandy clay, clay, loam and humus soil types. The water retention curve is described according to van Genuchten (see equation 2) and the hydraulic conductivity curve according to Mualem and van Genuchten. The parameters θ_r, θ_s, α, n, λ and K_s were determined based on data from soil samples that were collected from different locations spread out over the Netherlands. Hysteresis of the water retention curve was not included during the analyses and the Staring series only include the main drainage curve of the samples. Moreover, it should be noted that the saturated hydraulic conductivity reported in the Staring series is a fitted hydraulic conductivity based on unsaturated flow experiments and not the measured saturated hydraulic conductivity. Therefore the value of the saturated hydraulic conductivity might not be a good estimate for the actual saturated hydraulic conductivity. Another large uncertainty when using the parameters from the staring series in a seepage analysis through a dike body, is that soils in a dike body are compacted while the samples used for the Staring series are not. The saturated hydraulic conductivities for clay layers in the Staring series range between 10^{-2}–10^{-1} m/day. There is not many literature that give estimates for the conductivity of compacted clay. In the update of the technical report for the design of dike reinforcements, a hydraulic conductivity in the order of 10^{0} m/day (in original units: 10^{-5} m/s) of clay after compaction is mentioned (van Meurs & Kruse, 2017). However, it is unclear how this value was obtained. Benson et al. (1994) created a database of laboratory measurements of saturated hydraulic conductivities of compacted clay liners. The database contains only natural clay soils that were extracted from landfills in North America. The database shows hydraulic conductivities in the range of 10^{-6} -10^{-5} m/day (original units cm/s). However, since the measurements were from clays in clay liners, it is not possible to assume that such low saturated conductivities are also characteristics for clay used in dikes, since clay liners are very carefully constructed. It does however, give an indication in how low the conductivities of clay can get when compacted.

3 Suction in the case study dike: the factors of influence

The theory presented in chapter 2 shows that there are many potential influencing factors on the presence of suction in a dike. Based on the found literature, several initial conditions, boundary conditions and soil characteristic parameters can be identified that are of interest to be further explored in a sensitivity analysis. The initial conditions of interest are the height of the river level before a high water event, and the initial water content in the unsaturated zone. The boundary conditions that were found to be of importance were infiltration from the top due to precipitation, evapotranspiration and the shape of the high water wave. Furthermore, the hydraulic conductivity and the parameters that describe the water retention curve of the different soils in the cross section can have an influence. In this chapter, first the general set up of the analyses is presented (Section 3.1). After this, an analysis is done specifically to the influencing factors on the progression of the water table and on the progression of the wetting front separately. Finally, an analysis is done with real weather data in Section 3.6.

3.1 Methods

The theory has shown that suction in a cross section of a dike can be lost due to different processes. In the sensitivity analysis, the two processes (the high water and influences by the weather) were decoupled and researched independently of one another. The influence on the progression of the water table was researched by setting up a 2D seepage analysis in Geostudio Seep/W. Since precipitation and evaporation are mostly 1D processes, their effect was examined with simple 1D models in SWAP.

Schematization of the cross-section

The case study dike was schematized to a simple cross section where the top layer with a thickness of 1 meter was schematized as a cracked layer and the core of the dike was schematized as a clay layer. A sandy clay layer could be identified in the available CPTs, that separates the clay core of the aquifer. No differences could be observed in the properties of the blanket layer and the clay core, which is why they were modelled as one layer. An elaboration of the analysis of the soil data is included in appendix A.

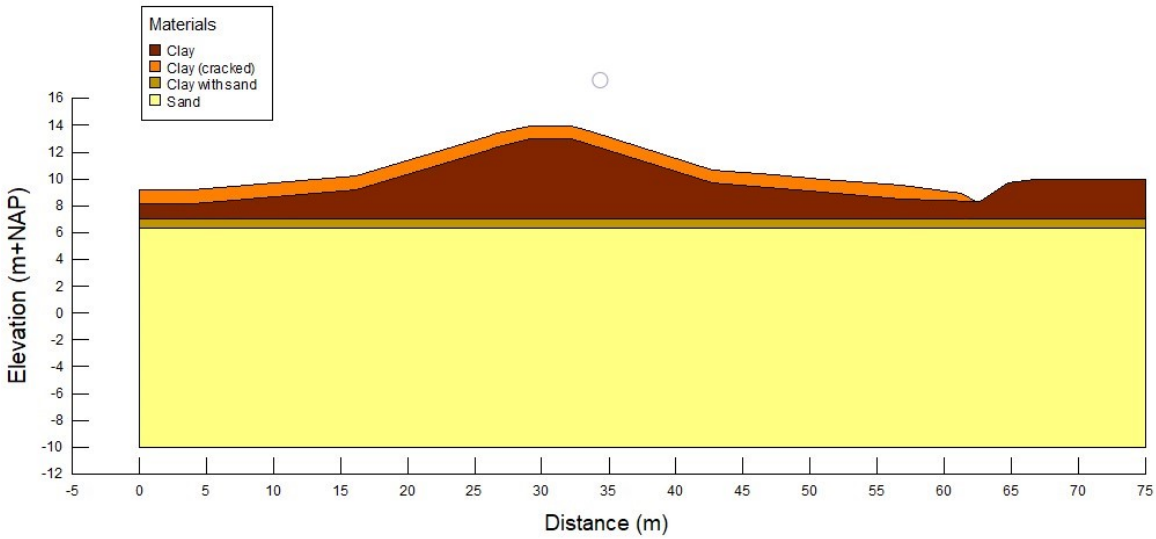

Figure 3.1: Schematization of the cross section of the Lathumsedijk at Duiven used as a case study in this report.

2D modelling with Seep/W

The methods used to obtain and process the data from Seep/W are briefly summarized here. The cross section of the case study dike was used in Seep/W by creating a grid. In the cracked clay layer and the clay core of the dike, a grid size of 0.1 meter was used. Since the pressure heads and conductivity vary a lot in the unsaturated zone, it is important that a fine grid is used. The sandy clay layer and the aquifer where schematized by grid cells with a size of 1 meter, since they are generally below the water table and there are less variations in

conductivity and pressure heads there. A transient seepage analysis will result in a lot of data (pore pressures on every grid point, for every time step), which can make it hard to provide insight in the variations over time and space. A schematization was made by making 5 vertical sections in the dike (see Figure 2.7, along which the pore pressures were exported for every time step.
With the data of the pressure heads along the 5 sections, the height of the water table could be determined along the sections over time. The position of the water table was determined with linear interpolation along the sections, to find the height at which the pressure head was 0 meter.

Quasi 2D modelling with SWAP

The sensitivity to the weather influences were analysed with 1D models and both synthetic and real weather data. Similar to the schematized cross section, the model set-up consisted of a cracked clay layer with a thickness of 1 meter and a clay core with varying heights. As initial condition, a hydrostatic condition can be chosen by defining the initial height of the water table, or an initial pressure head can be determined over the height of the soil column. The results of the 1D models can be transferred to create a 2D figure (as was included in chapter 2.5), by dividing the cross section in columns with a small width (0.25m) and performing the calculations for every column.

3.2 The water table and initial conditions

The initial condition in a transient 2D seepage analysis is generally given as a steady state calculation of a different situation or a specific time step of another transient analysis. The initial pore pressure distribution in a dike body has an effect in two main ways: The initial height of the phreatic surface has a large influence to what extend the phreatic surface will rise during a high water wave. Moreover, the initial water content of the soil determines the unsaturated hydraulic conductivity in the dike body. This can be included in the initial condition by applying a non-zero surface flux at the ground surface.

The initial water level in the river

To observe the influence of the initial height in the river 5 analyses were done, each with a different initial river level. The parameters that were used to define the characteristics of the soil layers are based on the soil types in the Staring series and included in Table 3.1.

Table 3.1: Parameters used for the soil layers in the analysis.

Soil layer description	**Staring series number**	Material model	θ_r **[-]**	θ_s **[-]**	α **[1/m]**	**n [-]**	K_s **[cm/day]**
Clay	B10	Sat/Unsat	0.01	0.448	1.28	1.135	3.83
Clay cracked	B07	Sat/Unsat	0.0	0.401	1.83	1.248	14.58
Clay + sand	O08	Sat	-	-	-	-	8.64
Sand	O01	Sat	-	-	-	-	22.32

The initial river stages that were considered were between 7 and 11 m+NAP with a step size of 1 meter and an initial surface flux of 0.1 mm/day was applied. After the initial condition (day 1) the water level in the river was heightened in one step to 13.64 m+NAP and the polder level was heightened to 9.5 m+NAP (see Section 3.3. A transient analysis of 36 days started with a time step of 1 day. Additionally, a steady state calculation was performed with the high water in the river to observe the height of the steady state water table. For every time step of the transient analysis the pressure head along the sections S1-S4 was determined and exported and the height of the water table was calculated with linear interpolation. The height of the water table along sections S1-S4 for every time step are included in Figure 3.3.

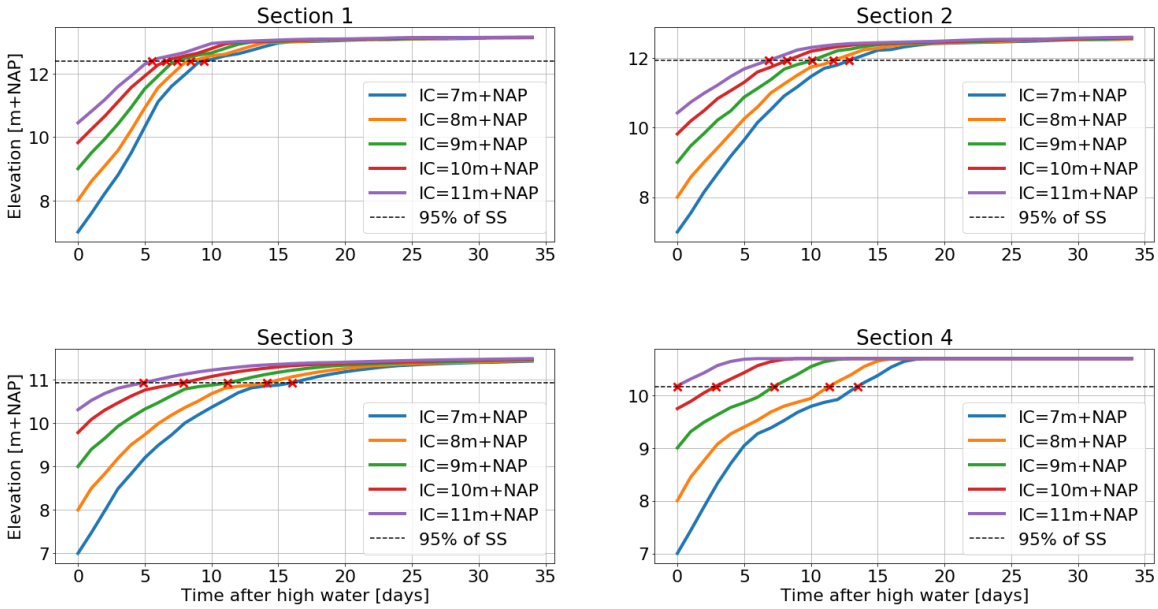

Figure 3.2: The height of the water table after a high water event along the four sections S1-S4 for varying initial conditions (IC) of the river stage.

The figure shows that the rate of the rise of the phreatic surface initially is high and decreases over time. This is a direct result of Darcy's law that states that the rate of flow is proportional to the difference in total head times the conductivity. The height of the water table for a steady state situation was calculated in a same manner with the results from the steady state calculation of the high water level in the river. Since a steady state situation is determined as the situation that would exist if the boundary conditions would be there for an infinite time, the steady state situation itself is never really reached. That is why the 95% level of the steady state situation was chosen as a reference level and the time before this height was reached for the varying initial conditions was determined (included in Figure 3.3).

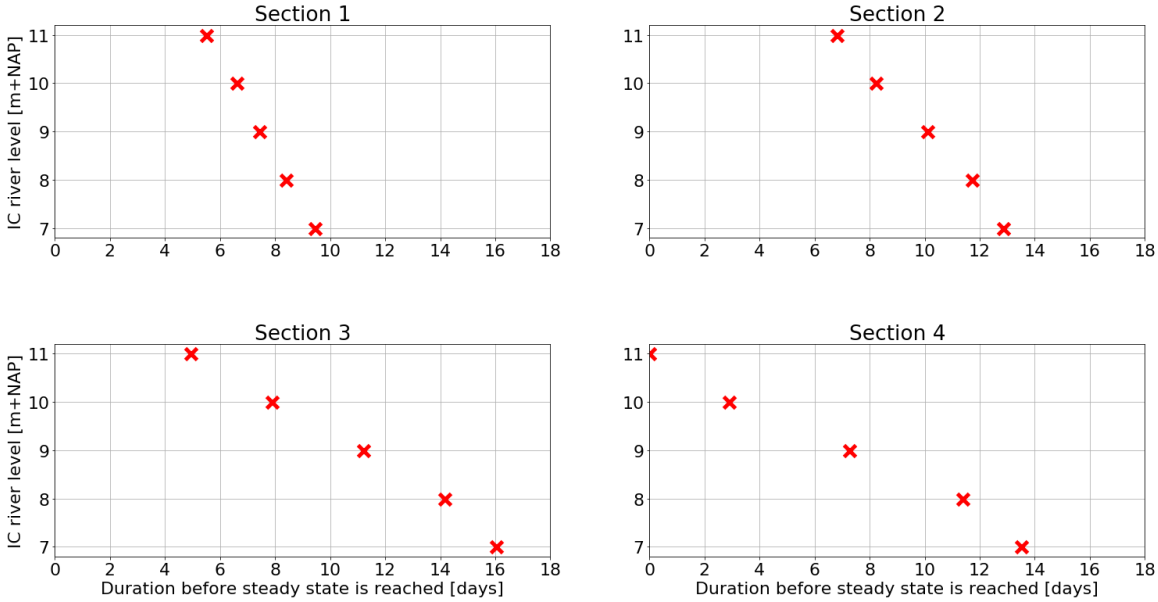

Figure 3.3: The duration before the 95% Steady state is reached along the four sections S1-S4 for the different initial river levels.

The graphs in Figure 3.3 show that the time it takes before a steady state is reached and the initial water level in the river have an approximately linear relation. Again, it can be referred back to Darcy's equation, which is also linear in the saturated area. In the unsaturated area, Darcy's law is not linear. However, since the area above the phreatic surface will have a similar water content and thus conductivity for all the 5 different initial

conditions (while naturally the height of the phreatic surface varies over the 5 situations), it is not surprising that the relation is approximately linear.

The initial water content in the dike

If infiltration and evapotranspiration are not considered, the area in a soil above the water table can be assumed to have a hydrostatic pressure distribution. However, a dike is subjected to the influences of the weather at all times. These processes influence the water content in the dike, which will influence the hydraulic conductivity and thus the flow of water through the dike. High water events in the Dutch Rhine and Rhine branches generally happen during winter, when there is a lot if precipitation in the Alpes and the south of Germany. Naturally during winter, there is also more precipitation in the Netherlands and therefore it is likely to assume that the water content in the dike body is already higher and suction less before a high water. This can be modelled by applying a small non-zero surface flux (smaller than the saturated hydraulic conductivity). An analysis was done to see how the applied surface-flux as the initial condition effects the time it takes until the water table reaches the 95% level of the steady state water table. The properties of the soil layers used in the analyses were equal to those specified in Table 3.1 and the varying applied surface fluxes were 0.01, 0.1, 0.5 and 1 mm/day. The initial river stage was 7 m+NAP. After the initial condition the water level in the river was again heightened in one step to 13.64 m+NAP and the polder level was heightened to 9.5 m+NAP. The height of the water table along the sections was determined similarly as in the previous sections. The height of the water table along the four sections are plotted over time in Figure 3.4. The time at which the water table reaches the 95% of the water table is also included in the figure.

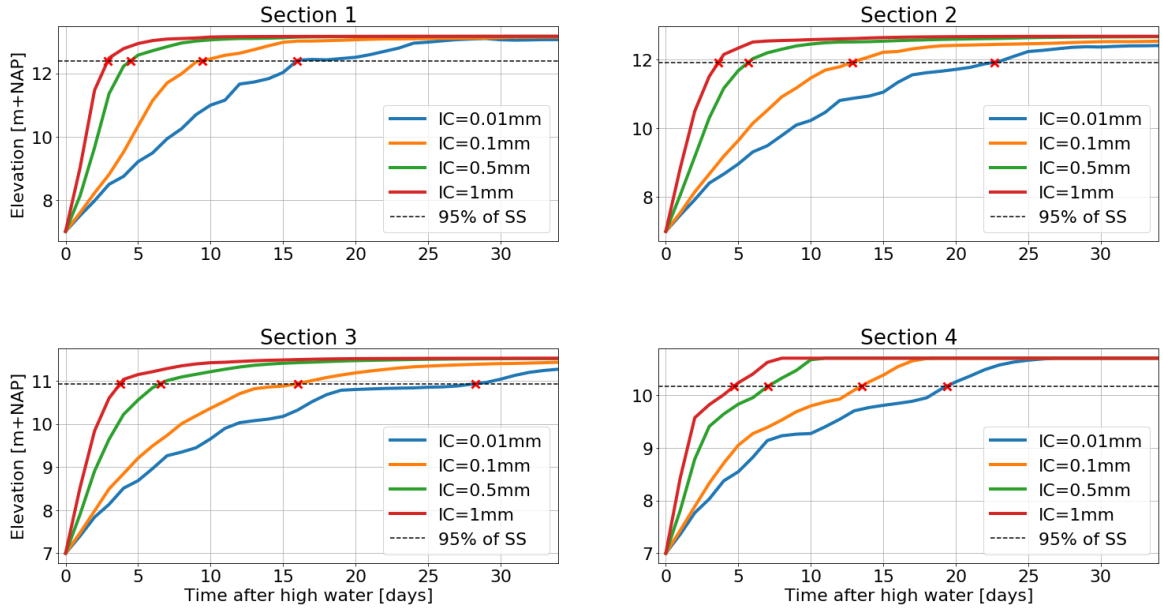

Figure 3.4: Height of the water table over time along the four sections S1-S4 for the different Initial Conditions (IC) of the infiltration rates.

The initial infiltration rates were plotted over the time it takes before the 95% height of the steady state water table is reached in Figure 3.5.

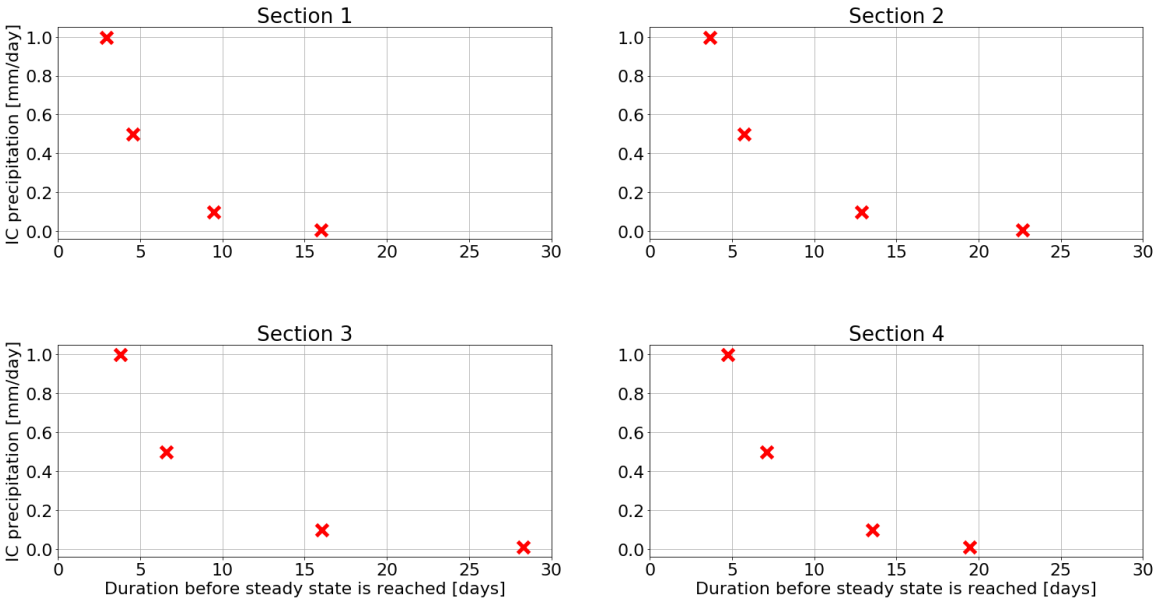

Figure 3.5: The duration before the 95% Steady state is reached along the four sections S1-S4 for the different initial infiltration rates.

The figures show that the relation between the initial precipitation flux and the time it takes before a steady state condition is reached is not linear. This is as expected, since the relation between hydraulic conductivity and water content is also highly non-linear. Comparing the figure with Figure 3.3, it is clear that the initial water content in the dike body has a larger influence on the result of the analysis than the initial water level in the river. Unfortunately, it is hard to determine the initial water content in the unsaturated zone, since it is heavily influenced through infiltration and evapotranspiration, processes that have a large natural variability. The initial water content in the unsaturated zone does not only have an influence on the rate at which the water table rises, it also affects the progression of the wetting front during infiltration. This will be elaborated on in section 3.5.

3.3 The high water wave

The high water wave in the river is an important boundary condition, with the two dominant characteristics the height of the peak of the wave and the total duration of the wave. The case study dike is situated along the river IJssel, which is a branch of the Rhine river. The statistics of the shape and peak height of the high water wave in the Rhine river have been extensively researched with models from GRADE, with the latest research to the shape and peak of flood waves in the Rhine river included in Chbab (2017). The height of the normative river level at the dike that is used for the design according to the Dutch standards is 13.64 m+NAP, which has on average a return period of approximately 10,000 year (see appendix D for a summary of the return periods and water levels at the case study dike). According to Chbab (2017), the number of days leading to the peak event and the number of days from the peak event until the water is lowered remains constant, independently of the peak height of the event. The median shape of a high water wave as well as the confidence intervals of the wave in the Rhine according to the latest research from grade is included in Figure 3.6.

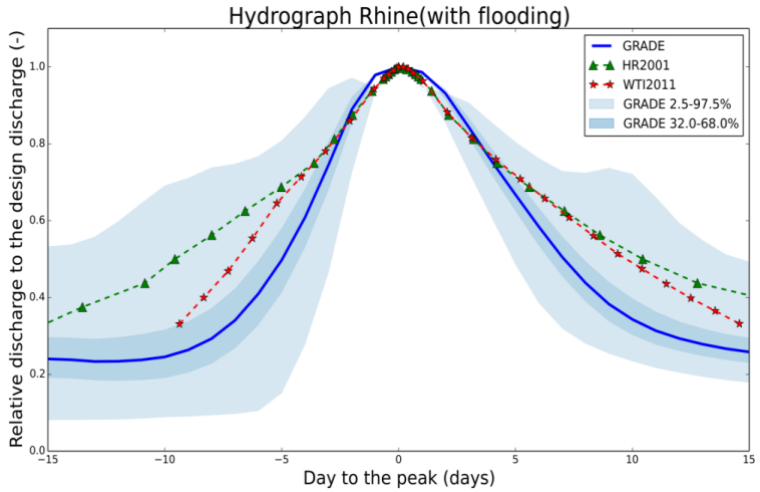

Figure 3.6: Shape of the discharge wave in the Rhine as calculated by GRADE (after Chbab (2017)).

The figure shows that there is little uncertainty regarding the duration of the peak event, while the rate at which the water rises does include uncertainty. Different rates of the rise and fall of the high water in the river were modelled with the objective to see how large the influence is on the final position of the water table (see Figure 3.7). In the analysis, the peak of the high water (13.64 m+NAP) and the initial water level (9.90 m+NAP) where kept constant to observe solely the influence of the rate at which the water rises (and falls) in the river. The parameters describing the properties of the soil layers were similar as in Table 3.1 and the initial surface flux was 0.1 mm/day for all analyses.

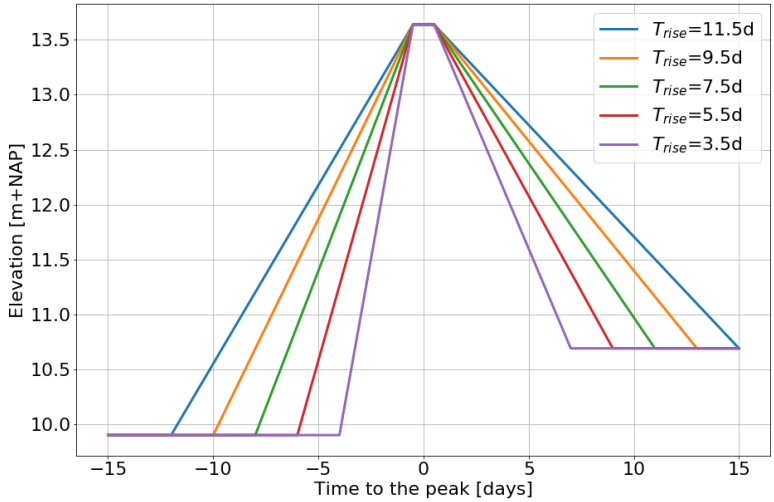

Figure 3.7: Shapes of the high water wave with varying rate of the rise and fall of the high water as used in the analyses.

The positions of the water table along the four sections after the start of the simulation are included in Figure 3.8 and show that a high water with a relatively slow rise results in a higher water table. This is as expected since the duration of the high water is longer, hence there is a large head difference for a longer time. The figures show that the difference of the maximum height of the water table between the simulations is especially large along section 1 and decreases along the sections that are situated more inland. The difference of the maximum height of the water table between the fastest and slowest rising water in the river is in the order of 1 meter along section 1, while this is smaller than 0.5 meter along section 4.

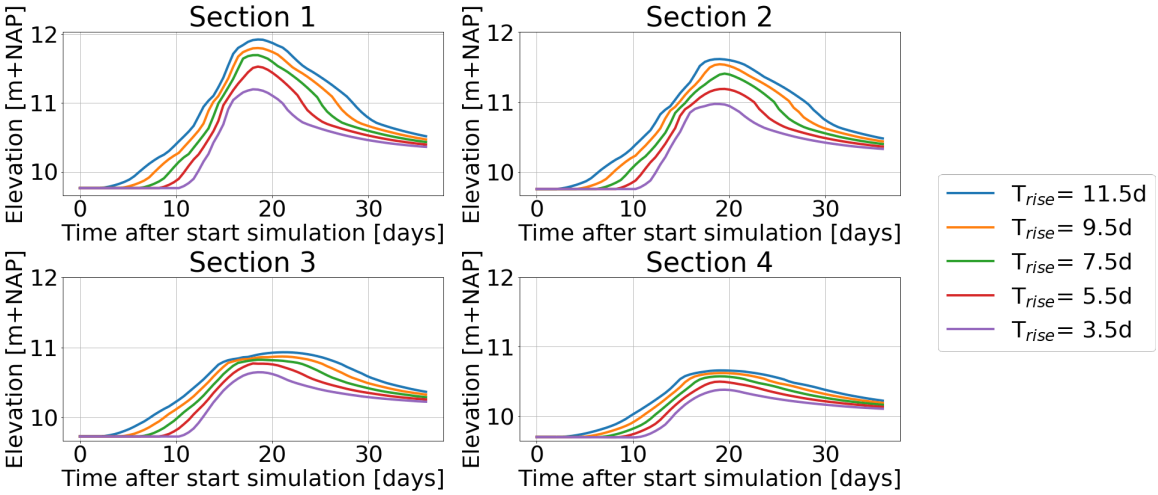

Figure 3.8: Height of the water table along sections S1 - S4 after the start the simulation with varying duration of the rise and fall of the high water, indicated by the duration of the rise of the water T_{rise}.

In the previous calculation, both the height of the peak and the initial water level in the river were kept constant at the situation of the normative event. However, since the interest of this report is to find the probability that suction remains over the cross section, it is interesting to see how sensitive the position of the water table is to the height of the river level with varying return periods, since suction in a dike might be lost due to a combination of a (high) river level and precipitation on the dike. For this reason, the highest probability of a situation where all suction is lost might be a situation with a river level lower than the normative event and hence a larger probability of occurrence. To observe the sensitivity of the position of the water table along the sections to the height of the river level with corresponding return period, statistics to the river levels at the case study dike are necessary, which can be determined with the discharges at Lobith and a stage-relation curve (included in Appendix D). Based on the return periods and discharges from GRADE and the stage-relation curve for the discharge at Lobtih and the river level near the dike, the peak river levels for the 1,250, 3,000 and 10,000 year return period were determined (Table 3.2). Both a river level for the median (50^{th} percentile) and the upper limit of the 95% confidence interval (the 97^{th} percentile) for the discharges at Lobtih were determined. Between the median of the 1,250 year return period and the median of the 10,000 year return period, there is only a difference in river level of 0.13 meters and between the 1,250 year median and the 10,000 year upper bound of the 95% confidence interval only 0.24 meters. It is expected that the differences in the position of the water table will also be marginal.

Table 3.2: Discharges at Lobith and river levels at the Lathumsedijk for varying return periods and percentiles of the confidence interval of the discharges.

Return period [year]	**Percentile**	**Discharge at Lobtih [m^3/s]**	**Water level at Lathumsedijk [m+NAP]**
1,250	50^{th}	14,970	13.40
1,250	97.5^{th}	16,230	13.52
3,000	50^{th}	15,520	13.45
3,000	97.5^{th}	16,980	13.60
10,000	50^{th}	16,270	13.53
10,000	97.5^{th}	18,100	13.64[2]

By using a schematized version of the median shape of the high water wave (Figure 3.6) and a duration of 1 day of the peak of the wave, the shapes of the high water wave were schematized and used as boundary condition (see Figure 3.9). The set-up of the analyses was, besides the shapes of the high water wave, similar to the analysis presented above. As an initial water level in the river, the river level before the start of the flood wave was used. The results of the analysis are included in Figure 3.10.

[2]The calculated height with linear extrapolation was slightly higher, but was adjusted to the height of the normative event

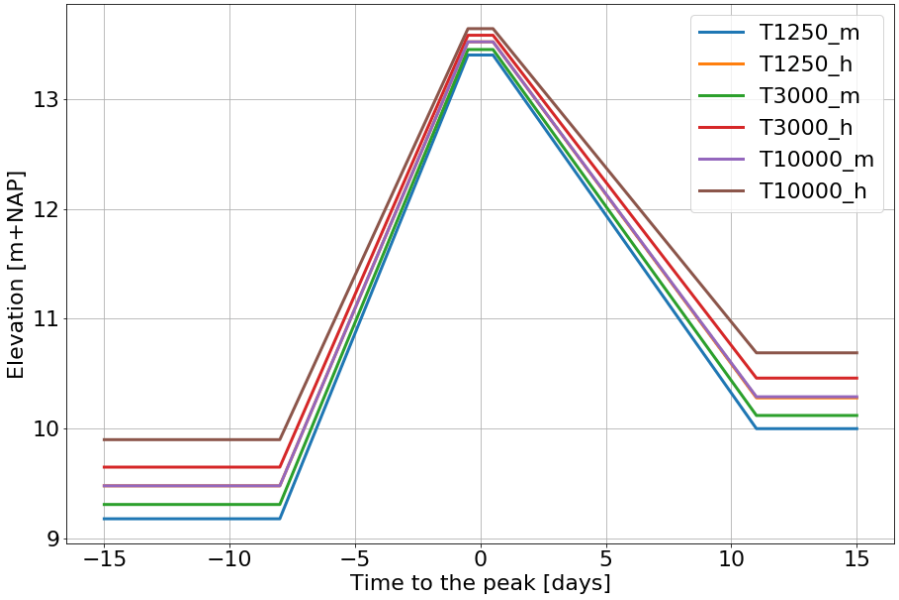

Figure 3.9: Schematized shapes of the flood wave at the case study dike with varying return periods for median scenarios (indicated with _m) and the upper 95% confidence interval (indicated with _h).

As expected, the figure shows that the differences between the height of the water table along the sections are small. Comparing the highest position of the water table during the high water, we see that along section 1 there is a difference of 0.6 meter between the 1,250 year median event and the 10,000 year upper bound of the 95% CI. This difference is more than the difference in maximum peak height, which can be explained by the higher initial river level. Following the advice of GRADE, the shape of the high water wave at Lobith is determined by taking the discharges relative to the design (peak) discharge for fixed numbers of days to the peak. Because of this, and the non-linear character of the stage-relation curve, the difference in water level before the flood event is larger than the difference in peak event. However, the difference is still not very large compared to the difference in return period.

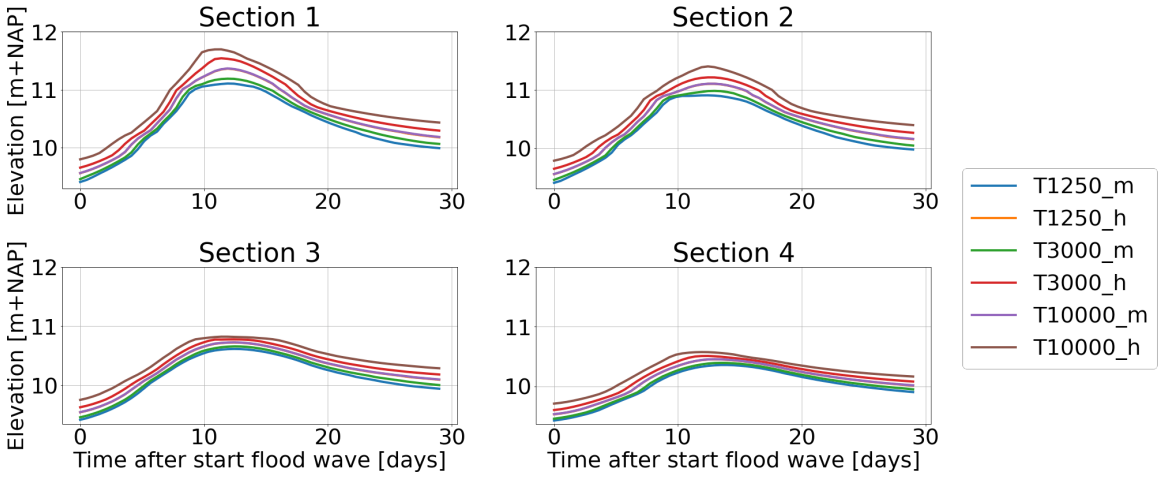

Figure 3.10: Water tables along the sections during high water waves in the river with varying return periods

3.4 Soil-specific parameters and variability

As mentioned in chapter 2.5, the Staring series can be used to estimate the parameters to determine the water retention curves and the hydraulic conductivity curves of different soils. However, the Staring series include average parameters of natural and agricultural soils and should be used with care when applied to seepage analyses. Moreover, it is not possible to determine with the information of a CPT or boring exactly what type

of soil is in the subsurface. For example: it is clear that there is a clay layer present from approximately 7.00 - 13.00 m+NAP (in the crest), but it is not clear if this is light, medium or heavy clay (which can be described with Staring series types B10 - B12). The use of these parameters is thus accompanied with a large uncertainty. It is therefore important to observe the extent of the effect of the chosen properties of the soil layers. The soil types can have an influence on both the progression of the water table as on the progression of the wetting front after infiltration (included in section 3.5). The analysis include the influence of the soil type for the cracked top layer and for the clay core of the dike. The influence of the aquifer and the sandy clay layer at 7.00 m+NAP were not included since the influence of these layers on suction in the dike will be minimum. First, the effect of the soil layer type of the cracked layer was examined. The cracked layer is a clay layer with some sand, cracks and other structures in it. It can be best described as a sandy clay layer, which corresponds to Staring series B07 - B09. The clay core of the dike is best described by Staring series B10 - B12. As mentioned in section 2.5, the saturated hydraulic conductivity in the Staring series itself includes uncertainty. For that reason, the influence of the saturated hydraulic conductivity of the clay core of the dike was also included in the analysis. This was done by setting up a calculation with a clay core with type B10, but with a hydraulic conductivity equal to 0.1 and 10 times the saturated hydraulic conductivity as included in the Staringseries.

The cracked clay layer

First, the sensitivity of the model to the characteristics of the cracked layer was observed. This was done by setting up the model with similar soil properties as in 3.1, but with a varying cracked layer between B07 - B09. The characteristics of the Staring series types B07 - B09 are included in Table 3.3. The parameter λ is not included in the table since it was set to 0.5 for all analyses (see section 2.5).

Table 3.3: Soil-specific parameters used in the analyses for the cracked clay layer from the Staring series (Heinen et al., 2020).

Staringseries number	θ_r **[-]**	θ_s **[-]**	α **[1/cm]**	**n [-]**	K_s **[cm/day]**
Cracked layer					
B07	0.0	0.401	0.0183	1.248	14.58
B08	0.01	0.433	0.0105	1.278	3.00
B09	0.0	0.430	0.007	1.267	1.75

The water retention curve and hydraulic conductivity for the soil types in Table 3.3 are included in Figure 3.11.

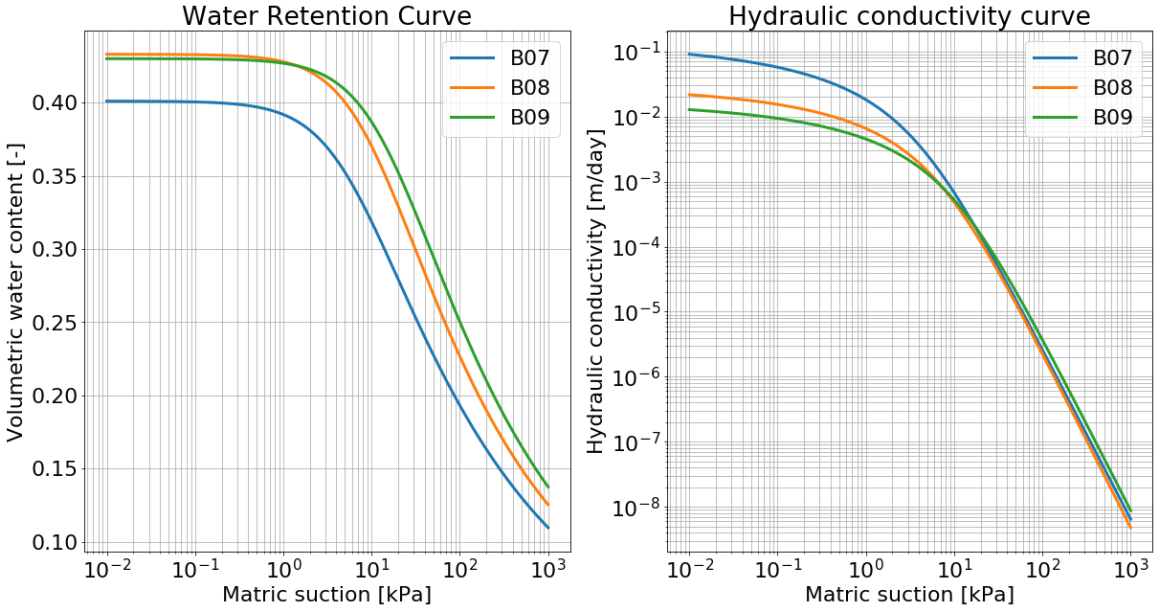

Figure 3.11: Water retention curves and hydraulic conductivity curves for sandy clay soil types from the Staring series, ranging from very sandy to slightly sandy (B07 - B09).

The inititial river stage was 7 m+NAP and the intitial surface flux was 0.1 mm/day. After the initial condition (day 1) the water level in the river was heightened in one step to 13.64 m+NAP and the polder level was heightened to 9.5 m+NAP. The rise of the phreatic surface over time along sections S1-S4 was observed for the three calculations. The results are included in Figure 3.12.

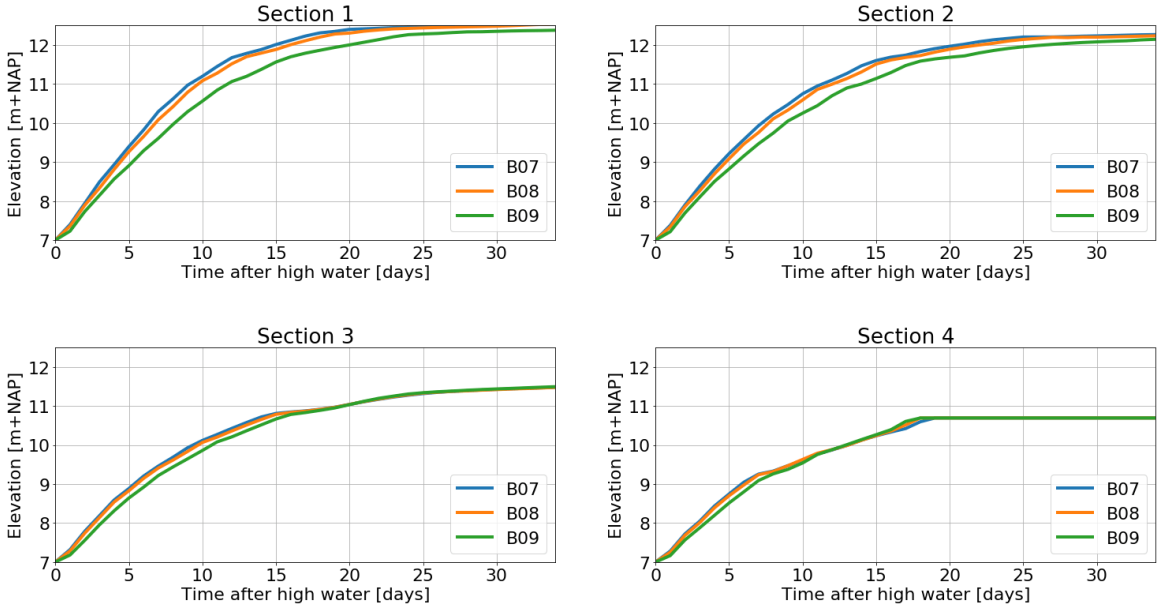

Figure 3.12: The height of the water table over time along the four sections S1-S4 for varying characteristics of the cracked clay layer.

The figure shows that the water table rises fastest when the cracked layer has the properties of the B07 (very sandy) clay type. Of the three included soil types, this is the one with the highest saturated hydraulic conductivity. It is therefore not surprising that the water table will rise faster: a higher hydraulic conductivity results in a larger flow of water, following Darcy's law. Observing the hydraulic conductivity curves in Figure 3.11, it can be seen that for high suction, the hydraulic conductivity of the three soil types is approximately similar, but that for lower suction (up to 10 kPa), B07 will have a higher hydraulic conductivity for a similar suction. Since suction in the dike body for this situation will be in the order of meters, this is in line with what is observed. Overall, the effect of the soil properties of the cracked layer is marginal.

The clay core

An analysis with similar initial and boundary conditions as in the previous analysis for the cracked layer was done. Again, the soil properties as in as in Table 3.1 were used, but now with varying properties for the clay core of the dike, ranging from B10-B12 and the B10 properties with altered saturated hydraulic conductivity. The soil-specific parameters used in the analyses are included in Table 3.4.

Table 3.4: Soil-specific parameters used in the analyses for the clay core of the dike from the Staring series (Heinen et al., 2020).

Staringseries number	θ_r **[-]**	θ_s **[-]**	α **[1/cm]**	**n [-]**	K_s **[cm/day]**
Clay layer					
B10	0.01	0.448	0.0128	1.135	3.83
B10 with $0.1K_s$	0.01	0.448	0.0128	1.135	0.383
B10 with $10K_s$	0.01	0.448	0.0128	1.135	38.3
B11	0.01	0.591	0.0216	1.107	6.31
B12	0.01	0.530	0.0166	1.091	2.25

The water retention curve and hydraulic conductivity curve for the soil types included in Table 3.4 are included in Figure 3.13.

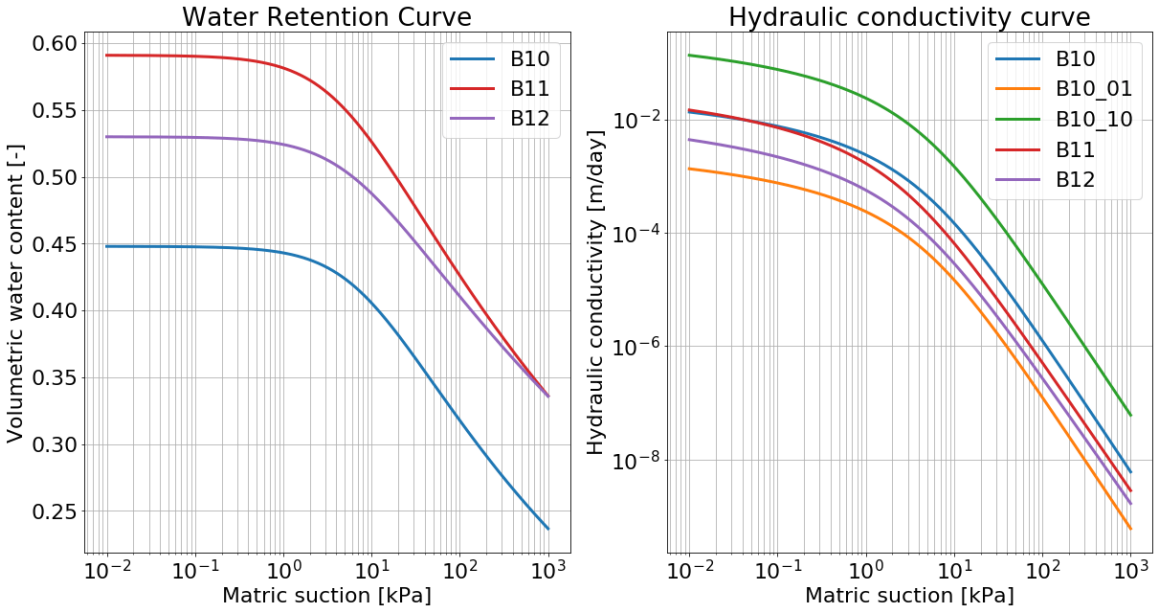

Figure 3.13: Water retention curve and hydraulic conductivity curves of Staringseries for clay soils ranging from light clay to heavy clay (B10 - B12), with an altered K_s for clay B10.

In total, this resulted in 5 analyses to observe the effect of the soil properties of the clay core on the progression of the water table along the four sections S1-S4. The results are included in Figure 3.14.

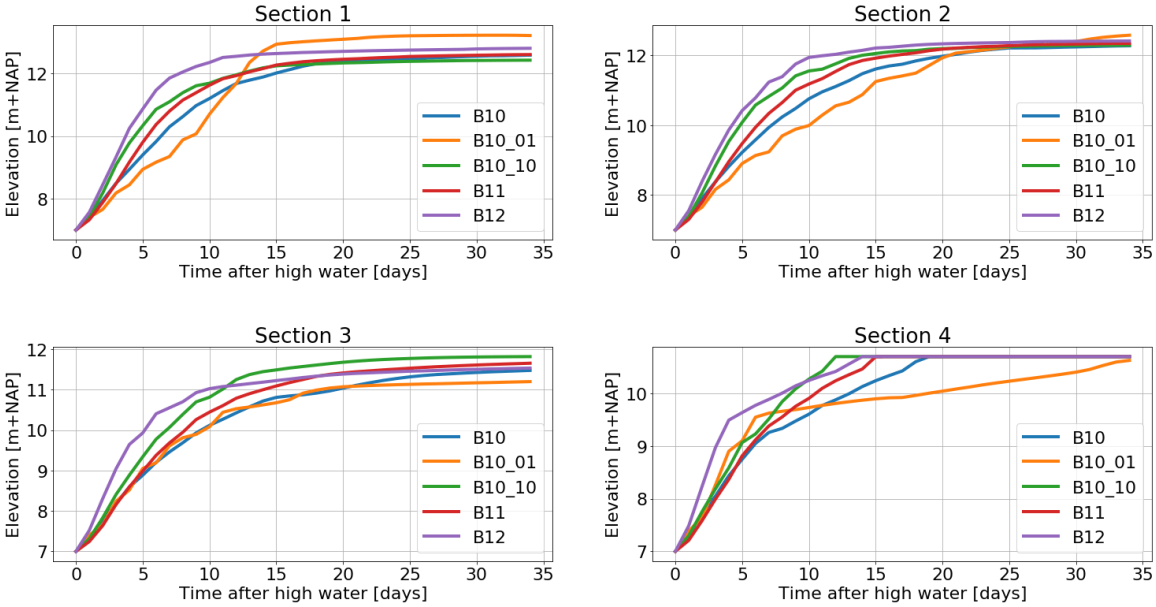

Figure 3.14: The height of the water table over time along the four sections S1-S4 during a high water event for varying characteristics of the clay core.

Observing this figure, a few things stand out. First of all, the scenario that results in the fastest rise of the water table after the start of the analysis is the scenario with clay properties of staring series B12. The hydraulic conductivity curves in Figure 3.13, show that B12 has the second lowest hydraulic conductivity for a similar suction between 0.01 and 1000 kPa, with only clay type B10_01 that has a lower hydraulic conductivity. While this is not as expected, it can be explained. The analyses were performed with an initial condition that included 0.1 mm rain and an initial water level of 7 m+NAP. This steady state initial condition will result in a similar initial water table for the five scenarios, however the initial pore pressure distribution in the vadose zone will vary. This can be observed when looking at the initial pressure heads along section 1 (included in Figure 3.15).

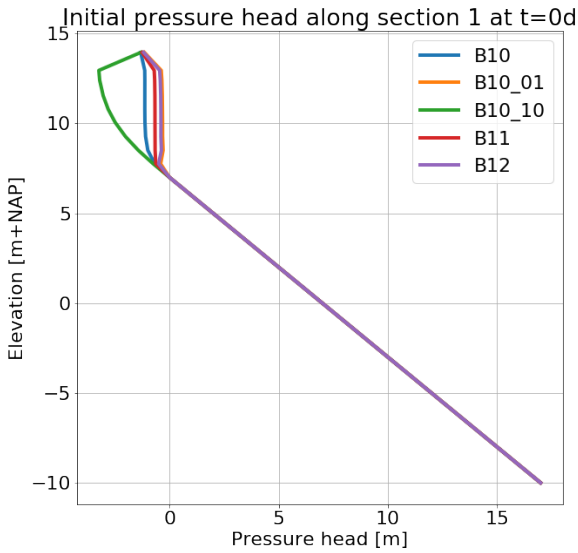

Figure 3.15: Initial pressure head along section 1 at t=0 for the five calculations with a varying clay core.

The figure shows that the initial pressure head distribution for the five scenarios varies in the vadose zone, due to the initial infiltration. Clay types B10_01 and B12 result in the least suction at t=0 and thus will have a higher saturation. Not only will less suction result in a higher hydraulic conductivity, a soil that has a higher effective saturation needs less water to fill up and be fully saturated. Figure 3.14 shows that the rise of the water table along section 1 and 2 is slowest for clay type B10_01 in the first days after the start of the calculation. This can be attributed to the lower saturated hydraulic conductivity. Hence, it can be concluded that it depends both on the saturated hydraulic conductivity and the shape of the water retention curve as on the initial saturation of the dike how fast the water table in a dike body will rise. To verify that indeed these processes are the reason for the varying results, a verification calculation was done with no initial infiltration. This will result in an initially linear pressure head in the unsaturated zone and hence with respect to the pressure head, a similar initial condition for the five scenarios. The results and interpretations of the calculation are included in appendix E.

Overall, it can be concluded that the soil-specific parameters of the clay layer can have a large influence on the position of the water table during a high water event. After a few days of high water, the difference between the heights of the phreatic surfaces can already be a few meters along section 1 and 2 depending on the chosen parameters (see Figure 3.14). Both the saturated hydraulic conductivity and the initial saturation contribute in this. In this calculation a steady state infiltration rate of 0.1 mm/day was used to calculate the initial saturation of the dike body. This raises the question what initial saturation can be expected in the dike cross section.

3.5 Infiltration in a 1D soil column

The analyses in the previous sections showed that seepage through a clay dike body is not straight forward and that there are numerous important influencing factors. The thusfar presented analyses suggest that especially the initial saturation of the dike body has a large influence on the progression of the water table. Moreover, the initial saturation also effects which soil type will result in the fastest rise of the water table. It is therefore not possible to select a soil type, or a specific soil property that will result in the governing situation with respect to the progression of the water table. Considering that the initial saturation is in reality a result of the weather and river level influences that the dike was subjected to, the 'initial saturation' will vary over the year. In this section, the influence of precipitation on suction in a 1D soil column is observed with different initial and boundary conditions. The analyses presented in this section were performed with the 1D model SWAP.

Soil layer characteristics

The analyses in section 3.4 showed that the chosen soil types for the cracked clay layer and the clay core influence the effect of precipitation on matric suction. In the analyses it was found that when a steady state initial condition with a non-zero surface flux is used, the chosen unsaturated properties have a large effect on what that means as an initial saturation and hence on the matric suction. What the analyses did not show is how heavy rain and the chosen soil profiles are connected. This subsection shows how the chosen Staring series profile for the cracked top layer and the clay core influence the maximum pressure head in a 1D soil column during

and after infiltration. The analyses were done with three different initial pressure heads and three different precipitation intensities.

The cracked clay layer

First, the effect of the chosen soil properties of the cracked clay layer was observed. A 1D soil column was considered with a height of 5 meters and the initial water table at 4 meters below Ground Surface (GS). The properties of the clay core were fixed as a B10 Staring profile. An analysis was done with three different initial conditions and three different intensities of precipitation. By varying the properties of the cracked layer between a B07, B08 and B09 Staring profile, this resulted in 27 analyses, in which the effect of evapotranspiration was not included. An overview of the varying boundary conditions (BC) and initial conditions (IC) is included in Figure 3.16. Three different combinations of precipitation intensity and duration were applied as the upper boundary condition, after which the model ran until day 90 after the start of the simulation (see Figure 3.17). The total precipitation was kept constant at 30 mm.

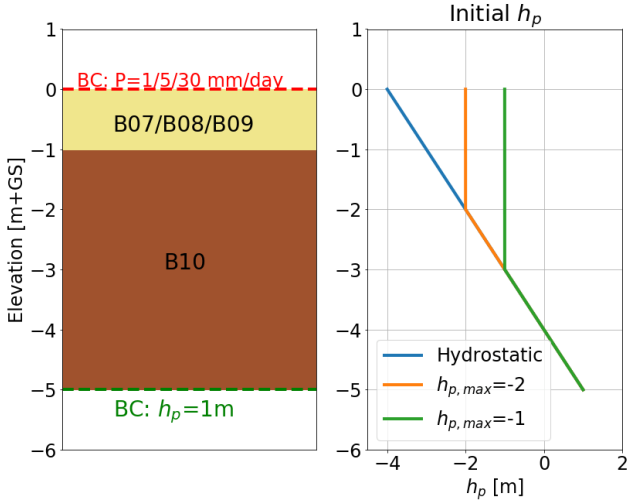

Figure 3.16: Set up of the analyses of the cracked layer including the boundary- and initial conditions.

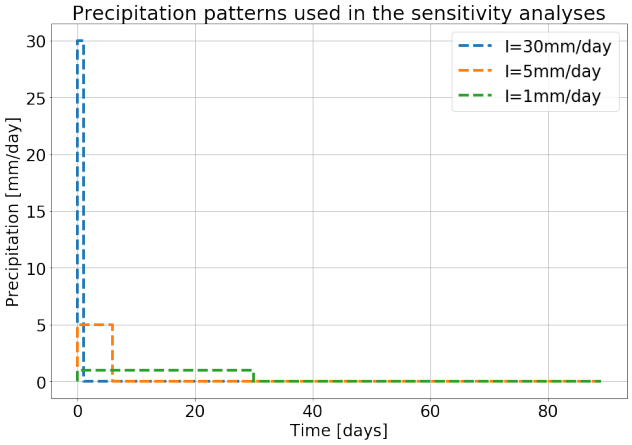

Figure 3.17: Precipitation over time used as the top boundary condition.

The results of the analysis were plotted by selecting the maximum pressure head during the entire simulation for every height (an envelope of all results). The results of the analyses with a hydrostatic initial condition, a maximum initial pressure head of -2 and -1 meter are included in Figure 3.18a, 3.18b and 3.18c respectively.

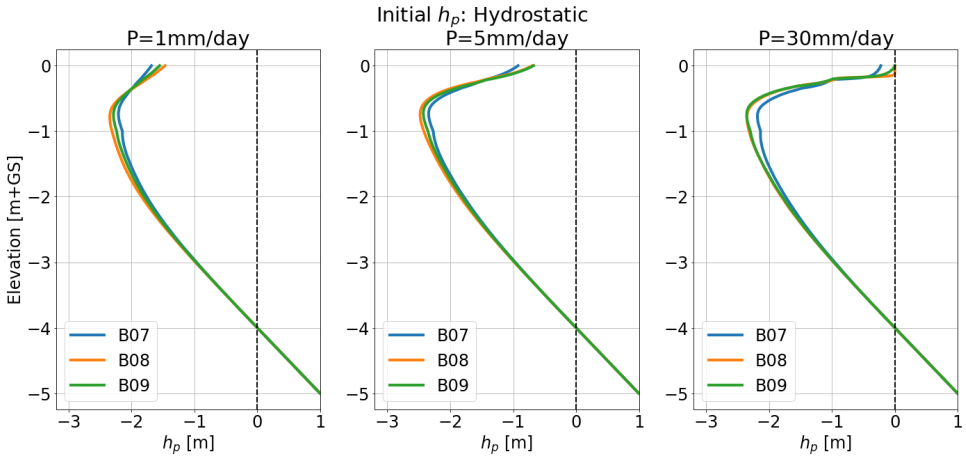

(a)

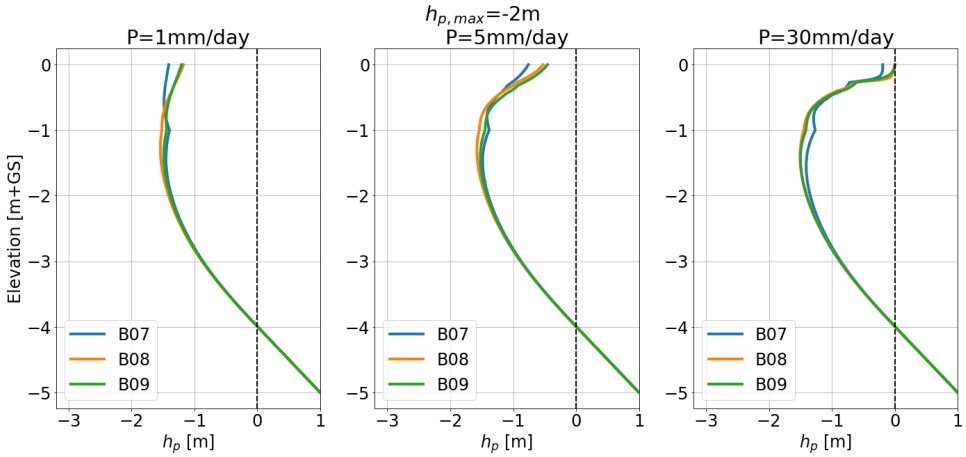

(b)

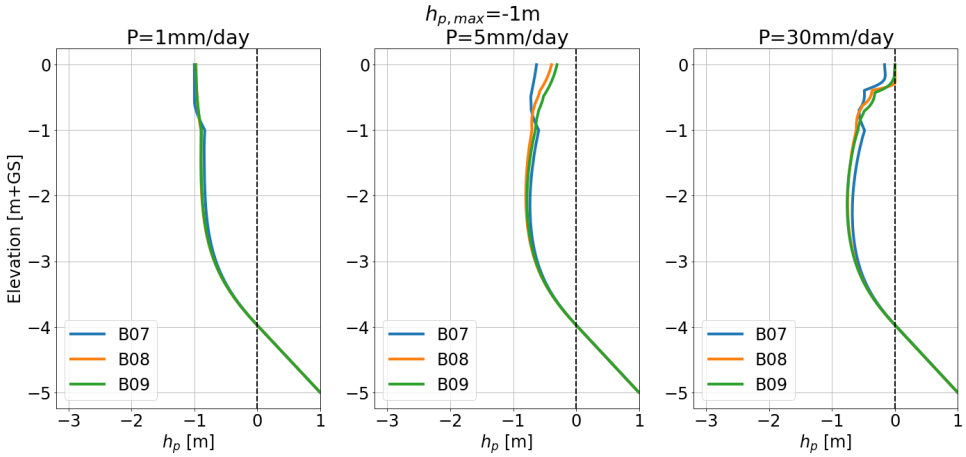

(c)

Figure 3.18: The maximum pressure head in a 1D soil column with a cracked layer with soil properties B7, B8, B9 after infiltration of varying intensities and duration with a hydrostatic pressure head (a), a maximum pressure head of -2m (b) and a maximum pressure head of -1m (c) as initial condition.

The figures show that profile B07 results in the lowest pressure heads in the upper part of the cracked layer, while it results in the highest pressure head in the lower parts of the soil column for every combination of initial and boundary conditions that were used in the analyses. It is relatively straightforward why the soil profile with the highest hydraulic conductivity results in the smallest wetting front: water can flow more easily through a soil with a higher conductivity which results in a smaller wetting front. While the water can flow relatively

easy through the cracked layer, when it reaches the clay core layer there is a lower conductivity and the water will stagnate. The profile B07 (with the highest K_s), has the largest difference with the clay layer (with type B10). As a result the pressure head in the clay core will be largest for a cracked layer with type B07. Moreover, the time it takes for the water to seep from the cracked layer into the clay layer is longer. As a result, the pore pressures are high for a longer duration, making the soil column more prone to saturate in the case of a subsequent precipitation event. Nevertheless, the differences between the results of the varying properties of the cracked layer are marginal.

The clay core and infiltration

A similar analysis as for the cracked clay layer was done for the soil properties of the clay core of the dike. The chosen soil properties of the cracked layer were fixed in this analysis, while the properties of the clay core varied over the types as given in Table 3.4. The set up of the analysis is presented in Figure 3.19 and the precipitation patterns used are similar as in Figure 3.17.

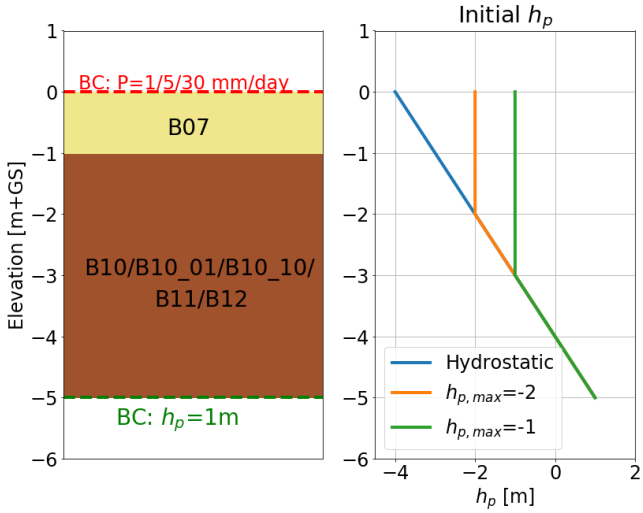

Figure 3.19: Set up of the analyses of the clay core layer including the boundary- and initial conditions.

The results are presented in the following figures, where the maximum pressure head during the simulation is plotted over the depth. The figures show that the chosen properties for the clay core have a larger influence on the maximum pressure heads as compared to the cracked clay layer. The soil profile with profile B10 and a 10 times larges K_s, results in the lowest pressure heads for all cases. Since the K_s is larger than the K_s of the cracked layer, the water can flow easily into the clay core. On the contrary, the soil types with a lower K_s than the cracked layer (all but B10_10), result in an increase of the pressure head 1 meter below ground surface. The water that flows through the cracked layer will stagnate when it reaches the clay core layer with a smaller K_s. The water content increases in the lower part of the cracked layer, increasing similarly the pressure head. This effect is largest for the profile with the smallest K_s, which is B10 profile with a decrease K_s by a factor 10. This results in the most suction loss over the profile. Note that at the end of the simulation (simulation time was a period of 30 days), the pore pressures in the profiles were still much higher than the starting values, for all initial conditions. As a result, when a subsequent rainfall event occurs, the soil profile will saturate much faster (similar to the effect of the initial pressure head). The figures suggest that the profile with Staring series type B10 and a reduced saturated conductivity and type B12 results in the most suction loss for the presented situations.

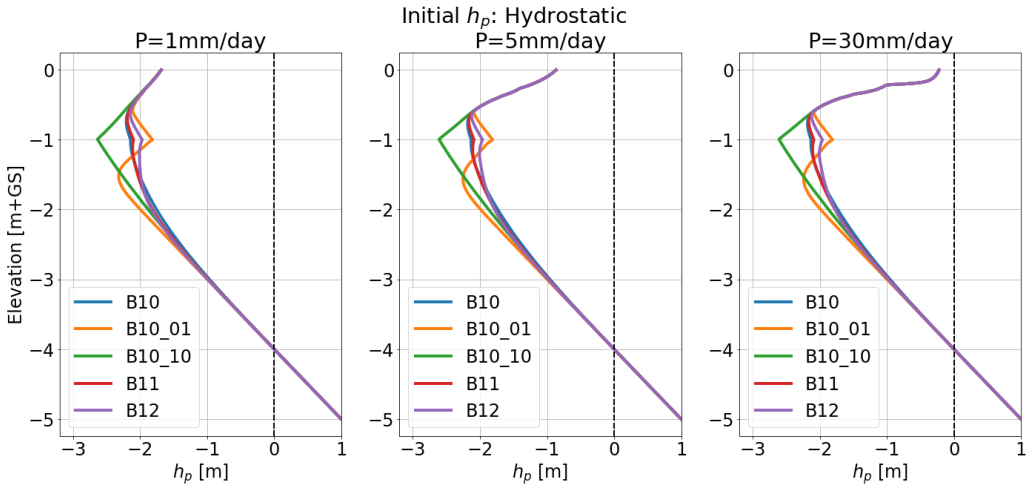

(a)

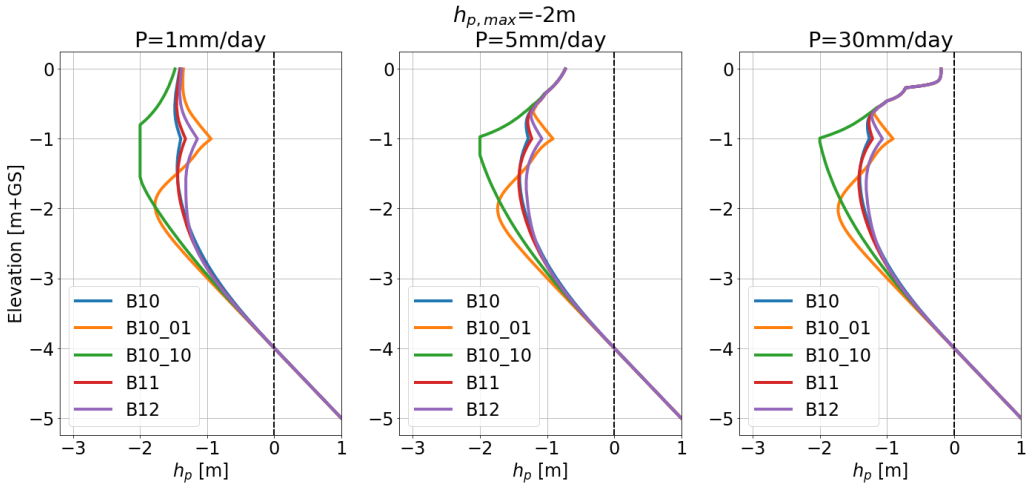

(b)

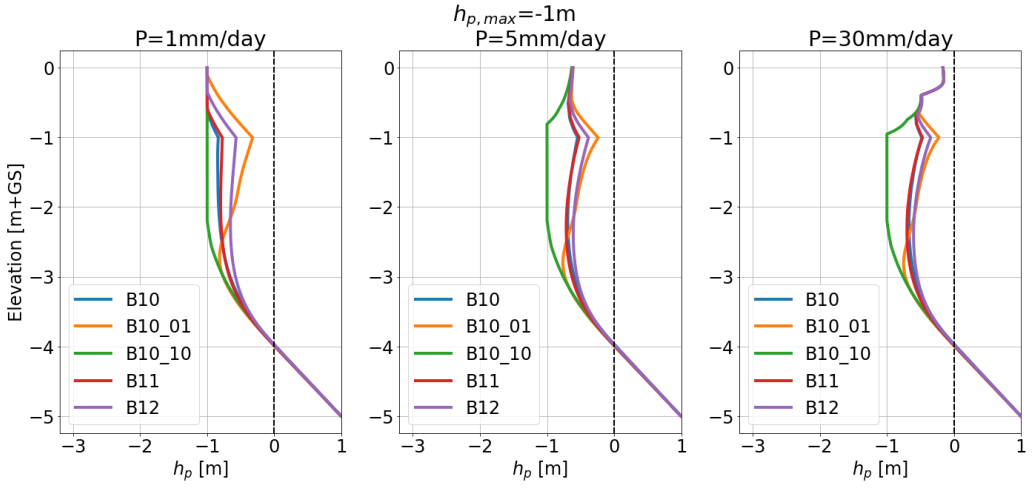

(c)

Figure 3.20: The maximum pressure head in a 1D soil column with a clay core with soil properties varying between B10, B10 with $0.1 \cdot K_s$, B10 with $10 \cdot K_s$, B11 and B12 after infiltration of varying intensities and duration with a hydrostatic pressure head (a), a maximum pressure head of -2m (b) and a maximum pressure head of -1m (c) as initial condition.

The results presented above make a comparison possible between the profiles for similar initial pressure head

profiles as distribution. However, the differences in pressure heads in the profiles after precipitation, raise the question whether this similar initial condition is valid. Putting this in real-life context; the pressure head in a clay dike before a certain (extreme) event occurs is a direct result of the recent precipitation and water table variations. Since the effect of the precipitation (and water table variations) are in turn dependent on the soil properties of that same dike, the pressure head distribution before an event of interest is also dependent on this and will not be the same for the different soil profiles (also shown in Figure 3.15). This means that the actual difference in pressure head between the soil profiles will thus be larger than presented in Figure 3.20.
Moreover, the figures show that different combinations of initial pressure head and infiltration event result in a decrease in suction (in an increase in the pressure head). As a result, there is not one combination of duration and intensity that will result in a large decrease of suction, this is always a combination of the precipitation and the pressure head before precipitation.

Influence of the bottom boundary condition

The boundary condition at the bottom of the soil column is set as a Dirichlet type boundary condition, which is determined by the initial height of the water table. The previous sections have showed that the height of the water table is determined by the river stage and that this varies between 7.00 m+NAP during daily conditions and 13.64 m+NAP during the normative event with a return period of approximately 10,000 years. As a result, the height of the unsaturated zone in the case study dike is generally somewhere between 0 and 7 meters. To observe the influence of the initial height of the unsaturated zone, a simple analysis of infiltration in a 1D soil column of 7 meter height with varying boundary condition was performed. The soil properties of the cracked and clay layer were Staring type B07 and B12 respectively and a the soil column was subjected to a 10 day precipitation event with an intensity of 10 mm/day. The analysis was done for situations with the initial water table 3, 4, 5 and 6 meter below ground surface and a maximum (negative) initial pressure head of -1 meter (see Figure 3.21a). The results (Figure 3.21b) show that the bottom boundary condition does not influence the shape of the wetting front at the top of the soil column. However, the first infiltration will reach a higher situated water table faster, resulting in a larger water table increase.

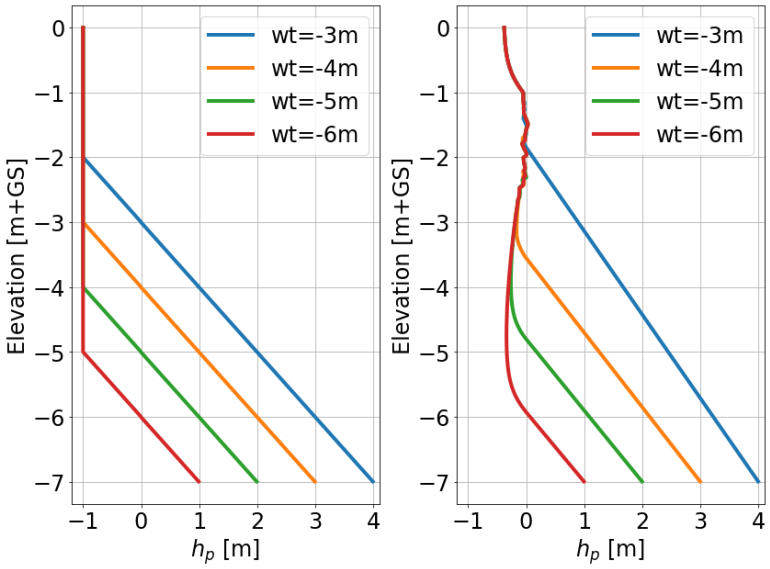

(a) Initial condition (b) Maximum pressure head

Figure 3.21: Initial condition and results for the analysis of the influence of the height of the water table on the pressure head after infiltration

3.6 The influence of precipitation

Figure 3.20 showed that different combinations of initial pressure head and precipitation result in a decrease in suction over the soil column. In these analyses, evapotranspiration was not specifically included (although one could argue that a combination of precipitation and evapotranspiration is included by setting an initial pressure head). Moreover, the analyses all included synthetic data for precipitation with constant infiltration rates per day for a specified duration. Naturally, in reality precipitation varies in time and is influenced by the seasons.

To find what type of precipitation events lead to the loss of soil suction, two analyses were done with historic daily meteorological data that cover a duration of 37 years (described in section 3.6). The first analysis was done by defining a 1D soil column in SWAP with a height of 5 meter and two layers. The top layer, representing the cracked layer, was characterized with soil properties similar to Staring series type B07 and a height of 1 meter. The bottom layer (4m high) was characterized by Staring series type B12. As an initial condition, a hydrostatic pressure distribution was chosen with an initial water table at a height 4 meters below the ground surface (see Figure 3.22). This chosen initial condition will influence the first few weeks or months of the analysis and will likely result in an overestimation of the amount of suction in the upper part of the soil column. However, since the data set is long, the effect of the initial condition decreases over time until it has no influence on the results. The bottom boundary condition was set to have a constant pressure head of 1 meter. This schematization represents a situation at the case study dike with a river level of 10.00+NAP in the river for a relatively long time, which happens on average approximately once per year. The second analysis was similar to the first analysis, with the only varying parameters the height of the second layer (7 meter) and the initial water table, which was 7 meters below the Ground Surface (GS). A water table that is 7 meters below ground surface corresponds to a section in the crest when the river level is at 7m+NAP, which can be seen as the daily water level during summer in the river. An overview of the set-up of the two analyses, their initial and boundary conditions is presented in the figure below.

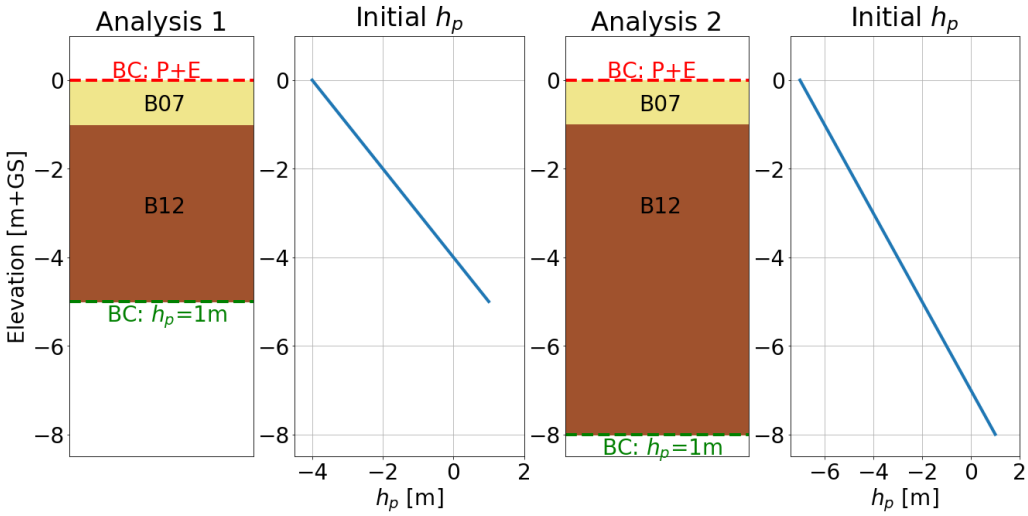

Figure 3.22: Schematization of the top and bottom boundary conditions (BC) and initial conditions used in the analyses 1 (left) and 2 (right). In this figure, P is the precipitation and E is evapotranspiration.

For the top boundary condition of the two soil columns the weather data from the dataset were used, which was translated to infiltration and evapotranspiration rates by SWAP. While translating precipitation (P) to infiltration in a soil column is rather straightforward, calculating the evapotranspiration (E) flux is not. An overview of the methods used by SWAP to compute evapotranspiration and the assumptions that were made in the analysis are included in appendix C.

Description of the data

The dataset that was used in the analyses consist of daily meteorological data form January 1980 until December 2016. The data were collected by the KNMI at the meteorological station in De Bilt, situated 60 km from the case study dike, where similar weather conditions can be expected. The data consist of daily data regarding solar radiation, minimum and maximum air temperature, wind speed, rain (mm/day) and humidity. An overview of the monthly and annual rain statistics is given in Table 3.5 and the average precipitation and number of rainy days per month are plotted in Figure 3.23. The figure shows that on average July is the wettest month of the year, while there are relatively few rainy days, indicating days with intense rainfall. January, November and December have on average most rainy days.

Table 3.5: Monthly and annual statistics for precipitation means, extremes, average number of rain days and maximum precipitation in one day in De Bilt (The Netherlands) for the period 1980 - 2016

Month	**Mean [mm]**	**Max [mm]**	**Min [mm]**	**Days $\geq$ 1 mm**	**Max per day [mm]**
January	72	133	4	18	30
February	56	139	0	15	25
March	62	134	11	16	35
April	42	97	0	13	34
May	61	138	5.6	14	41
June	68	181	18	14	50
July	86	179	15	15	59
August	76	180	6	15	51
September	75	211	9	14	44
October	83	188	20	16	64
November	79	148	11	18	46
December	78	169	17	18	37.1
Annual	838.9	1240	576	185	64

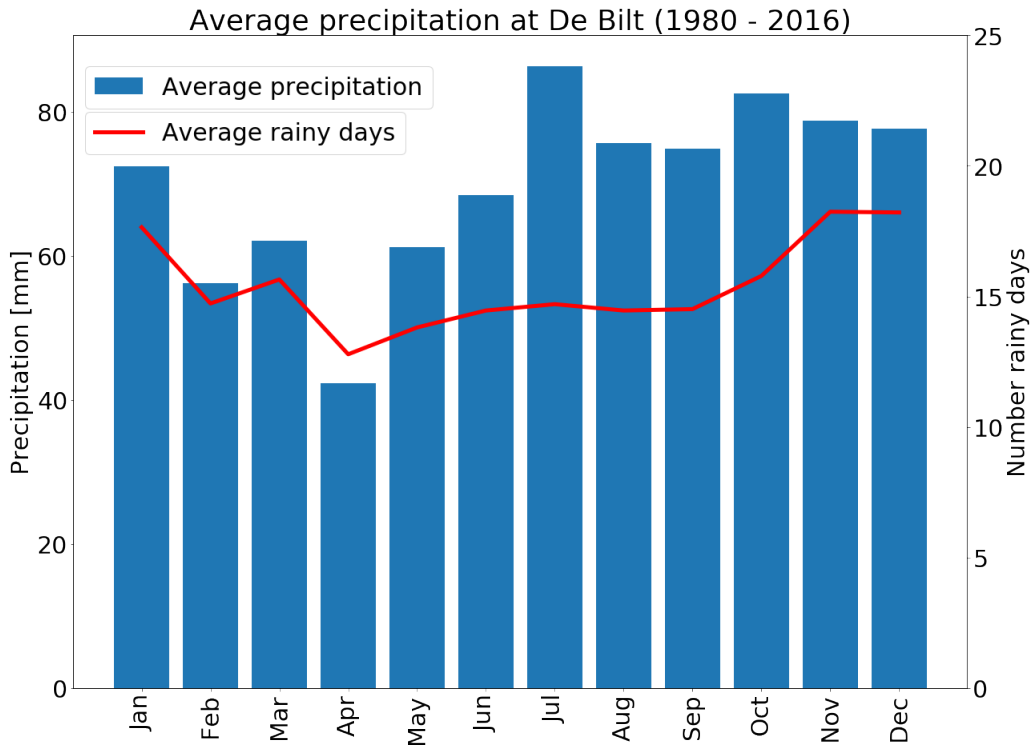

Figure 3.23: Average precipitation and number of rainy days per month recorded at the meteorological station De Bilt between 1980 and 2016.

Methods used for analyzing the data

The goal of the analyses was to find the events that have led to full saturation of the soil columns, where full saturation is assumed when $h_p \geq 0$m. The analyses were performed by taking the following steps:

- With the boundary and initial conditions as described above, the two analyses were performed with SWAP with a duration of 37 years.
- The days where $h_p \geq 0m$ at a depth -1.005 m+GS, -1.505 m+GS and -2.005 m+GS were selected. Multiple depths were used to ensure that all days where a wetting front with a pressure head larger than 0 meter infiltrated the clay column were found. When subsequent days resulted in $h_p \geq 0m$, only the first day

was selected, as it was assumed that this was the result of the same extreme weather event. A distance between the events of four days was used.

- For all the events, a plot was made of the precipitation a week previous to the first day where $h_p > 0m$.
- For all the events, the pressure head was plotted over the depth of the column for the dates corresponding to a week previous to the event until two weeks after the event.

From the analyses it followed that there were 8 events that led to saturation of the soil column at a depth between -1.005 and -2.005 m+GS (see Table 3.6). However, this does not necessarily mean that the entire soil column was saturated after the event. With the plots that were made of the pressure head over the depth of the soil column, it was determined whether the event led to full saturation of the soil column. All plots of the pressure heads and the precipitation corresponding to the 8 events are included in Appendix F.

Table 3.6: Summary of the precipitation events that led to saturation of the soil columns of the two analyses at a depth between -1.005 and -2.005 m+GS.

Event number	**First day of saturation**	**Season**	**Saturation of entire soil column WT = -4m**	**Saturation of entire soil column WT=-7m**
1	1981-03-13	Winter	Yes	No
2	1994-01-01	Winter	Yes	No
3	1994-12-30	Winter	Yes	No
4	1998-03-09	Winter	No	No
5	1998-10-30	Autumn	Yes	Yes
6	1998-11-03	Autumn	Yes	Yes
7	2003-01-04	Winter	No	No
8	2004-01-21	Winter	No	No

Since events 5 and 6 took place right after each other, they are considered one event from here. The results show that during the simulation there were 4 and 1 events that led to a fully saturated soil column for the situation with the water table -4.0 and -7.0 m+GS respectively. Moreover, all the events took place during autumn or winter. In appendix F, a full overview of the precipitation intensities and daily pressure heads in the column is presented, together with the analysis of the results. It is noted that even though events 1,2 and 3 did not result in full saturation of the entire soil column in analysis 2, the pressure heads were very close to 0m (in the order of -0.1m) in the entire column. The conditions that led to the suction loss in events 1,2,3 and 5/6 are summarized in Table 3.7. For most cases, saturation occurred after consecutive days of rainfall and the average precipitation rate is also included in the table.

Table 3.7: Summary of the conditions previous to the events that led to saturation of the entire soil columns.

Event number	**Description of rain**	**Total precipitation [mm]**	**Days of precipitation**	**Average precipitation [mm/day]**	**Initial h_p [m]**
1	3 days medium-high	67.5	3	22.5	-0.5
2	1 peak	34.3	1	34.3	-0.1
3	1 peak + 2 days medium	59	3	19.6	-0.3
5 + 6	13 days rain	183.7	13	14.1	-0.2

Since the results of the analyses suggest a strong correlation with the seasons, a plot was made that included all daily precipitation records with an intensity $\geq$ 20 [mm/day] and the 8 high intensity events that resulted in the full saturation of the soil column. The plot is included in Figure 3.24 and shows that, while there are relatively many high intensity daily rainfall events during the summer months, those events do not result in the saturation of the soil columns.

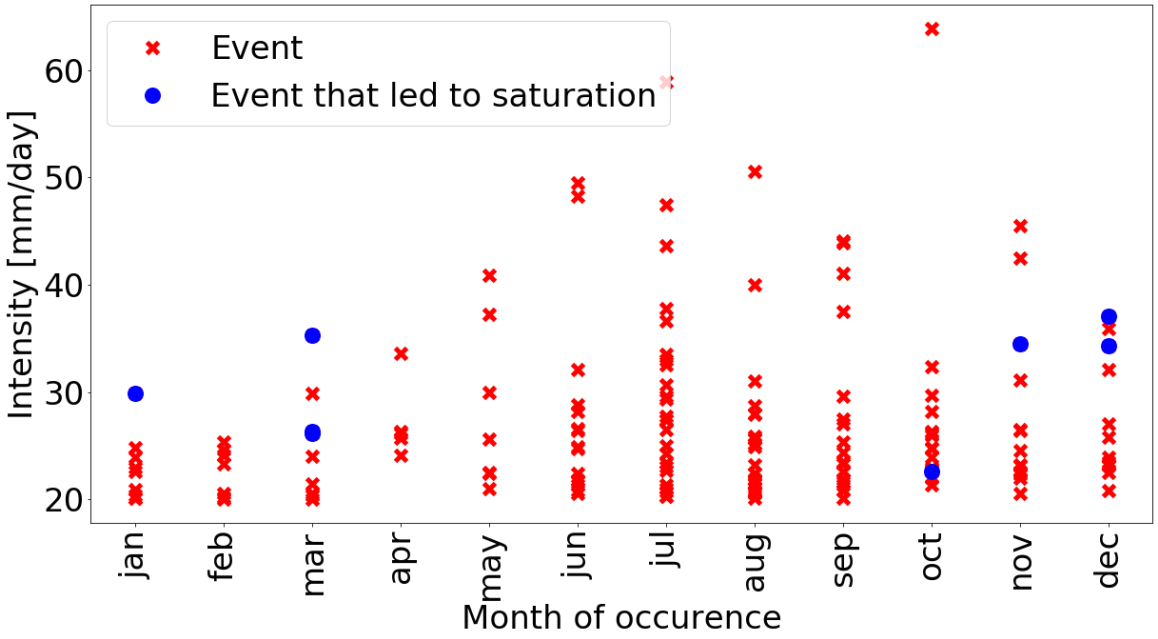

Figure 3.24: Daily precipitation events $\geq$ 20mm/day recorded at meteorological station De Bilt from 1980-2016 sorted by the month of occurrence and whether or not it resulted in saturation at a depth between 1 and 2 meter below the ground surface.

The results of this analysis raise the question whether averaging of rainfall over the days results in similar results when compared to the results of the actual data. In section 4.2, intensity, duration, frequency curves are presented that provide information on the frequency of a precipitation depth with a given duration, which can be translated to an average intensity per day. However, this is not seen in reality. Take for example the situation of event 5/6. Over a duration of 13 days the total precipitation depth was 184 mm, resulting in an average intensity of 14.1 mm/day. The measured and averaged precipitation per day are included in Figure 3.25 and show that there are many peaks that deviate a lot from the average. To see what the influence is of averaging the total precipitation over the duration, one more analysis was done with the set-up of analysis 2 (see Figure 3.22) for the year 1998. The meteorological data file was altered by changing the rainfall depths of the 13 days to the average daily rainfall of 14.1 mm. A schematized version of the pressure head on 31 December 1997 was used as the initial condition for the analysis (see Figure 3.26), since this was the day before the start of the simulation.

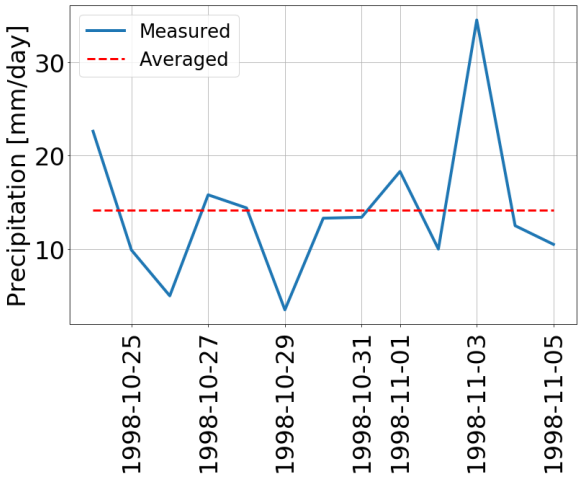

Figure 3.25: Measured and averaged daily precipitation in De Bilt.

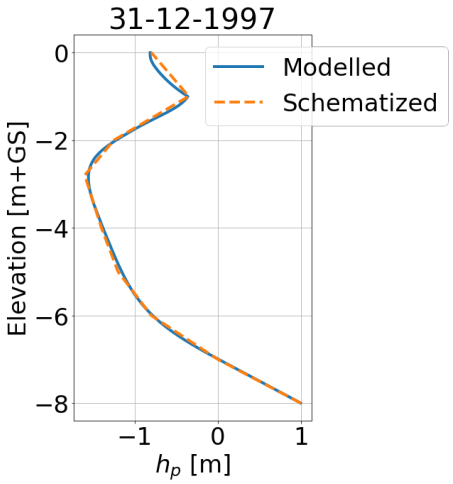

Figure 3.26: Modelled and schematized pressure head on December 31st 1997.

The results from the original analysis and the averaged analysis are compared in Figure 3.27. The figure shows that there are some differences between the two models, but that the wetting fronts are generally similar. After

days where the average precipitation data is below the actual data, the averaged run underestimates the pressure heads in the column and vice versa. For this case, the averaged data does result in a total suction loss, similar to the case with measured data. However, when using the average intensities for a given duration it should be kept in mind that it might not be the governing situation for the given precipitation depth with respect to suction loss.

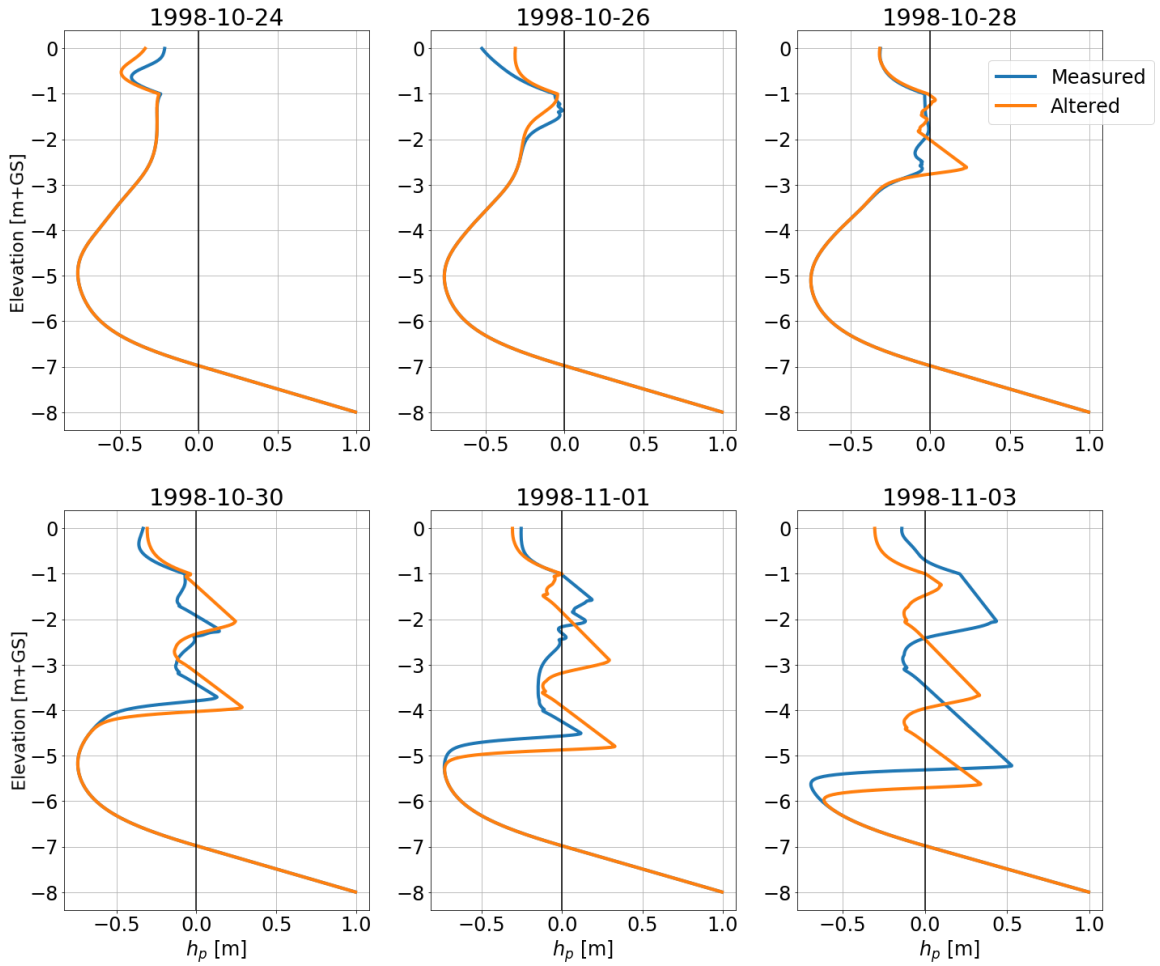

Figure 3.27: The pressure head in a 1D soil column on different dates obtained with measured meteorological input data and altered data that uses a 13 day average between 24 October and 05 November 1998.

3.7 Conclusions after the sensitivity analysis

The analyses presented in the previous sections showed how both nature- and modelling related factors can influence the magnitude of suction in the cross section of the case study dike. From the presented analyses, the following can be concluded:

- It is unlikely that a steady state position of the water table related to the maximum river level is reached during a high water in the river. The rate at which the water table rises is mainly influenced by the initial water content in the dike, which is in turn related to the meteorological conditions previous to the high water event. It is thus expected that a high water event during winter will result in a higher position of the water table in the dike than a high water event during summer (see Figure 3.4).

- The number of days over which the river level rises and falls during a high water wave can be expected to remain constant, independent of the peak height of the event. Moreover, the difference in the peak river level that can be expected once every 1,250 years and 10,000 years is not large (in the order of 0.1m). As a result, the difference between the highest position of the water table of a 1,250 year and a 10,000 year event is also in the order of a few decimeters. Moreover, the analysis showed that the position of the water table has a marginal effect on the progression of the wetting front during infiltration. When

searching for a combination of precipitation and river level events after which all suction will be lost in a soil column, a high water event with a smaller return period in combination with heavy precipitation will likely be governing. Since a similar height of the water table can be expected for the varying river levels, but the probability of occurrence of a lower river level is much larger.

- The choice of the unsaturated soil properties of the cracked layer have a marginal influence on the position of the water table during a high water event and on the maximum pressure head during infiltration. The unsaturated properties of the clay core have a significant influence on the position of the water table. The combination of a low hydraulic conductivity and a high saturated water content result in the highest water table, especially in the first few days of a high water. Moreover, this also results in the governing situation (with respect to the amount of suction), when infiltration occurs. The pore pressures (and hence the water content) will remain high for a longer period, resulting that when a subsequent high water or precipitation event occurs, suction in the the dike will be lost even faster.

- The saturation of the soil previous to extreme events has a large influence on both the progression of the water table as on the influence of precipitation on the matric suction. The history of the soil (with respect to meteorological influences and high waters) has the largest influence on whether or not a precipitation event will lead to saturation of the soil column. That is why even though most rain falls (and on relatively little days) during summer months, this generally does not lead to saturation of the soil column. Due to evapotranspiration the water content in the top layer of the soil during summer will be lower than in winter. A low water content in the top layer will result in more runoff and less infiltration.

- Saturation due to precipitation is most likely to occur during winter time. The analyses showed that the soil column was also saturated once during autumn, but this was after very long and intense precipitation. The analyses suggest that the governing situation for a soil column with a relatively low water table is when there are multiple days of consecutive rainfall above 10 mm. When the water table is relatively close to the ground surface (for example during a high water event in the river), one larger precipitation peak can also result in full saturation of the soil column when the initial pressure head is already high.

4 Suction in the case study dike: return periods and the influence on slope stability

The previous chapter has shown how initial and boundary conditions influence the magnitude of soil suction in the case study dike. The largest influencing factors that were found are the saturation of the unsaturated zone previous to extreme events and the soil characteristics of the clay core. Naturally also the height and duration of extreme boundary conditions showed to be of importance (high river stage and precipitation). Especially the initial saturation was found to have a large influence, both on the progression of the water table during a high water as on the extend of the wetting front during precipitation. The initial saturation of the soil is a result of a combination of evapotranspiration, precipitation and high waters in the river, which makes it one of the hardest things to determine. In this section first the median suction throughout the cross section is calculated based on a quasi 2D calculation of the 37 year analysis (Section 4.1). Based on these results, the median saturation during winter and summer can be estimated and the probability that part of the dike is saturated can be estimated with the obtained empirical distribution of pressure heads in the dike. However, in this distribution the variations of the water level are not included and since it is a time series of 37 year, it does not include (many) extreme precipitation events. To include a strength increase due to suction in stability analyses, we also need to know the expected suction during extreme precipitation in combination with a high water event. Multiple scenarios are calculated that include a combination of high waters in the river and precipitation on the dike. The probabilities of occurrence for the (extreme) events can be estimated by assigning return periods. The return periods of high waters at the dike are based on the analysis results for the discharges at Lobith in GRADE (included in Appendix D). The probability of occurrence of precipitation events with a given intensity and duration is obtained by constructing Intensity, Duration, Frequency (IDF) curves. The initial saturation is estimated with help of the results of the 37 year analysis in section 3.6. An overview of the variations in initial and boundary conditions that led to the scenarios is presented in section 4.2 and the results of the analyses of the scenarios are included in Section 4.3. Since the objective of this research was to see if a strength increase due to matric suction can be included in stability analyses, four scenarios were analyzed to see how the stability of the dike is influenced for given expected suction during a high water event (Section 4.4). An estimation of the expected strength increase is made with a Monte Carlo analysis in Section 4.5.

4.1 Probability of saturation based on the time series

With the quasi 2D analysis, the 37 year analysis was repeated to calculate the pressure heads in the upper part of the inner slope of the case study dike. With this analysis, the median pressure head can be calculated over the dike. Since a large seasonality is expected, the median pressure head in the dike cross section during a winter month (January) and a summer month (July) were calculated. In this calculation, the water table was kept constant at a height of 8.00 m+NAP, which is the daily water level in the winter. The calculation was performed for a clay core with properties B10 and a cracked layer B07. The 37 year analysis in the previous section was performed with clay core properties B12. In Figure 4.3, a comparison is presented of the median pressure head during winter and summer for both clay core properties. This figure shows that the pressure head calculated with B12 is approximately 0.25 meter higher than when calculated with B10. When calculating the probability of saturation, it is therefore assumed that the dike is fully saturated when $h_p \geq$ -0.25 m. The median pressure heads during winter and summer are included in Figure 4.1.

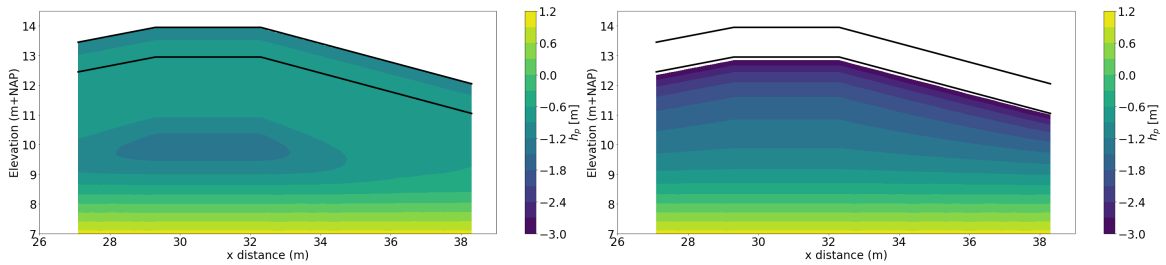

(a) January (b) July

Figure 4.1: Median pressure heads in the cross section based on the results of the 37 year analysis during winter (4.1a) and summer (4.1b). The median pressure head in the cracked layer during summer is -21 m.

The suction in the cracked layer is higher than the levels of the contour plot show, because otherwise the

distribution of pressure heads in the core could not be observed. The median pressure head in the cracked layer during summer is -21 meter. Observing the figures, it can clearly be seen that during winter the influence of precipitation is observed over a larger depth in the dike. It is emphasized once more that these figures show the median pressure heads without considering water level variations. The probability of saturation (where saturation is defined as $h_p \geq$ -0.25 m) is included in figure 4.2.

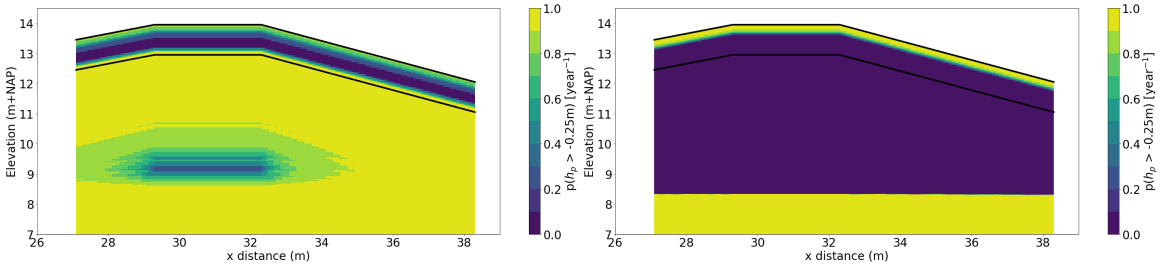

(a) January (b) July

Figure 4.2: Probability of saturation per year during winter (4.2a) and summer (4.2b) based on the 37 year time-series.

The figures shows that during summer, the probability of saturation is 0 in the core of the dike. This means that during the 37 year analysis, the core was not saturation once during the month July. During winter, the inner part of the core is saturated less than the part closer to the ground surface. These figures show the probability of saturation due to precipitation per year. Again, the figures do not include water table variations. When observing this figure, it is clear that the area that can be expected to remain unsaturated during a high water in winter (located in the upper part of the inner slope) is relatively prone to become fully saturated.

4.2 Scenario Analysis: set-up

In the scenarios, variations regarding the soil properties, initial pressure head, high water waves and precipitation were used. How and why they were included is elaborated on in this section.

Soil properties

The soil-specific parameters that describe the unsaturated zone have proven to have a large impact on both the rise of the water table as on the progression of the wetting front and they should therefor be included in the scenarios. In the scenarios a clay type was chosen that results in relatively much suction and a clay type that results in relatively little suction (considering similar conditions). The Staring series includes parameter estimates for three different clay types in the upper part of the subsurface (B10, B11, B12). The analyses in the previous chapter have shown that when B12 (heavy clay) is used, the water table progresses relatively fast (during wet months) and precipitation also has a large influence on suction. For type B10 (light clay), the opposite is true and hence this was selected as a 'favorable' situation. Clay type B11 showed similar results as B10 and is therefore not included. The scenario where B12 is used can be seen as an unfavorable scenario (regarding the presence of suction) and scenarios with B10 as favorable. It should be noted that, based on the lutum content in the samples taken from the case study dike, the clay seems to match Staring series type B10 better (see also Appendix A). The soil properties of the cracked layer turned out to be of less relevance, hence the decision was made to keep the properties of the cracked clay layer fixed at Staring series type B07 (very sandy clay) in all analyses.

The initial pressure head

To get a reasonable estimate for the initial pressure head, the results of the year by year analysis (section 3.6) were used together with the fact that the saturation in a dike body during winter will on average be higher than the saturation in summer. The scenarios were split up in scenarios that occurred during a winter month (January) and a summer month (July). From the results of the 37 year analyses, the median pressure head in January and in July were plotted together with their 33% and 95% confidence intervals, to observe the variation (see Figure 4.3). To create a more complete picture, the 37 year analysis was repeated for a clay core with properties B10 and a water table 7m below the ground surface.

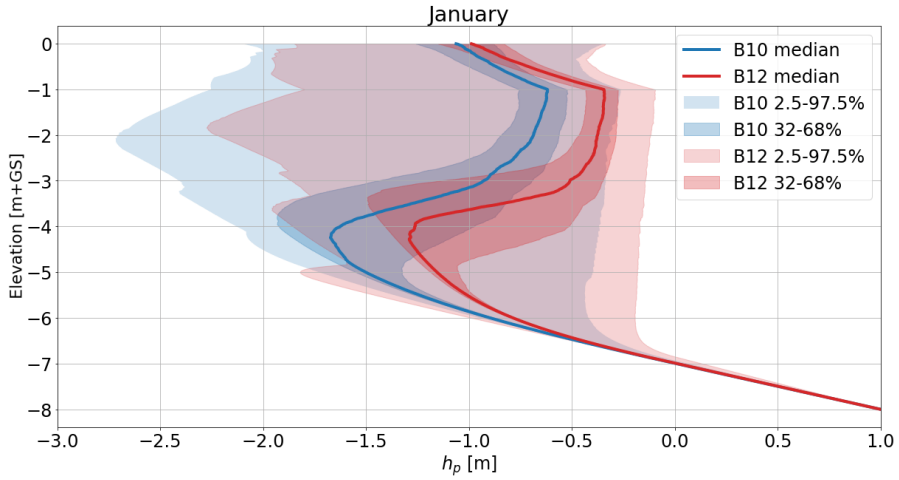

(a)

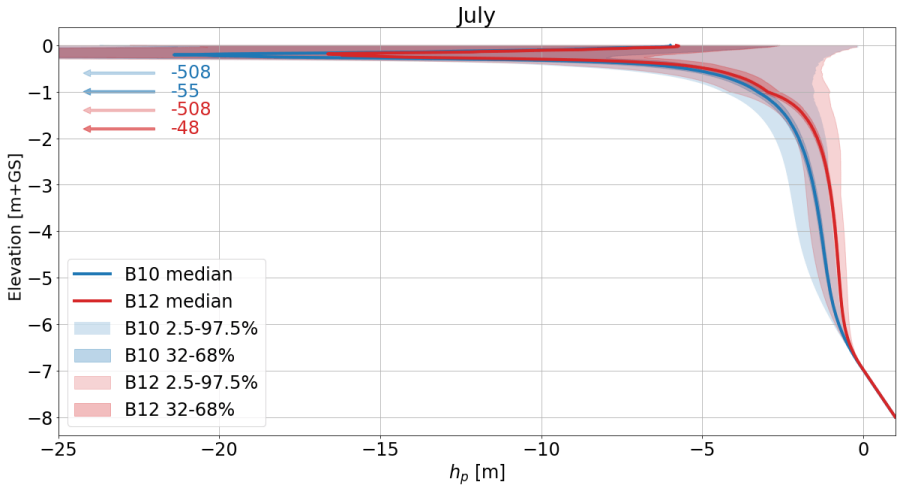

(b)

Figure 4.3: The median and confidence intervals of the pressure heads in a 1D soil column in January (a) and July (b) for a clay core properties B10 and B12.

While these figures could easily be translated to initial pressure heads in SWAP, this is not the case in Seep/W, since an initial pressure head can not manually be specified. The pressure heads were imitated by applying rain and evaporation on the dike before the high water event. However, these initial pressure heads did not match exactly with what is found in the 1D analysis. A comparison from what was found with SWAP and the modelled initial pressure head along section S1 is included in Figure 4.4a and 4.4b. The figures show that during summer the initial condition used in Seep/W underestimated the amount of suction in the top layer, but that the pressure head in the dike body matches well. Due to the lower suction in the top part, precipitation can infiltrate more easily. During winter, there is a deviation from the median found with SWAP of a few decimeters. The modelled suction is slightly lower, which means that the progression of the water table is slower. These implication will be considered when analysing the results.

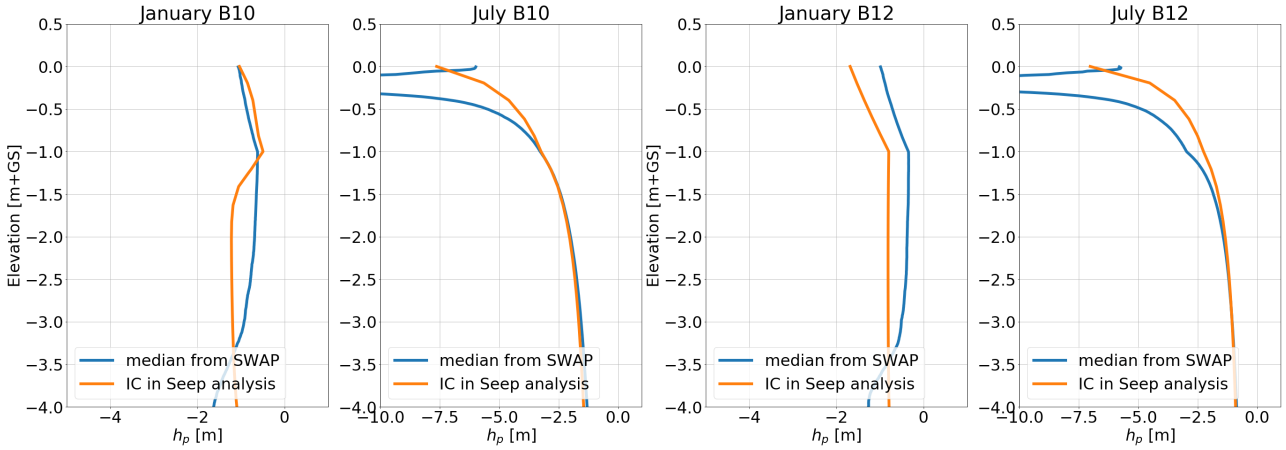

(a) B10 (b) B11

Figure 4.4: Comparison of the median pressure head in SWAP and the initial pressure head used in Seep/W for the four scenarios.

Discharges and water levels

As described in section 3.3, the water levels for certain return periods can be determined with the return periods for discharges at Lobith and a stage relation line (included in Appendix D). From the results in section 3.3, it can be concluded that events with extremely high return periods (for example 10,000 year), will only result in slightly higher water tables than events with a much lower return period (for example 1,250 year). For that reason, events with a maximum return period of 1,250 year are included in the scenarios. In the scenarios, also an initial water level (or height of the water table) has to be determined. The median discharge at Lobith in January (± 2,500 m^3/s) and July (± 2,000 m^3/s) are used as initial conditions, as presented in Figure 4.5.

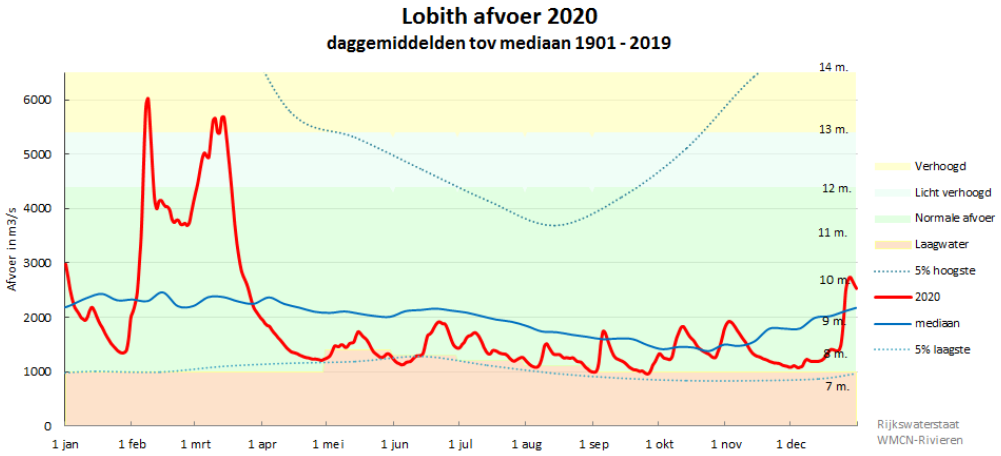

Figure 4.5: Discharge statistics for the year 2020 (after Rijkswaterstaat (2020))

The plots of the median pressure heads in the 1D soil column indicate a strong seasonality of the saturation in the dike (which also follows from literature). To get a feeling about the occurrence of high waters in the Rhine river, a plot was made of all high waters recorded in the Rhine at Lobith (Figure 4.6). A high water level in the Netherlands is considered when the river level at Lobith is larger than 14.00 m+NAP, which corresponds to a discharge of 6,731 m^3/s. For the plot daily discharge data for the years 1930-1988 and 1996-2021 was used (no data was available for the years 1989-1996).

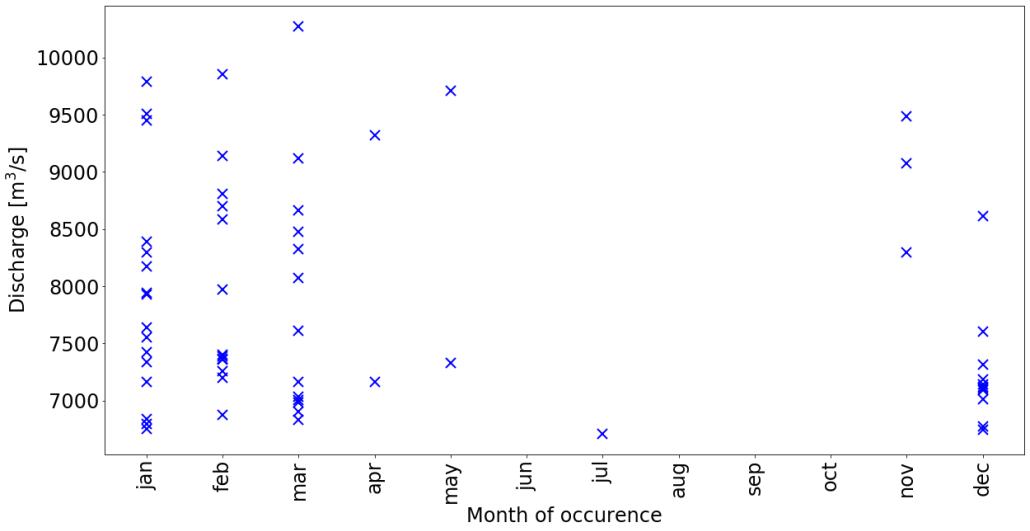

Figure 4.6: High discharges per month measured in the Rhine at Lobith for the years 1930-1988 and 1996-2021.

Precipitation

Obtaining information regarding the return periods of certain precipitation events can be done by creating IDF curves. For the analysis, daily precipitation data from the years 1906 - 2021 was used from meteorological station De Bilt. To obtain IDF curves, the General Extreme Value (GEV) distribution was fit to the data, together with the block maxima method (a method where the maximum value over certain time block, typically a year, is selected). The GEV distribution has three parameters that define the shape of the probability density function (pdf, see equation 23), the shape parameter (ξ), the scale parameter (σ) and the location parameter (μ). ξ determines the behaviour of the tail of the distribution and the GEV with ξ equal to zero is the Gumbel distribution.

$$f_{\text{GEV}}(x;\mu,\sigma,\xi) = \frac{1}{\sigma}\exp\left(-\left[1+\xi\left(\frac{x-\mu}{\sigma}\right)\right]^{-1/\xi}\right)\left[1+\xi\left(\frac{x-\mu}{\sigma}\right)\right]^{-1/\xi-1} \quad \{z : 1+\xi(z-\mu)/\sigma > 0\} \tag{23}$$

The IDF curves were created with the following steps.

1. The daily data was summed to obtain precipitation depths for two-daily rainfall, three-daily rainfall etc. up to a duration of thirteen days.
2. From the obtained daily and multiple daily data, the annual maxima were selected.
3. To every set of annual maxima (corresponding to a certain duration) the GEV distribution was fit, obtaining the most likely estimates of the shape, location and scale parameters.
4. With the obtained parameters, a return period curve of the precipitation depths was plotted for each duration.

To obtain the estimates for the parameters with maximum likelihood estimation the GEV sub-package of the statistical function package of Python (scipy.stats.genextreme) was used. The probability density functions of the found distributions are compared to the histogram of the data in Appendix G. A plot with the return period curves of the precipitation depth belonging to the varying duration is presented in Figure 4.7. Typically, one more step is taken where the found precipitation depth is divided over the duration to obtain mean intensities. This step was not taken, as the previous section showed that a mean intensity is not only very unlikely, but might also not result in the governing situation with respect to suction loss. The step to go from precipitation depth over a duration to mean intensity is trivial. The figure show that the daily and two daily lines cross each other at a return period of 350 years. Naturally this is not possible and it is result of the tail behaviour of the fitted distributions.

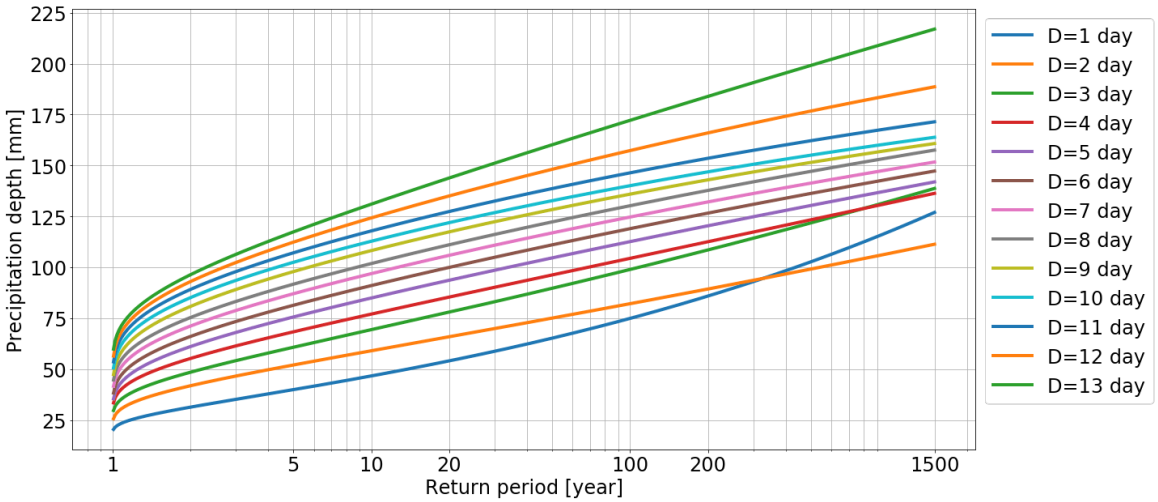

Figure 4.7: Return period plot for the precipitation depth over a varying duration.

Since the results in section 3.6 showed that averaging precipitation over a duration can lead to variations in the size and extend of the wetting front, the information from Figure 4.7 was included in a different way. To create random patterns of rainfall that add up to the total precipitation depths from the IDF curve, the following steps were taken:

1. From an array A=[0, 1, 2, ..., 39] a random sample of size n was taken, with n being the duration (in days). The sample was taken with the possibility of repetition.
2. All values in the sample were divided over the total sum of the array, such that the numbers in the sample sum up to 1. All values in the sample were then multiplied by the total precipitation.
3. This process was repeated ten times, such that there were ten varying arrays with synthetic rainfall data that correspond to the same precipitation depth, but with different rainfall patterns. Due to round off errors, the total precipitation depth could vary 1 mm from the desired precipitation depth.

Naturally, many more combinations can be made for a precipitation depth over a specified duration. However, as the goal of the applied approach was to include some of the variation in the analyses, 10 was considered sufficient.

Scenarios

With the variations discussed above, the twelve scenarios presented in table 4.1 were considered.

Table 4.1: Initial and boundary conditions used in the scenarios

scenario	**Month**	**Soil type core**	**River level h_{peak} [m+NAP]**	**RP h_{peak} [yr]**	**Precipitation [days, total mm]**	**RP precipitation [yr]**
1.1	January	B10	8.00	-	13, 184	200
1.2	January	B12	8.00	-	13, 130	10
1.3	July	B10	7.00	-	13, 220	1,500
1.4	July	B12	7.00	-	13, 220	1,500
2.1	January	B10	11.00	2	10, 115	10
2.2	January	B12	11.00	2	10, 100	4
2.3	July	B10	11.00	2	13, 220	1,500
2.4	July	B12	11.00	2	13, 220	1,500
3.1	January	B10	13.40	1,250	10, 115	10
3.2	January	B12	13.40	1,250	10, 100	4
3.3	July	B10	13.40	1,250	13, 220	1,500
3.4	July	B12	13.40	1,250	13, 220	1,500

The sequence of the scenarios is of influence on the final result: a high water in the river that happens after a rainy day may result in a different amount of suction in the dike than a situation with rainfall after a high water. Since the interest of this report is the influence of matric suction on the stability of a dike, the suction should be in the dike during the high water event. For that reason, the scenarios were modelled such that first the precipitation occurred and after the precipitation stopped, the high water event started.

4.3 Scenario Analysis: Results

The first four scenarios consider a situation with extreme precipitation and no high water in the river and were performed to show what type of precipitation event leads to saturation of the whole cross section of the dike, during median river level conditions in a relatively wet and a dry month. The four scenarios are a combination of typical conditions with respect to initial saturation and river level in January and July, for both B10 and B12 soil properties of the clay layer (scenarios 1.1 - 1.4 in table 4.1). Since a steady river level is considered in these scenarios and to reduce computational time, they were calculated with the 1D model. In the approach it was considered that if saturation occurred over the full height of a column situated in the crest of the dike, that would also result in saturation of the other parts of the cross section, since the vertical distance between the water table and the ground surface is largest under the crest. Another benefit of the 1D model is that variations in the precipitation per day could be included for the total precipitation per duration that were calculated with the IDF curves. With the methods described in the sub-section about precipitation, 10 random precipitation events were calculated. For each of the 10 combinations, the maximum pressure head over the soil column is included in Figure 4.8. The figures show that in January, the chosen precipitation events lead to full saturation of the soil column, for some of the random precipitation events (not all). They were chosen such, that a precipitation event with a slightly smaller return period would not lead to full saturation of the soil column. The results suggest that if there is a long duration of precipitation (13 days) in January with a total precipitation depth between 130 and 184mm, it is likely that this will lead to full saturation of the dike. The return period of these event is between 10 and 200 years, and is this return period thus only refers to a precipitation event. Cases 1.3 and 1.4 were subjected to 220 mm op precipitation, spread out over 13 days (with a return period of 1500 years). The figures show that, although such an event will lead to saturation of the upper layer of the dike, in the core of the dike suction will remain.

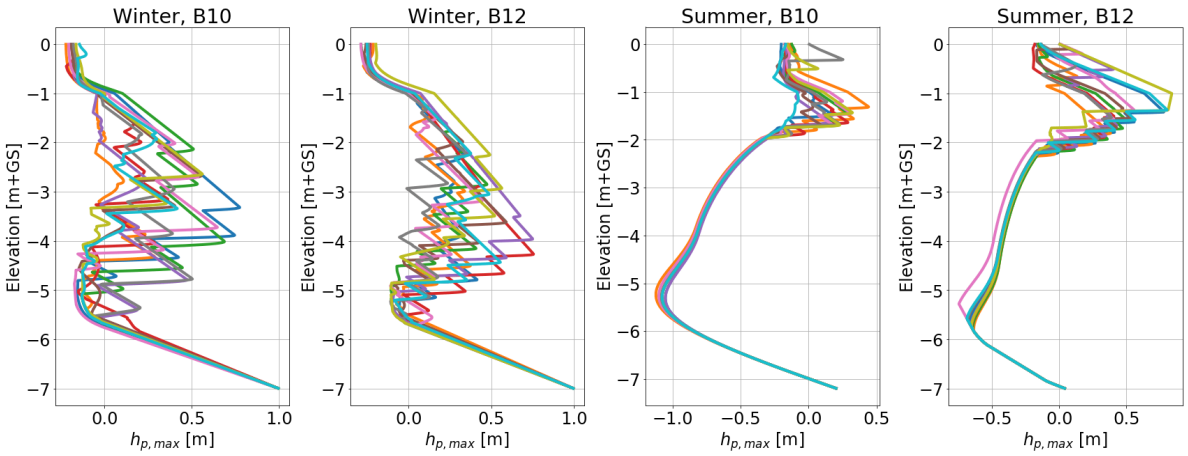

(a) 1.1 (b) 1.2 (c) 1.3 (d) 1.4

Figure 4.8: Maximum pressure head after 10 combinations of precipitation events for scenarios 1.1-1.4.

Scenarios 2.1-2.4 consider a high water in the river that happens on average once every 2 years in combination with precipitation. The precipitation events were chosen based on the results from scenarios 1.1-1.4. Since the precipitation events for 1.1-1.2 resulted in full saturation, events with a smaller return period were chosen for scenarios 2.1-2.2. For scenarios 2.3-2.4 the same events were used as in 1.3-1.4, to see the combined effect of heavy precipitation and a high water event. The scenarios were modelled in Seep/W, to model the progression of the water table. In Seep/W, the precipitation was not divided randomly over the duration of the precipitation, but was kept constant at the average intensity. From the results of the analysis, the maximum pressure head during the simulation was selected and plotted in Figure 4.9.

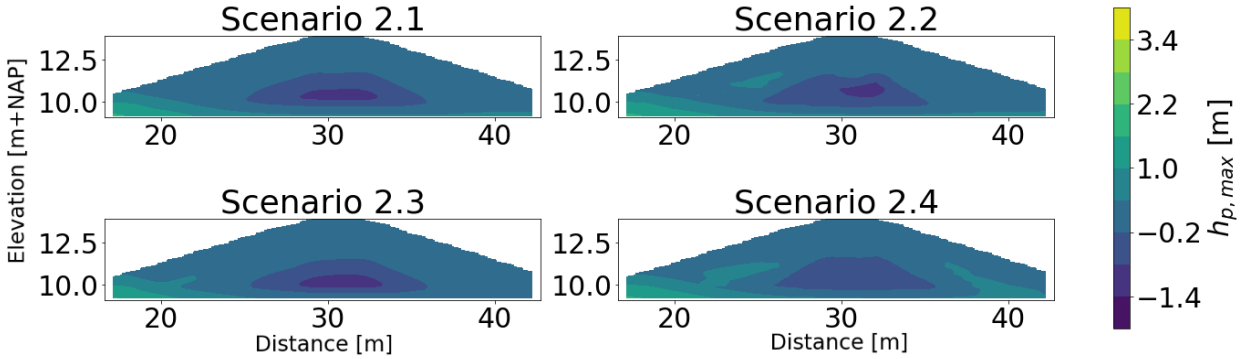

Figure 4.9: Maximum pressure head in the dike after a high water event with a return period of 2 year and precipitation for scenarios 2.1-2.4

The results show that it is very unlikely that the dike will be fully saturated during summer when there is a high water event with a peak height of 11.00 m+NAP. Even when there is a precipitation event with a duration of 13 days and a return period of 1500 years, there remains suction in the core of the dike (scenario 2.3-2.4). The area over which suction is present is approximately similar for the scenario with favorable and unfavorable soil characteristics of the core, but for the favorable case (2.3) the magnitude of suction is slightly higher. For the two scenarios in January, there is also some suction in the core of the dike, but the return periods of the precipitation events are much smaller (10 and 4 years).

Finally, four scenarios were created that considered a high water with a return period of 1,250 year and precipitation. The figures show that there is some suction in the river cross section at all times during these scenarios, but that it is very low (around 0.2m).

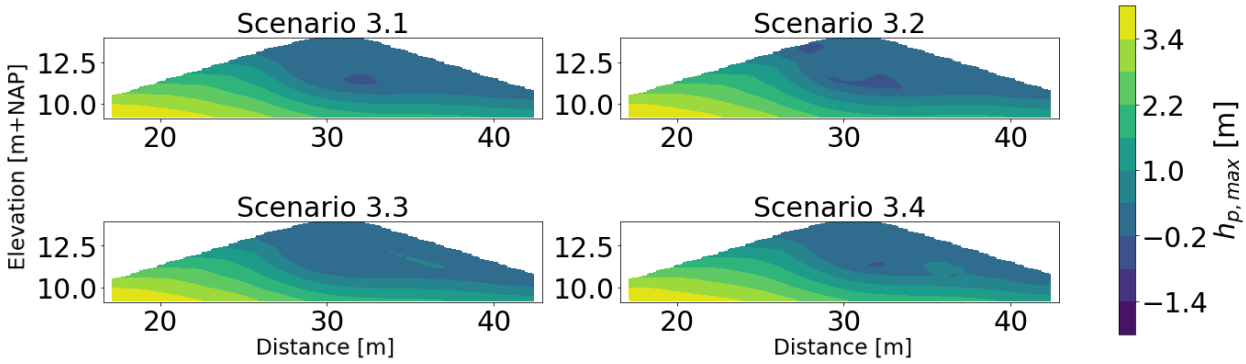

Figure 4.10: Maximum pressure head in the dike after a high water event with a return period of 1250 year and precipitation for scenarios 3.1-3.4

Conclusion after scenario analysis

The results of the quasi-2D analysis and the analysis of the scenarios show that during most extreme events there is some suction present in the dike, although for some events in very low amounts. The quasi-2D analysis shows that during winter the median suction in the core of the dike is between -1.5 and -0.5 m and during summer between -2.5 and -1 m. Moreover, the probability of saturation during winter from the quasi-2D analysis is around 1 year^{-1} and during summer 0 year^{-1}. From the scenarios it follows that the type of events that result in complete saturation are the precipitation events with a long duration and a high intensity that occur during winter months. The scenarios show that precipitation events that have a return period of 10-200 years, can result in full saturation of the case study dike, considering a median January situation as starting position. However, considering that on average 50% of the time the pressure head in the dike is initially already higher, full saturation of the dike after only precipitation likely occurs more often. This is also what can explain the difference in result from the quasi-2D and the scenario analysis. The average return period can be estimated to be between 1 and 10 years. The results also show that during summer, it is very unlikely that the dike will be

fully saturated. During a high water event with a return period of 1,250 years and precipitation with a return period of 1,500 years, there is some (although very little) suction left in the dike. Considering that extreme events were combined in these scenarios, the probability that the extreme events happen simultaneously is lower than the individual probability of occurrence. As a result the return period of the two events occurring together is even higher. If the events can be assumed to be uncorrelated, the probability of occurrence in the product of the two individual probabilities. It is unclear if that assumption is reasonable, since some correlation can be expected. The results of the two analyses are included in Table 4.2.

Table 4.2: Summary of the median pressure head in the dike core and the probability of saturation during winter and summer.

Month	**median pressure head in the core [m]**	**Return period of full saturation [yr]**	**Probability of full saturation [yr^{-1}]**
January	-1.5 – -0.5	1–10	0.1 – 1.0
July	-2.5 – -1.0	>1,875,000[3]	<5.3 10^{-7}

4.4 The strength increase due to matric suction

The strength increase due to matric suction can be included in stability analyses by adding an apparent cohesion to a soil layer. The influence that the apparent cohesion has on the stability of the dike depends on three things, namely the magnitude of the apparent cohesion, the size of the area to which the apparent cohesion is added and the position of that area. The position of the soil layer is important because the critical slip plane should go through the soil layer with the apparent cohesion to see an effect on the factor of safety. The results from the previous section showed that suction during a high water in the river in combination with extreme precipitation is generally between 0 and 1 meter. In this section a situation is calculated with a high water event and average precipitation to get an indication of the magnitude of the matric suction in the dike and the corresponding strength increase during average weather conditions. The scenarios were calculated with a 2D seepage analysis in Seep/W, from which the results were used in a stability analysis with the software D-stability of Deltares.

When there is a river level of 14.00 m+NAP in the Rhine at Lobith, there is a high water situation in the Netherlands and from a river level of 16.50 m+NAP (with a discharge of 11,800 m^3/s) there is an extreme high water and additional measures are taken. This corresponds to a peak height of 13.00 m+NAP at the case study dike, which is similar to the high water situation in 1995. This river stage at the case study dike is used as the peak of the high water wave event in this analysis, together with the median shape of the high water wave from GRADE. Four scenarios were set up with this high water as the boundary condition. Two in an average wet month (January) and two in an average dry month (July), where they are calculated with favorable and unfavorable soil properties. As initial conditions, the results from the 1D analyses were used. In the analyses, the following steps were taken:

1. The high water event was schematized with the median shape from GRADE and the peak at 13.00 m+NAP.
2. The initial pressure head in the dike was estimated with the results from the 1D analyses, where the median pressure head in January and July were used (Figures 4.4a and 4.4a).
3. The average precipitation in January and July was used, where the intensity per day was calculated as the mean total precipitation per day divided over the mean number of rainy days (see table 3.7).
4. A plot was made with the maximum pressure heads during the simulation. The area where $h_p \leq 0$m, was schematized and used in the stability calculation.
5. All water tables were plotted to obtain the maximum position of the water table. The schematized maximum water table during the simulations was used as the water table in the D-stability calculation.
6. The stability calculation was performed and the critical slip plane and safety factor were determined for the situation where the unsaturated area is schematized as a drained soil layer, with zero apparent cohesion.

[3]Calculated assuming that the events heavy precipitation and a high water in the river are uncorrelated, which is probably over simplistic. The value should only be used as an indication that the event of full saturation in summer is very small.

7. The stability calculation for the found critical slip plane was repeated for situations with an increasing apparent cohesion from 0.5 to 10 kPa. These are values to be expected for matric suction between 0 and 2 meter according to Figure 2.6.

The set-up in D-stability

A previously existing geometry in D-stability of the cross-section was used as a base case. The cross section is included in the following figure and the properties of the layers are included in table 4.3. The properties of the layer "Dike material cohesion" are the ones used in the unsaturated area.

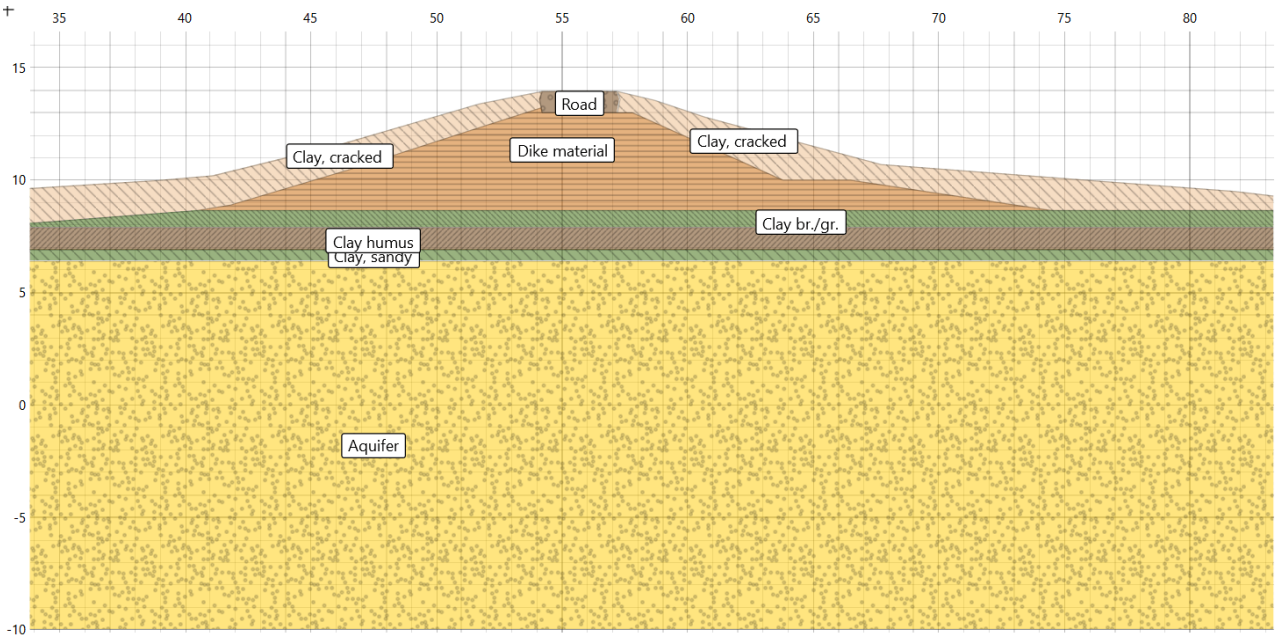

Figure 4.11: Original cross-section of the case study dike in D-stability

Table 4.3: Shear strength properties and soil characteristics for the different layers in the stability model.

Layer	**Shear strength model**	**Dry unit weight [kN/m³]**	**Wet unit weight [kN/m³]**	**Friction angle**	**Strength increase exponent**	**Cohesion [kPa]**
Clay, cracked	Mohr-Coulomb	18	18.3	32.7	-	0
Road	Mohr-Coulomb	20	21	32.3	-	0
Dike material	SU-table	19	19.5	-	0.45	-
Clay br./gr.	Shansep	18	18.3	-	0.88 (S=0.24)	-
Clay humus	Shansep	14	14	-	0.85 (S=0.25)	-
Clay, sandy	Mohr-Coulomb	18.8	19.1	33	-	0
Aquifer (sand)	Mohr-Coulomb	18	20	32.3	-	0
Dike material cohesion	Mohr-Coulomb	19	19.5	30	-	[0-10]

The scenarios

The results from the 1D analysis were used as a basis to create the initial condition in Seep/W, where the median pressure head was used as initial conditions for the four scenarios and the average precpitation was applied as boundary condition. On average there is 72 mm precipitation in January spread out over 18 days

(see table 3.5). The water table for each time step was plotted in Seep/W (figure 4.12a) and the maximum pressure head was plotted in python (figure 4.12b). Note that there is data for each grid point, and that linear interpolation is used to make the figure with the maximum pressure heads. As a result of the grid that was used, the right slope does not seem straight. However, besides this the plot is correct and validated with figures from Seep/W.

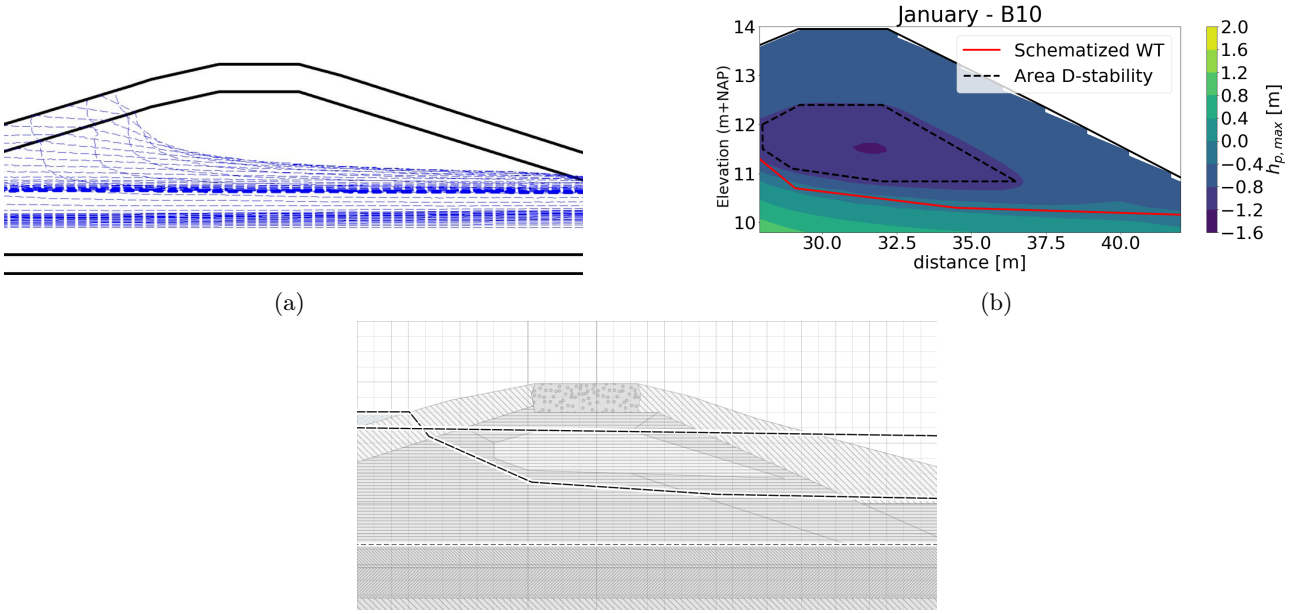

(a) (b)

(c)

Figure 4.12: The results of analysis in January with soil properties B10. The water table in the dike (a), the maximum pressure head and the area that where suction remains present (b) and the schematized layer in D-Stability (c)

With figures 4.12a and 4.12b the D-stability calculation was adjusted (see figure 4.12c) and the schematized area was given the properties of "Dike material cohesion" as defined in table 4.3. The situation with 0 cohesion was used to find the governing slip circle and for that circle (included in appendix H) the factor of safety was determined for situation with a varying cohesion between 0-10 kPa that was added to the soil.

For the other 3 scenarios a similar approach was used. The figures of the water tables over time, the maximum pressure heads, the schematization in D-stability and the governing slip plane are included in Appendix H. The results show that the area that remains unsaturated is larger during summer. Due to the higher suction the progression of the wetting front is slower. Also, since there is very high suction in the top layer of the dike, a lot of water that falls on the dike during summer does not infiltrate, but runs off. The results also show that the area that remains unsaturated is larger for the scenario with B12, but overall there is less suction in this area which will lead to less apparent cohesion. For all four scenarios, the schematized area in D-stability was given a varying apparent cohesion ranging from 0 to 10 kPa and the safety factor was determined. A plot of the results is included in figure 4.13, in which the safety factors were translated to a reliability index with equation 24. In this equation γ_n is the safety factor and β is the reliability index (Kanning et al., 2017). The reliability index can also be expressed as a probability of failure per year using the cumulative standard normal distribution.

$$\gamma_n = 0.15 \cdot \beta_{T,c\ \text{toss}} + 0.41 \tag{24}$$

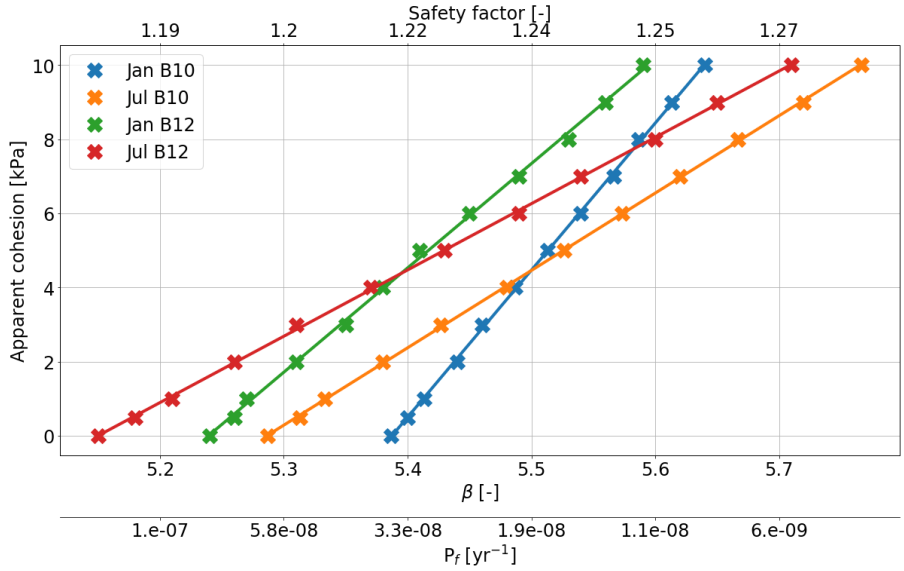

Figure 4.13: Safety factor for macro stability for a varying apparent cohesion added to the zone that remains unsaturated for 4 cases.

The figure shows that an increase in the safety factor is found for an increasing apparent cohesion for all four cases and that the relationship between the two is approximately linear, where the slope depends on the area in the dike where the cohesion is added to. A different plot was created that shows the relative increase in the factor of safety compared to a situation with 0 kPa apparent cohesion (see Figure 4.14).

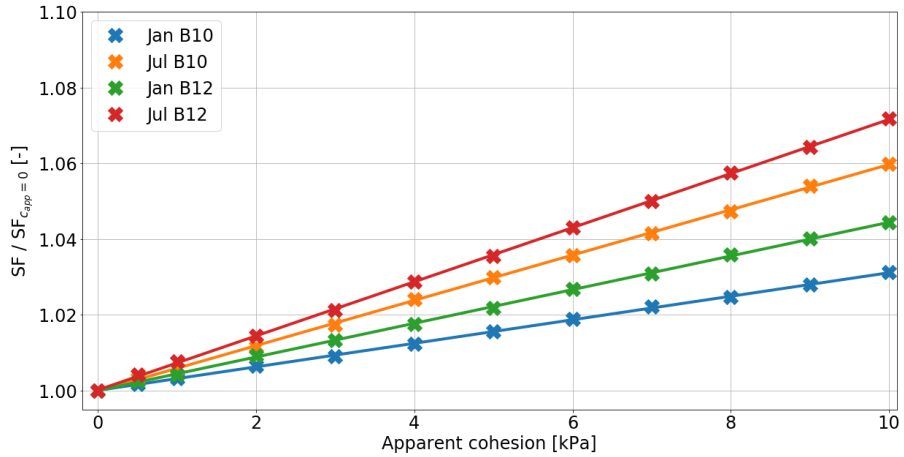

Figure 4.14: Relative safety factor for macro stability for a varying apparent cohesion added to the zone that remains unsaturated for 4 cases.

The two figures show that the largest gain per increasing apparent cohesion in the factor of safety is found during summer, when the area that remains unsaturated is largest. Remarkable is that the situation during summer initially has a lower factor of safety than the situation in winter, while the modelled water tables in summer are lower than in winter. To put this in perspective, one additional calculation was done per case where the entire core of the dike is modelled assuming undrained behaviour following the SU-table ('Dike material' in table 4.3), which is the way according to the Dutch standard to model soil layers with a low permeability. The results of these calculations are included in table 4.4, together with the results assuming drained behaviour with 0 and 10.0 kPa apparent cohesion.

Table 4.4: Safety factors found with an undrained clay core layer and a drained layer with cohesion and 10 kPa.

Scenario	**SF [-] with SU table**	**SF [-] drained $c' = 0$ kPa**	**SF [-] drained $c' =$ 10 kPa**
January B10	1.30	1.218	1.256
July B10	1.341	1.203	1.275
January B12	1.30	1.196	1.249
July B12	1.34	1.182	1.267

This shows that when modelling the entire dike core while assuming undrained behaviour of the soil, the found factor of safety is higher than when assuming drained behaviour, independent of whether there is an apparent cohesion (up to 10 kPa). This explains why the found safety factors for the cases in summer are lower than those in winter (per soil type), since in summer a larger part remains unsaturated and is modelled with Mohr-Coulomb. These results deviate from what is expected, since analyses with undrained soil behaviour generally lead to less favorable results (van Duinen, 2014). It therefore raises the question whether assuming undrained soil behaviour for clay layers really is the conservative approach and if clay above the water table should be modelled as drained or undrained.

Considering that most high waters occur during winter, the focus of the study is on the cases during January. The figures show that for these two cases, after adding 5-6 kPa apparent cohesion to the simulated area, the probability of failure per year is reduced by a factor of 5, which can be seen as a significant decrease from an engineering perspective. However, when a dike is not sufficient according to the norm, a smaller decrease can also be seen as significant. Based on these results, the question remains how much apparent cohesion can be expected, which will be elaborated on in the next section.

4.5 The influence on the probability of failure

The analysis in the previous section and Figures 4.13 and 4.14 show that the factor of safety given a water level in the river, depends on the apparent cohesion and that the function is approximately linear. This same figure also suggests that the area over which the apparent cohesion is added determines the slope of this relationship, such that the following is true:

$$SF = f(c_{app}, \text{Area}, \text{stage}) \tag{25}$$

Where 'Area' is the area over which the apparent cohesion is added. Moreover, in Section 2.4 the expected relationship between suction and apparent cohesion for clay soils was determined, which showed that the apparent cohesion depends on the suction and on soil-specific parameters. With the results of the Monte Carlo analysis presented in that section, a distribution for the apparent cohesion of a clay can be determined, that shows the relation between c_{app} and suction. Moreover, the area over which the apparent cohesion is added is determined by the height of the water table, which is again dependent on the river stage. This means that the only unknown parameter to determine the safety factor given a river stage, is the amount of suction in the area. The average expected amount of suction over the area can be estimated with the results of the 36 year 1D analysis. By using the empirical results of the 36 year analysis for a clay core type B10, a first indication can be obtained of the expected increase in the safety factor for the case study dike. This was done for four different river levels: 11.00, 12.00, 13.00 and 13.64 m+NAP. The steps that were taken to do this were the following:

1. First, the 37 year analysis was repeated as a quasi 2D analysis to obtain results and statistics over the cross-section. In this analysis, the position of the water table was fixed at 8.00 m+NAP, which is the daily river stage during winter. By setting the position of the water table at this height during the entire simulation, the assumption was made that the height of the water table does not significantly affect the pressure head change due to infiltration and evaporation above the water table. This assumption was shown to be reasonable with Figure 3.21, that showed that the influence of the position of the water table is negligible on the wetting front.

2. For the four river levels, the maximum height of the water table was estimated, based on the previous analyses presented in this report. For a river level of 11.00, 13.00 and 13.64 m+NAP, multiple 2D calculations were already done, so the position of the water table could be estimated relatively easy. The position of the water table for a river stage of 12.00 m+NAP, was estimated based on these results.

3. The area above the water table was schematized as the area where suction is expected, with a margin of 0.5 meter. Meaning, that the area starts from half a meter above the water table. This margin was included to account for the schematization of the water table position.

4. Over this area, the average suction per day was determined for the months January, February and March. By excluding the results of the other months, the assumption was made that the high water occurs during these three months. In reality, a high water can also occur during the other months, although the probability that a high water occurs during summer is lower than during winter. As a simplification, it is thus assumed that the high water occurs in the first three months.

5. With the empirical distribution of average suction in the area per day, a (normalized) histogram was created that shows the probability of occurrence of the average suction per day during the months January, February and March.

6. With the crude data that was used to create Figure 2.6, a distribution was determined for the expected apparent cohesion given a suction. However, as Figure 4.16 shows, this function is not constant over the range of suction and both the expected value and the variance increase for an increasing suction. By analysing the samples for suction values up to 50 kPa, it shows that the Lognormal distribution can be used to describe the data and that the parameters have to be determined for every value of the suction.

7. The area that was determined in step 3 and the water table were schematized in D-Stability and the safety factor was determined for an apparent cohesion c_{app} = [0, 1, 3, 5, 7, 9] kPa. Through these points a linear line was fitted with linear regression to determine a continuous relationship between the apparent cohesion and the safety factor.

8. With this relationship, the empirical distribution for the suction and the fitted distribution for the apparent cohesion, a Monte Carlo analysis was performed to observe the expected variation of the Safety Factor. This variation shows the variation of the SF given a high water in the river and assuming that it occurs during the months January, February or March between 1981 and 2016.

The results of the intermediate steps of the calculation of a situation with a river stage of 11.00 m+NAP are presented here. Similar results for the other 3 calculations are included in Appendix I. The data obtained with the 37 year calculation of the pressure heads in the dike were first cleaned by selecting only the results in the months January, February and March. Next, the area that remains unsaturated during a river stage of 11.00 m+NAP was schematized (see Figure I.1a). All the daily data of the quasi 2D analysis that falls within this area was selected and the mean value over the area per day was computed as the representative value. Naturally, in reality there is some variability over the area, but as this calculation is meant as an indication, the mean value was used. A histogram was made of the values and is included in Figure I.1b. Ideally, a continuous distribution was used in the analysis. However, after trying to fit multiple continuous probability functions in Python (in total 87), it was concluded that there is no distribution that fits the data well enough and that the empirical distribution should be used. This was concluded after performing a Kolmogorov-Smirnov test to determine the goodness of fit of the fitted distributions. Figure I.1b shows that there are several peaks in the distribution, which is why it is not surprising that there is no distribution that fits this data well. Since the average value on one day has an effect on the average value of the subsequent day, the data in the histogram is not mutually independent. This is why the results of this analysis only say something about the 36 year that is in the time-series. However, the results can be used as an indication for the expected strength increase due to suction.

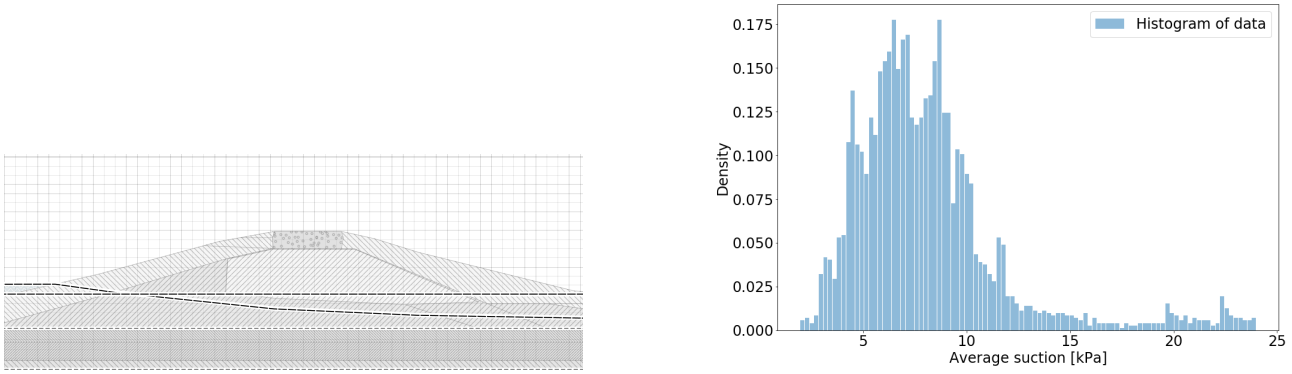

(a) (b)

Figure 4.15: Schematized area and water table (a) and the average daily suction over this area during January, February and March during 1981-2016.

As explained in step 6, it was found that the Lognormal distribution can be used to describe the distribution of the expected apparent cohesion for a given amount of suction. This was verified by performing a Kolmogorov–Smirnov test for every suction ($0 < \psi < 50$ kPa), which resulted in that p>0.05 for every case. However, the shape of the distribution and thus the parameters do change (see Figure 4.16). To properly include this in the Monte Carlo analysis, the distribution was estimated based on the Monte Carlo samples for a given value of the suction.

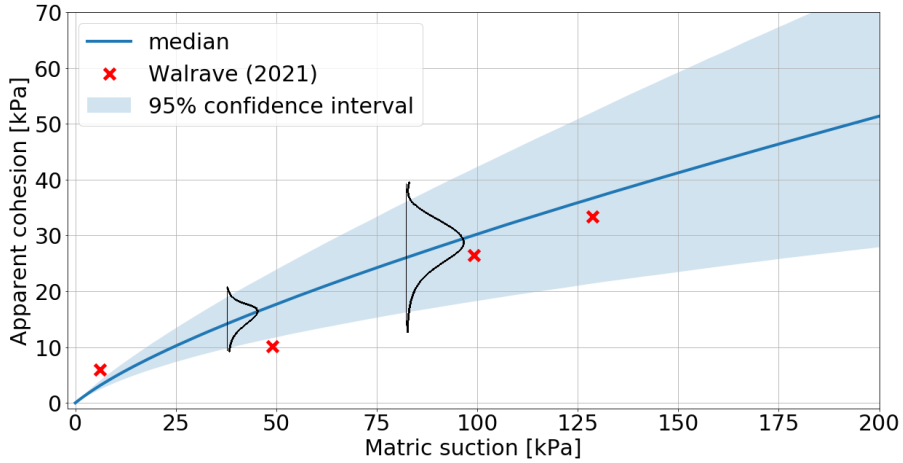

Figure 4.16: Relationship between suction and cohesion. The drawn distributions are meant to illustrate how the distribution changes over the range of suction and are only indicative.

To obtain a linear relation between the apparent cohesion and the safety factor, the analysis in D-stability was repeated following step 7 and the results for the four cases are displayed in Figure 4.17. The decision was made to find the critical slip-plane for every separate calculation of varying cohesion (rather than keeping one slip-plane fixed, as was done in the previous section), to try to estimate the safety factor of the entire dike. As a result, the points are not exactly on the linear line. A linear line was fitted through the data, while keeping the intercept fixed. This was done because the linear line has to go through this point, since this is the case with 0 kPa apparent cohesion. The figure shows that especially for the 11 m+NAP case, this results in a line that has some variation from the found points and that it slightly underestimates the increase in safety factor for low apparent cohesion.

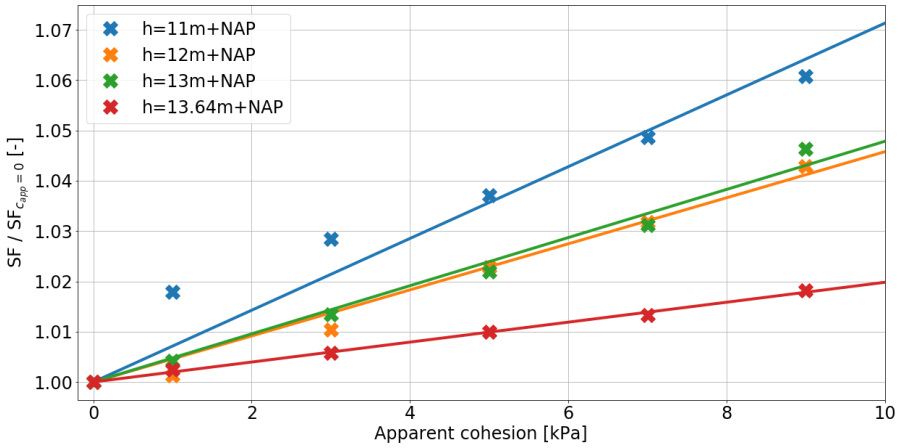

Figure 4.17: Safety factor for macro stability as a function of apparent cohesion

The only parameter to determine the relation between the relative safety factor and the apparent cohesion is the slope (included in Table 4.5) and has the following form:

$$\frac{SF}{SF_{c_{app}=0}} = a \cdot c_{app} + 1.0 \tag{26}$$

The slopes for the four cases are included in Table 4.5, in which also the SF for 0 kPa cohesion is included.

Table 4.5: Slopes of the linear relation between apparent cohesion and relative safety factor

River stage [m+NAP]	**slope a**	**SF$_{c_{app}=0}$ [–]**
11.00	0.0061	1.726
12.00	0.0049	1.446
13.00	0.0050	1.187
13.64	0.0020	1.205

With the found distributions and relationships, a Monte Carlo analysis was performed with 10^6 samples. The results of the simulation of both the apparent cohesion and the change in SF are included in Figure 4.18. In the figures the median of the sample is indicated in red and this shows that the median of the apparent cohesion is 3.63 kPa and that the median of the increase in the safety factor is 1.022. The median values and the 95% confidence intervals for the four cases are included in Table 4.6. The safety factor for the situation with no apparent cohesion (SF$_{c_{app}=0}$) is included in Table 4.5.

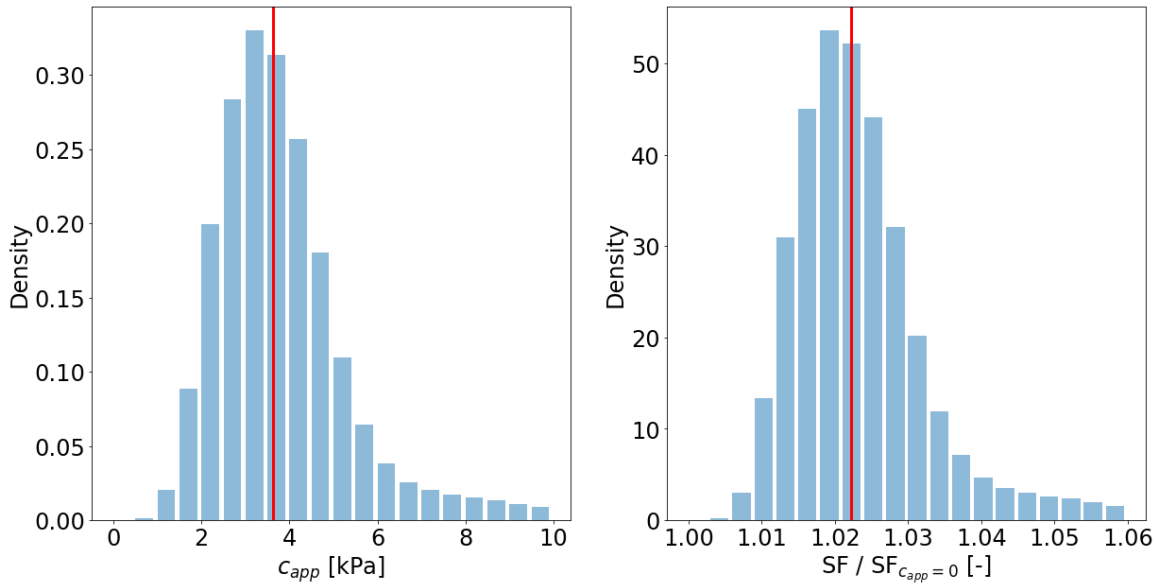

Figure 4.18: Histogram of the results of the apparent cohesion (left) and the influence on the safety factor (right) of a Monte Carlo simulation with 10^6 samples.

Table 4.6

River stage [m+NAP]	**Median c_{app} [kPa]**	**95% CI c_{app} [kPa]**	**median relative SF [–]**	**95% CI relative SF**
11.00	3.63	(1.72 – 8.56)	1.022	(1.011 – 1.052)
12.00	3.58	(1.65 – 8.51)	1.018	(1.008 – 1.04)
13.00	3.55	(1.62 – 8.52)	1.02	(1.008 – 1.042)
13.64	2.62	(1.22 – 6.21)	1.005	(1.002 – 1.012)

The table shows that both the expected apparent cohesion and the increase in safety factor are larger when the water table is lower in the dike. When the normative event is used (13.64 m+NAP), the expected factor of safety is 1.21, where we can be 95% sure that it is between 1.207 and 1.22. The safety factor without an added apparent cohesion is 1.205.

5 Discussion

The previous two chapters included the results of the sensitivity analysis and the scenario analysis. In this chapter the results will be interpreted and put in context. The objective of the research was to determine where in a dike cross-section an increase in soil strength due to suction can safely be included in stability analyses and under what conditions this is reasonable. To help reach this objective, several research questions were defined. These research questions were:

1. Which factors have a large influence on the development and reduction of soil suction?
2. When does suction result in a significant increase in the factor of safety of the macro stability?
3. What is the probability that a significant soil suction will remain present throughout a high water event in location (x_i, y_i) of the initially unsaturated zone?
4. What is the return period of full saturation of the cross section of the dike?

While the presented research in this report aimed at answering these research questions as complete as possible, several assumptions were made that potentially influenced the results. The structure of this chapter is such that first the results are interpreted, after which the limitations and other influences are discussed.

The results of the research show that the saturation of the soil previous to extreme events determines for a large part how the extreme event influences suction in the dike. This saturation is in turn a result of the external conditions that the dike was subjected to previous to the event. The characteristics of the soil layers in a dike have also shown to be of importance on the suction in the dike. From the theory it was already clear that sandy soils show different behaviour when compared to a clay, which is mainly due to the size of the grains and pores. However, the analyses have shown that also the soil water retention curves and hydraulic conductivity curves for different types of clay can have a large influence on the overall development and reduction of suction. The results suggest that the unsaturated parameters with the largest influence are the saturated hydraulic conductivity and the saturated water content.

The results in section 4.4 show that, for the suction to have a significant impact on the safety factor of the stability of the case study dike, the apparent cohesion that is added should be at least 5 kPa. However, when a dike is assessed that is just or just not sufficient according to the norm, a smaller cohesion might also result in a significant increase in the safety factor. Whether or not an apparent cohesion results in a significant strength increase depends also on the size of the unsaturated zone. This zone is larger during less extreme high waters in the river. The analysis in Section 4.4 raised the question how much extra strength a soil gains from suction. The theory in Section 2.4 showed that this is soil-specific and that it depends on the plasticity index, the unsaturated properties and on the effective friction angle. With these variations and the variations in suction in the cross section over the days, the Monte Carlo analysis in Section 4.5 showed the variations in apparent cohesion and safety factor that can be expected. These results showed that when the river stage is between 11.00 and 13.64 mm+NAP, the expected suction is between 0.5 and 1 meter during the months January, February and March and that the expected apparent cohesion is between 2 and 4 kPa. The analysis showed that when the river stage is higher, and hence the water table is higher, the expected average suction over the area is also less. This can be explained by that the area in the dike close to the ground surface is more easily influenced by the weather and the suction during wet months will generally be lower locally. For the normative event, the analysis shows that the increase of the safety factor is 0.02 - 0.12 %. In the case of the case study dike this can not be seen as a significant increase. However, since it also depends on the area that remains unsaturated, an apparent cohesion in this range might results in a significant increase for other dikes, where the crest is situated higher above the normative event. It should be noted that these results are based on the results from the 37 year analysis and therefore extremes events are not included in this.

The varying scenarios in Section 4.4 and the simplified Monte Carlo analysis in Section 4.5 were used to try to find an answer to the third and fourth research question. Initially, the intention was to perform a probabilistic analysis directly with a seepage model to determine what the probability is that a significant suction is present over a cross section. However, due to the large computational time of the 2D numerical model, this was not possible. Instead, the scenarios were calculated to observe how much suction is present during extreme conditions in the dike and to find the return period for the event that all suction is lost in the cross section. The results show that in winter precipitation events with a return period of 10 to 200 years and a median initial saturation

result in a total loss of suction. The results from the quasi-2D analysis based on the 37 year time-series show that this is in the order of 1 year. Therefore, the return period of full saturation is assumed between 1 and 10 years. If a high water event would occur after heavy rainfall, there would be no additional strength in the dike. However, that means that heavy precipitation and a high water event have to occur at the same time (or more specifically: the high water shortly after heavy precipitation). Determining the probability of that happening is difficult, since the two seem to be correlated. Since most high waters occur during winter, when suction is already low due to the relatively wet months and little evapotranspiration, this can not be ignored when estimating the probability. Due to time limitations, the combined probability of occurrence of such events could not be included in this research. However, this should be of interest for further research.

Modelling uncertainties and limitations

One of the limitations of the presented research is in the included variability of the parameters used to define the soil layers. Variations in soil properties were included, also in the part of the research where scenarios were calculated, but the curves were kept constant as the curves for clay soils that are included in the Staring series. The Staring series was initially used because it includes many soil samples, which are all collected in the Netherlands and there are no other databases of this size available. However, the samples that are used in the collection are all from soils collected in nature and from agricultural land, while dikes are man-made. As a result, clay in dikes is often compacted, which might change the (unsaturated) properties of the clay. Moreover, the core of the dike was modelled as a large layer with homogeneous soil properties. In reality it can be expected that there are layers in the dike core with varying properties, due to the historic build up of the dike and also within layers there will be some heterogeneity. Considering this, together with the results from the sensitivity analysis that show that the soil-specific parameters can have a large influence, it should be noted that actual suction might deviate from the values in this report. However, the presented research can be used as an indication of how much suction can be expected during daily and extreme conditions in a river dike with a clay core. It would be beneficial to have a better indication of the unsaturated properties of clay samples from dikes, where especially a better estimate of the saturated hydraulic conductivity would be useful.

Another source of uncertainty in the models, is in the way evapotranspiration is simulated. Evapotranspiration was calculated with the Penman-Monteith equations. For this calculation, some assumptions had to be made which, although substantiated, still include a large uncertainty. Examples of these assumptions are the average grass cover of the dike and the depth to which the roots of the grass extend (see appendix C). Since there are no measurements at the case study dike that can be used to calibrate the measurements to, the uncertainty remains. Nonetheless, we can compare the results (for example the plots of the median pressure heads in figure 4.3), to what is known in literature and from measurements at other locations. In the measurements of Deltares on dike section Oijen and Westervoort (along the Maas) suction of 80 kPa was measured at a depth of 1 meter. Comparing this to the results of the 1D model, it shows that the lower bound of the 95% confidence interval is around 4 meter suction, which is approximately half of what was measured by Deltares, although much higher suction is modelled at a depth of 0.5m. The difference in results can be due to the modelling assumptions, a different soil profile or due to different climatic conditions during the measurements. The models presented in this report assumed 'clean' clay, while in the specific dike section where Deltares measured, the clay is characterised as sandy clay. Also the time step of one day could be why this difference is observed, resulting in different infiltration and evapotranspiration rated than what is observed. The comparison that was made in Appendix B showed that the chosen time step of a day has an influence on the modelled pressure head, when compared to a time step of an hour. Since in reality precipitation intensities are also not constant over an hour, this could explain the differences between the measured suction by Deltares and the modelled suction in this report. To decrease uncertainty, it would be very beneficial to calibrate the models used in this report to field measurements of suction (or water content).

One more very important source of uncertainty is in the relation between suction in the soil and the apparent cohesion. With the help of the Monte Carlo analysis in Section 2.4, this uncertainty was included in the research. However, when comparing the results of that analysis to measurement data of Walrave (2021), deviations were found, especially for low suction values. Since these low suction values showed to be the important values for engineering practice in river dikes, the research results can be improved if this relationship can be adjusted or validated by more measurements.

Finally, the expected strength increase in Section 4.5 was calculated with a mean value of the suction over the unsaturated area. It is unclear if this assumption is reasonable, with respect to the expected strength increase. This could be improved by calculating the expected suction over smaller areas and modelling these areas with

varying apparent cohesion in the stability calculation.

6 Conclusion

The objective of the work presented in this report was to determine where in a dike cross section an increase in soil strength due to suction can be included in stability analyses. To reach this objective, a modelling study was performed with a cross section of an existing clay dike along the IJssel, in the eastern part of the Netherlands.

From the results it can be concluded that most of the time there is some suction present in the upper middle part of the cross section of the case study dike. However, when there is a long period with heavy rain, the water content increases such that the pressure heads are above 0 meter and suction is lost. Such an event has a return period between 1 and 10 years. Such an event occurs most likely during the winter months, when there is little evaporation or transpiration. It can therefore be concluded that based on these results, an increase in strength due to suction should not be included when assessing the stability of dikes, since a strength increase due to suction should only be included if we can be confident that that suction will be present during a high water event in the river. Moreover, high waters in the Rhine happen most of the time during the winter months, when suction can be expected to be already low on average.

The research showed that there are numerous factors that have an influence on suction in the case study dike. One of the most important factors that was found was the saturation of the soil previous to an (extreme) event. This showed to be of great importance to the influence of the event: a high saturation before a high water in the river, results in a higher water table in the dike during the event. Moreover, the results show that the properties of the clay in the dike that are used to determine the water retention curve and hydraulic conductivity curve have a large influence on suction in the dike. They have an influence on both the expected suction, as on the apparent cohesion of the soil given an amount of suction. Generally a clay with a low hydraulic conductivity and a high saturated water content results in less suction in a dike. Due to the low hydraulic conductivity the water in the soil will dissipate slow, which results in a high water content for a relatively long time. When a subsequent event occurs (either a high water in the river or precipitation), there is little water needed to fully saturate the soil and the hydraulic conductivity is higher. Moreover, evapotranspiration has a large influence on suction and is especially high during summer. In summer the water content in the upper layer of the dike is very low, which decreases the hydraulic conductivity locally to a great extent. As a result, during precipitation, water will run off instead of infiltrating in the soil. Moreover, a large part of the water that does infiltrate, will not reach the core of the dike, since it will mostly evaporate or be absorbed by the roots of grass. This process results in a large seasonality with respect to suction in the dike. Because of this, it is very unlikely that the dike will be fully saturated during summer, which was shown by various implemented scenarios. Even if a precipitation event with a duration of 13 days and a return period of 1,500 years occurs together with a high water with a return period of 1,250 years, it is likely that there will remain suction in the core of the dike. In the winter months the probability that all suction will disappear is higher, and the return periods of complete saturation varied between 1 and 10 years based on precipitation alone.

During wet months, the average suction in the unsaturated area is generally between 0.5 and 1.5 meter. The area over which this suction is present depends on the height of the water table and thus on the river stage. It was found that for this amount of suction, an apparent cohesion between 2 and 4 kPa can be expected. Subsequently, the increase in the factor of safety associated with these suction values is between 0.5 and 2%, where the influence of the suction decreases for higher river stages. For the normative event in the river, an increase in safety factor between 0.02 and 0.1% can be expected.

6.1 Recommendations

Based on the work in this report, some recommendations can be made for follow up research. Although the research has tried to provide a complete analysis regarding the uncertainties that are associated with modelling unsaturated/saturated flow problems, some assumptions had to be made due to time limitations or because they were outside the scope of the research. This can be improved in follow up research with the following recommendations.

Validation with measurements

As mentioned in the discussion chapter, uncertainties remain due to the lack of data for calibration. Although some uncertainty will always remain, confidence in the presented models can be increased by calibrating the models to measurements from the field. To do this, ideally suction is measured at various depths in the crest of

a dike, throughout a year. With measurements for calibration, also new insights can be gained regarding the soil specific parameters and the variations of these properties within the dike.

Increase confidence in soil-specific parameters

Another way to decrease uncertainties in the results of the models would be to increase confidence in the shape and variations of the water retention curves for clay soils in a dike. The research in this report showed that the unsaturated properties of clay in the core of a dike can have a significant influence on both the position of the water table during a high water event and to what extend the dike is influenced by the weather. In this research profiles from the Staring series were used, while it is unsure if clay that is used in dikes, usually compacted, has similar water retention curves. A few measurements of unsaturated properties of clay in dikes would already shine light on this, where especially the saturated hydraulic conductivity is a parameter of interest.

Soil models for unsaturated soil

The research showed that using an undrained soil model above the water table can result in a higher safety factor. This raises the question how the area that remains unsaturated should be modelled. Moreover, the research has shown that suction in the dike body can be as low as 0.2 meter and even completely disappear during winter. It is unclear if such low suction, in the area above the water table, behaves as an undrained material. A better understanding of clay soil that are near saturation, while above the water table, is needed.

References

Benson, C., Zhai, H., & Wang, X. (1994, 02). Estimating hydraulic conductivity of compacted clay liners. *Journal of Geotechnical Engineering; (United States)*, *120:2*. doi: 10.1061/(ASCE)0733-9410(1994)120:2(366)

Bishop, A. W. (1959). The principle of effective stress. *Teknisk Ukeblad*, *39*, 859-863.

Chbab, E. (2017). *Basisstochasten wbi-2017* (Tech. Rep.). Deltares.

Cheng, Y., & He, D. (2020, 08). Slope reliability analysis considering variability of shear strength parameters. *Geotechnical and Geological Engineering*, *38*. doi: 10.1007/s10706-020-01266-w

Chowdhury, M. (2020, 04). Elastic storage in aquifer.

Corey, A. (1977). Mechanics of heterogeneous fluids in porous media. *Water Resources Research*, 150.

de Kleine, D. (2021, 02). *High water in the ijssel river at derxen.* Retrieved from https://www.wdodelta.nl/hoogwater-in-de-zomer

Duong, T. T., Do, D. M., & Yasuhara, K. (2019). Assessing the effects of rainfall intensity and hydraulic conductivity on riverbank stability. *Water*, *11*(4). Retrieved from https://www.mdpi.com/2073-4441/11/4/741 doi: 10.3390/w11040741

Gillham, R. (1984). The capillary fringe and its effect on water-table response. *Journal of Hydrology*, *67*(1), 307-324. Retrieved from https://www.sciencedirect.com/science/article/pii/0022169484902488 doi: https://doi.org/10.1016/0022-1694(84)90248-8

GoogleEarth. (2021). *Lathumsedijk and surroundings 5159'10"n, 600'15"e, elevation 21 km.* Retrieved from https://earth.google.com/web/

Heinen, M., Bakker, G., & Wösten, J. (2020). *Waterretentie- en doorlatendheidskarakteristieken van boven- en ondergronden in nederland: de staringreeks: Update 2018* (No. 2978). Wageningen Environmental Research. (Project number: KB-33-001-021) doi: 10.18174/512761

Jamalinia, E., Vardon, P. J., & Steele-Dunne, S. C. (2020). The impact of evaporation induced cracks and precipitation on temporal slope stability. *Computers and Geotechnics*, *122*, 103506. Retrieved from https://www.sciencedirect.com/science/article/pii/S0266352X20300690 doi: https://doi.org/10.1016/j.compgeo.2020.103506

Kanning, W., Teixeira, A., van der Krogt, M., & Rippi, K. (2017). *Derivation of the semi-probabilistic safety assessment rule for inner slope stability* (Tech. Rep.). Deltares.

Kroes, J., van Dam, J., Bartholomeus, R., Groenendijk, P., Heinen, M., Hendriks, R., ... van Walsum, P. (2017). *Swap version 4: Theory description and user manual* (No. 2780).

Le, H. T., Verhagen, H. J., & Vrijling, H. (2016). Damage to grass dikes due to wave overtopping. *Natural Hazards*, *86*, 204-224. doi: https://doi.org/10.1007/s11069-016-2721-2

Morel-Seytoux, H. J., Meyer, P. D., Nachabe, M., Tourna, J., van Genuchten, M. T., & Lenhard, R. J. (1996). Parameter equivalence for the brooks-corey and van genuchten soil characteristics: Preserving the effective capillary drive. *Water Resources Research*, *32*(5), 1251-1258. Retrieved from https://agupubs.onlinelibrary.wiley.com/doi/abs/10.1029/96WR00069 doi: https://doi.org/10.1029/96WR00069

Mualem, Y. (1976). A new model for predicting the hydraulic conductivity of unsaturated porous media. *Water Resources Research*, *12*(3), 513-522. Retrieved from https://agupubs.onlinelibrary.wiley.com/doi/abs/10.1029/WR012i003p00513 doi: https://doi.org/10.1029/WR012i003p00513

Rehman, Z. u., Mahmood, K., Kim, J., & Ashraf, M. (2015, 08). The effect of soil type on matric suction and stability of unsaturated slope under uniform rainfall. *KSCE Journal of Civil Engineering*, *20*, 1294-1299. doi: 10.1007/s12205-015-0796-z

Richards, L. A. (1931, November). Capillary Conduction of Liquids Through Porous Mediums. *Physics*, *1*(5), 318-333. doi: 10.1063/1.1745010

Rijkswaterstaat. (2018). *Verhanglijn rijn.* Retrieved from https://www.helpdeskwater.nl/@245949/betrekkingslijnen-rijn/

Rijkswaterstaat. (2020). *Lobith: waterstanden en afvoeren.* Retrieved from https://www.rijkswaterstaat.nl/water/waterdata-en-waterberichtgeving/waterdata/lobith-waterstanden-en-afvoeren

Rijkswaterstaat. (2021). *Hoogwaterbeschermingsprogramma (hwbp).* Retrieved from https://www.rijkswaterstaat.nl/water/waterbeheer/bescherming-tegen-het-water/maatregelen-om-overstromingen-te-voorkomen/hoogwaterbeschermingsprogramma

Ronen, D., Scher, H., & Blunt, M. (2000). Field observations of a capillary fringe before and after a rainy season. *Journal of Contaminant Hydrology*, *44*(2), 103-118. Retrieved from https://www.sciencedirect.com/science/article/pii/S0169772200000966 doi: https://doi.org/10.1016/S0169-7722(00)00096-6

Szymkiewicz, A. (2013). *Modelling water flow in unsaturated porous media.* doi: 10.1007/978-3-642-23559-7

Vanapalli, S. (2001, 09). A simple experimental procedure for determining the fitting parameter, for predicting the shear strength of an unsaturated soil..

Vanapalli, S., Fredlund, D., Pufahl, D., & Clifton, A. (1996, 01). Model for the prediction of shear strength with respect to soil suction. *Canadian Geotechnical Journal - CAN GEOTECH J*, *33*, 379-392. doi: 10.1139/t96-060

Vanapalli, S., Wright, A., & Fredlund, D. (2000, 10). Shear strength behavior of a silty soil over the suction range from 0 to 1,000,000 kpa..

Van der Meer, M., Niemeijer, J., Post, W., & Heemstra, J. (2004). *Technisch rapport waterspanningen bij dijken.*

van Duinen, A. (2014, 07). *Memo: Ongedraineerde schuifsterkte bij toetsspoor macrostabiliteit in wti 2017 - informatie voor besluitvormingsproces* (Tech. Rep.). Deltares.

van Genuchten, M. T. (1980). A closed-form equation for predicting the hydraulic conductivity of unsaturated soils. *Soil Science Society of America Journal*, *44*(5), 892-898. Retrieved from https://acsess.onlinelibrary.wiley.com/doi/abs/10.2136/sssaj1980.03615995004400050002x doi: https://doi.org/10.2136/sssaj1980.03615995004400050002x

van Meurs, G., & Kruse, G. (2017). *Update inzichten in gebruik van klei voor ontwerp en uitvoering van dijkversterking* (Tech. Rep.). Deltares.

van Woerkom, T. (2021). *From dike history to reinforcement practice.* Retrieved from https://storymaps.arcgis.com/stories/2d14e8423ce445ffa336dcb24f04ca1f

Vogel, T., Cislerova, M., & Šír, M. (1985, 01). Reliability of indirect estimation of soil hydraulic conductivity. *Vodohosp Cas*, *33*, 204-224.

Vogel, T., Van Genuchten, M., & Cislerova, M. (2000, 11). Effect of the shape of soil hydraulic functions near saturation on variably-saturated flow predictions. *Advances in Water Resources*, *24*, 133-144. doi: 10.1016/S0309-1708(00)00037-3

Walrave, N. (2021). The influence of initially unsaturated clay on the macro-stability of river dikes. Retrieved from https://repository.tudelft.nl/islandora/object/uuid%3A1fc4c228-06f2-4872-afe2-31c408f74748

Wösten, J., Veerman, G., de Groot, W., & Stolte, J. (2001). *Waterretentie- en doorlatendheidskarakteristieken van boven- en ondergronden in nederland: de staringreeks: Vernieuwde uitgave 2001.* Wageningen, Alterra, Research Instituut voor de Groene Ruimte. (Alterra-rapport 153)

A Analysis of the soil data

The research in this report is centered around the case study dike. In this appendix, the schematization of the cross section is presented. The dimensions of the dike were readily available, so only the varying soil layers had to be determined.

Schematization of the cross section

The available data of the soils are presented in table A.1.

Type of data	Location of the data	Quantity
CPT	Crest	6
CPT	Halfway in the slope	8
Manual boring	Crest	14
Manual boring	halfway in the slope	9
Mechanical boring	Berm	1

Table A.1: Available data of the Lathumsedijk, Duiven.

With this data, first the different layers in the dike were determined with the CPTS. From these CPTS, the governing one was chosen and and the layers were schematized. The final schematization of the cross section is included in figure A.1.

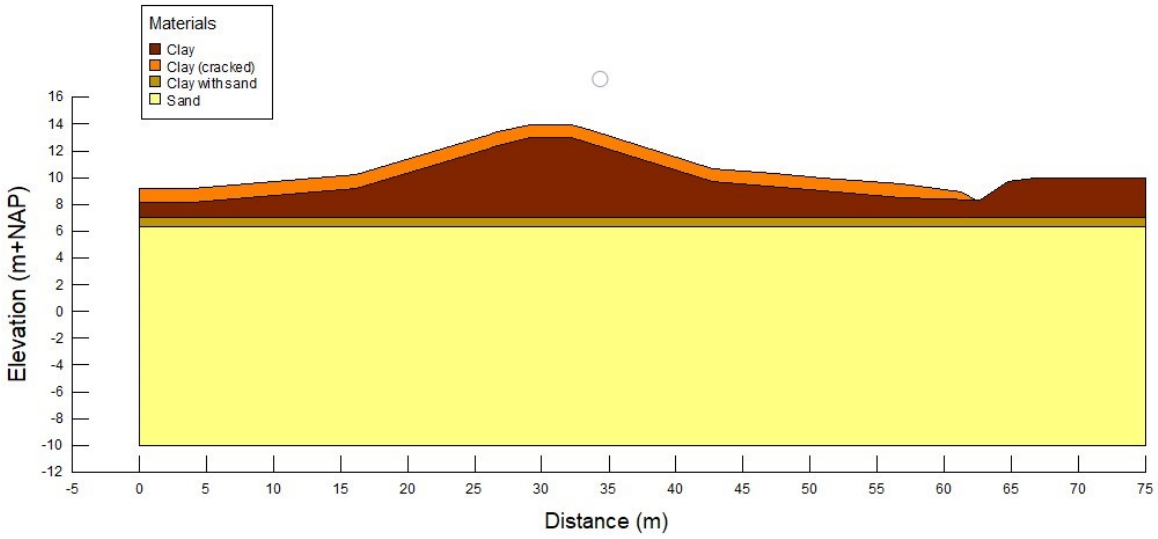

Figure A.1: Schematization of the cross section of the Lathumsedijk Duiven used as a case study in this report.

When analysing the CPTs and schematizing the cross section, the following observations were made.

- The CPTs that were performed in the crest show that the crest of the dike is between 13.93 and 13.98 m+NAP. Following the existing cross section, a height of 13.95 m+NAP was used in all analyses.
- Over the different CPTs, the heights of the layers varied slightly. The CPT that was chosen as the governing one, was the CPT where the aquifer was at the lowest elevation, and the blanket layer and clay core were thus largest (in vertical direction).
- From boring B001 it follows that the upper sand layer is coarse sand with some gravel and that it is brown. This layer is also the layer where cracks are present.
- From the CPTs and borings, it could not be derived what the (unsaturated) properties are of the varying layers. In the analyses in thesis report a variation in the parameters is included based on Heinen et al. (2020), as given in Table A.2. The parameters used for the sandy clay layer and the aquifer were fixed in this report. These layers are generally below the water table, and can thus be modelled as saturated layers. Therefore the unsaturated properties did not have to be determined.

- In some CPTS a small sand layer could be identified in the clay core of the dike. Due to time limitations, these variations within the core of the dike were not included in the analyses in this report. The clay core and the blanket layer were schematized as a layer with homogeneous properties. The effect of these layers with varying soil properties is unknown.
- The historic build up of the dike is not included in the schematized cross section. Over the years, the dike has been heightened numerous times. These extra added layers might have varying properties. In the CPTs this could not be observed. Due to time limitations, possible variations in the different historic layers are note included in the cross section.
- The case study dike has a road in the crest of the dike, which is a cycling path made of asphalt concrete. This asphalt concrete is highly impermeable and water can not penetrate. Water that falls on the road as precipitation will run off to the side of the road, where it can infiltrate the dike, or it will run off the dike. If it infiltrates the dike next to the road, it will enter a sandy layer on which the road is constructed. The water will spread out under the dike and enter the cracked layer. Generally, the road will act as a barrier and will result in more run-off over the dike and less infiltration into the soil. Since this is not the normative situation and many river dikes do not have such a road on the crest of the dike, the decision was made to not include it in the analyses. Instead, the cross-section was made without the road and it was assumed that the cracked layer is also present there.

Table A.2: Variation of the (unsaturated) soil parameters used in the research in this report (after Heinen et al. (2020))

Soil layer	θ_r **[-]**	θ_s **[-]**	α **[1/m]**	**n [-]**	K_s **[cm/day]**
Clay	0.01	[0.448 – 0.591]	[1.28 – 2.16]	[1.091 – 1.135]	[0.383 – 6.31]
Clay cracked	[0.0 – 0.1]	[0.401 – 0.433]	[0.7 – 1.83]	[1.248 – 1.278]	[1.75 – 14.58]
Clay + sand	-	-	-	-	8.64
Sand	-	-	-	-	22.32

Atterbergse limits

From the manual borings there is data available regarding the Atterbergse limits. This is of interest in this report since the plasticity index influences the relationship between apparent cohesion and suction (see Section 2.4) and because the soil of the case study dike can be compared to other clay types. For multiple samples the Atterbergse limits were determined. the samples showed that the lutum content of the clay in the dike has a mean of 33[%] and a standard deviation of 13 [%]. This means that most samples of the clay can be characterized as a light to medium heavy clay according to Heinen et al. (2020). However, some samples have a lutum content larger than 50, which indicates a heavy clay.

The plasticity index of the different samples are plotted in Figure A.2, where the elevation of the samples is indicated on the y-axis. The figure shows that most samples have a plasticity index around 20-25 [%]. In the figure also the unit weight is given.

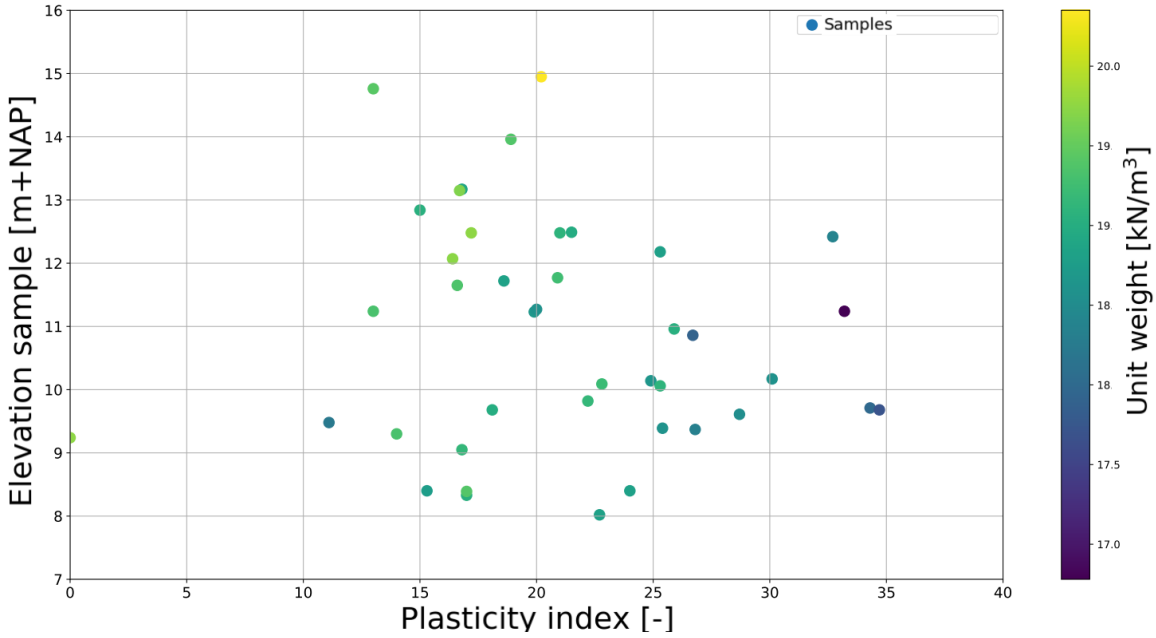

Figure A.2: Plasticity index of the samples taken in the dike, plotted over the elevation of where the sample was taken. The unit weight is indicated by the color.

To use the information about the plasticity index in the analysis, a distribution has to be fitted to the data. A Lognormal distribution showed to be te best fit (Figure A.3), although the figure shows that the distribution varies from the data for the upper part and lower part. Since the sample is relatively small and no better fitting distribution could be found, this Lognormal fit is accepted.

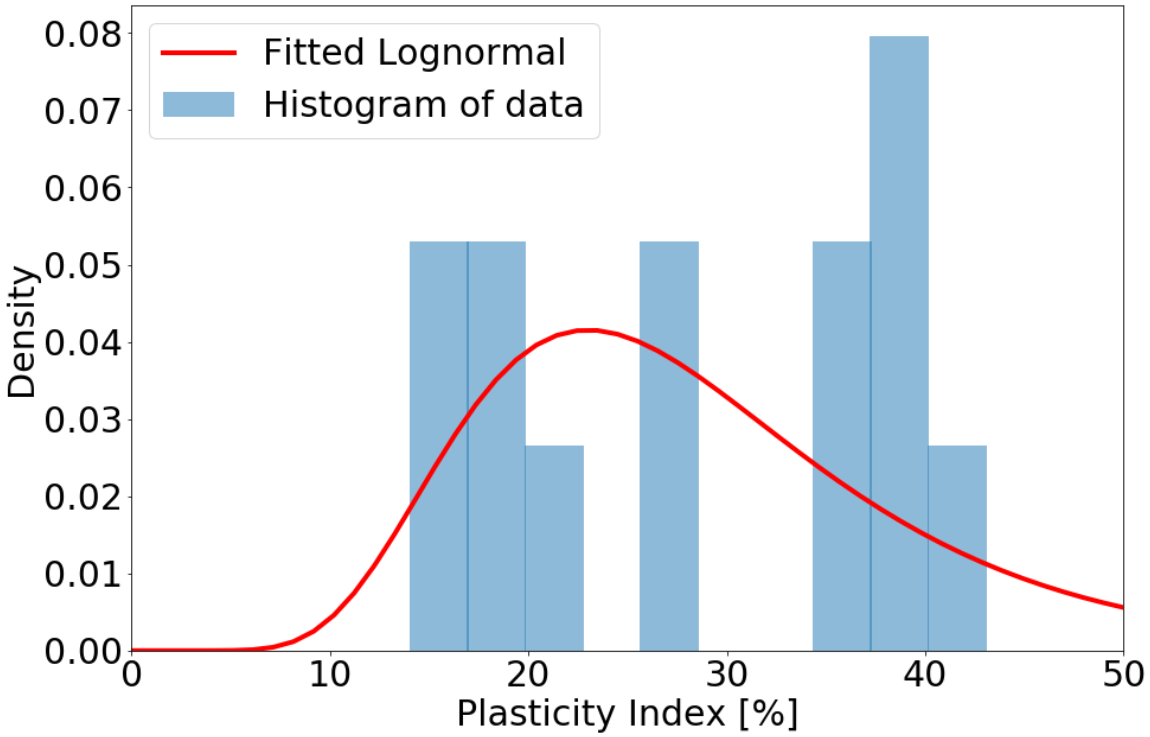

Figure A.3: Histogram of the plasticity index and a fitted Lognormal distribution with parameters shape=0.39, location=0 and scale=26.7.

B The effect of averaging precipitation and evapotranspiration

The time steps that are used in the analyses in this report are all one day. When modelling the rising river level, this is generally valid as this is a relatively constant process (see for example figure 3.6). For precipitation this is different. The precipitation pattern over a day is a random pattern with varying intensities. By using the amount of precipitation that falls in one day in a time, the results of a simulation might vary a lot from what is seen in reality. When suction is high at the surface of a soil, the hydraulic conductivity is locally very low. When precipitation falls on that soil, it will infiltrate with the rate of the hydraulic conductivity and the rest of the infiltration will run off. This is especially true for a dike (due to the slope) since ponding can not occur. When an average of a day is taken of the precipitation, really the intensity is lower (the rain event is spread out after all). When applying this to the numerical model, a larger part of the precipitation might 'infiltrate' in the soil than what is observed in reality. On the other hand, a precipitation event with a higher intensity results in a larger wetting front. In that way, averaging over a day might be an underestimation (since hydraulic conductivity will be larger in reality and there is a larger gradient).

To validate the chosen time step, or at least be aware of its implications, two comparison calculations were made between a simulation with hourly precipitation data and with daily precipitation data. Naturally, hourly precipitation data is also already an average. The first comparison calculation was made for a relatively wet year (1998, figure B.1) for a relatively dry year (2003, figure B.2) . The set-up of the calculation was a 1D soil column with a height of 5 meters and the water table 4 meter below the top of the soil column. The top 1 meter of the column was characterized with soil properties similar to Staring series B07, and the bottom layer with Staring series B12. For both calculations, the median pressure head in July and December were plotted, together with the 95% confidence interval to indicate the variation.

The results for the relatively wet year for the two simulations are very similar. Only a small underestimation during summer can be observed for the simulation with daily data. The figure suggests that the schematization of daily precipitation is valid, when compared to daily precipitation. The results in figure B.2 for the relatively dry year show larger variations, also during winter. It is interesting that during winter, the daily weather records result in an overestimation of the pressure head, while during summer they result in an underestimation of the pressure head. This can be if there are large peaks in precipitation and radiation, that deviate a lot from the average. The figure shows that by using daily weather data, the pressure head is around 0.5 higher than when calculating with hourly data. As mentioned, also hourly data is averaged and the pressure heads observed in real life probably deviates more.

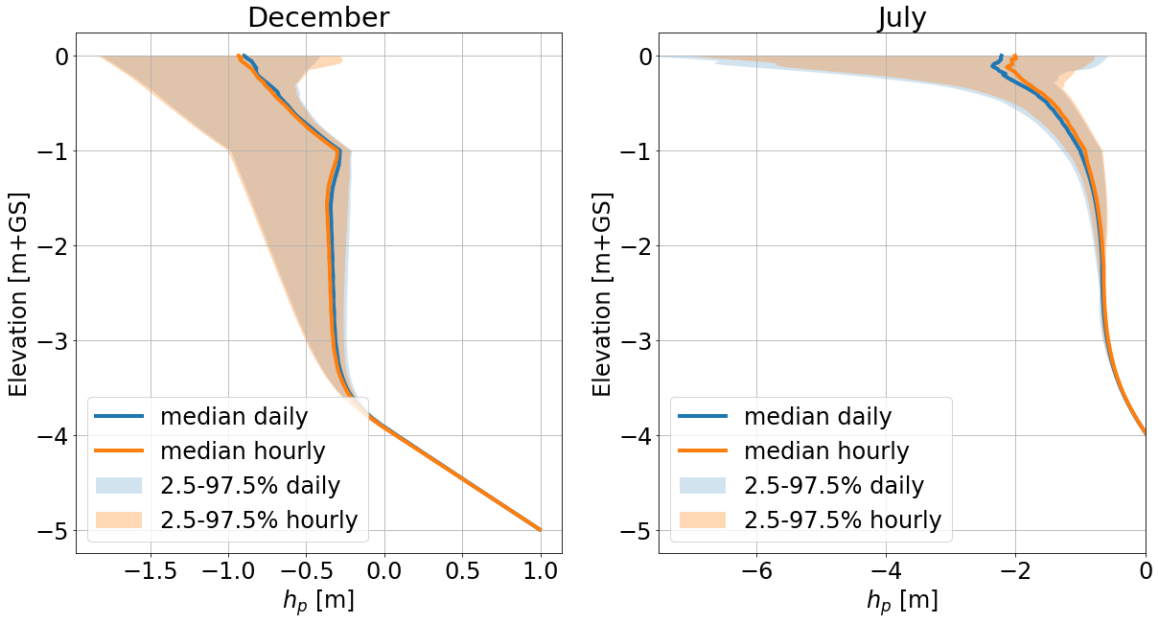

Figure B.1: Median pressure head and 95% confidence interval in December and July 1998 for an analysis with hourly and daily precipitation data

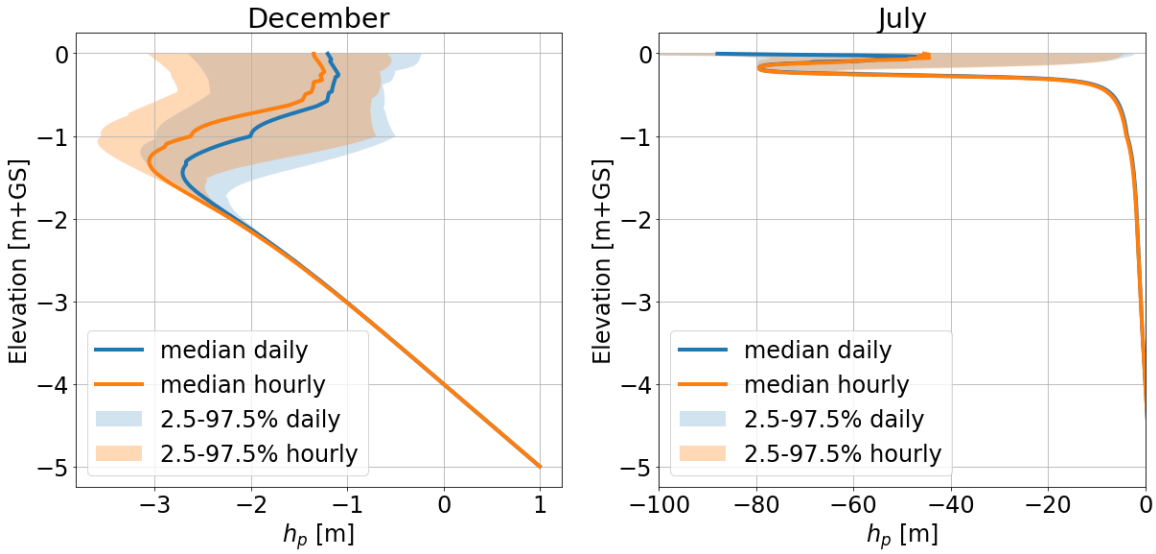

Figure B.2: Median pressure head and 95% confidence interval in December and July 2003 for an analysis with hourly and daily precipitation data

C Simulating evapotranspiration with SWAP

Measuring evapotranspiration fluxes is not as easy as measuring precipitation and therefore it has to be calculated with the help of models. In SWAP there are multiple ways to simulate both evaporation and transpiration. In this chapter an overview of the theory as well as justification for the chosen parameter is given. The different chosen parameters and models are included to ensure the repeatability of the research.

Transpiration of water happens due to the extraction of water through the roots of plants, which happens throughout the depth over which the roots extend. On the other hand, evaporation happens only at the ground surface. As a result, during a dry period evaporation fluxes will decrease very fast while transpiration might continue for a longer period. The method applied in this research can be split up in the following steps:

1. Basic meteorological data is used as input.
2. The Penman-Monteith formula is used with reference data for a uniform grass cover to calculate the potential evaporation and potential transpiration of a dry grass land.
3. The potential evapotranspiration is split up into potential evaporation and potential transpiration based on how much of the soil is covered.
4. The actual transpiration is calculated based on the potential transpiration and on the water content in the root area.
5. The actual evaporation is calculated based on the potential evaporation, the water content in the soil and a maximum soil water flux.

The steps will be elaborated in the following sections.

Potential evapotranspiration

First the potential evaporation and transpiration are determined based on the atmospheric conditions and on the characteristics of the plants with the help of the Penman-Monteith formulas for transpiration and evaporation as presented in equation 27 and 28.

$$T_p = \frac{(1 - W_{\text{frac}}) \left(V_{\text{c}} \frac{\Delta_{\text{v}}}{\lambda_{\text{w}}} (R_{\text{n}} - G) + \frac{p_1 \rho_{\text{a}} C_{\text{a}}}{\lambda_{\text{w}}} \left(\frac{e_{\text{sat}} - e_{\text{a}}}{r_{\text{a,can}}} \right) \right)}{\Delta_{\text{v}} + \gamma_{\text{a}} \left(1 + \frac{r_{\text{s,min}}}{r_{\text{a,can}} LAI_{\text{eff}}} \right)} \tag{27}$$

$$E_{\text{p}} = \frac{(1.0 - V_{\text{c}}) \frac{\Delta_{\text{v}}}{\lambda_{\text{w}}} (R_{\text{n}} - G) + \frac{p_1 \rho_{\text{a}} C_{\text{a}}}{\lambda_{\text{w}}} \left(\frac{e_{\text{sat}} - e_{\text{a}}}{r_{\text{a, soil}}} \right)}{\Delta_{\text{v}} + \gamma_{\text{a}} \left(1.0 + \frac{r_{\text{soil}}}{r_{\text{a, soil}}} \right)} \tag{28}$$

The different variables are elaborated on in the following table.

Table C.1: Variables used to calculate potential evaporation and transpiration.

Variable	Description	Unit	Value
T_p	Potential transpiration of a dry canopy	d^{-1}	calculated
W_{frac}	Fraction of time that the crop is wet	[-]	Based on precipitation data
V_c	Vegetation cover	[-]	calculated with LAI and light extinction
Δ_v	slope of the vapour pressure curve	kPa $C-1$	Calculated with temperature and saturation vapour pressure
λ_W	Latent heat of vaporization	Jkg^{-1}	calculated with air temperature
R_n	Net radiation flux at the canopy	$Jm^{-2}d^{-1}$	difference between incoming and outgoing radiation
G	Soil heat flux	$Jm^{-2}d^{-1}$	0
p_1	Unit conversion factor	sd^{-1}	86400
ρ_a	Density of air	kgm^{-3}	calculated with air temperature
C_a	Heat capacity of moist air	$\mathrm{kg}^{-1}\mathrm{°C}^{-1}$	calculated with λ_W, γ_a, and air pressure
e_{sat}	Saturation vapour pressure	kPa	calculated with air temperature
e_a	actual vapour pressure	kPa	calculated with air temperature
$r_{a,can}$	aerodynamic resistance of canopy	sm^{-1}	calculated with crop height, windspeed factor and vegetation cover
γ_a	Psychometric constant	$kPa°\mathrm{C}^{-1}$	-
$r_{s,min}$	minimal stomatal resistance	sm^{-1}	
LAI_{eff}	effective leaf area index	[-]	3.0
r_{soil}	soil resistance of a wet soil	sm^{-1}	30
$r_{a,soil}$	actual soil resistance	sm^{-1}	Calculated with V_c

For a more in depth elaboration of the calculation of the varying factors, the reader is referred to (Kroes et al., 2017). The assumed values that were used in the analyses are included here.

Transpiration due to grass

One of the most important assumptions that has to be made is the rooting depth of the grass. A value of 0.3m was chosen since Le et al. (2016) found that most roots in a dike are within the upper 0.3m of the soil. A constant root density was used. For the height of the grass, a constant value of 0.12m over the year was used. No rainfall interception was applied, assuming that all rain that reaches the grass will also reach the soil.

D Statistics of discharges and river levels

Obtaining statistics of water levels and discharges is not as straight forward as obtaining, for example, statistics of precipitation. Discharges in the river are not only influenced by meteorological aspects, but also by the management of the river upstream. The Rhine river for instance, is heavily managed in both Switzerland and Germany, which influences the discharges that we measure in the Netherlands. The most recent statistics used in the Netherlands are based on simulations with GRADE that can take such things into consideration. The statistics from GRADE include the median and 95% Confidence Interval (CI) of the discharge at Lobith. The discharge at Lobtih can be translated to river levels at different locations with a stage-relation curve. The stage-relation curve for the discharge at Lobith and the location of the case study dike is presented in the following figure. For the highest discharge linear extrapolation was used from the four highest measured data points to obtain a linear line and estimate the highest water levels.

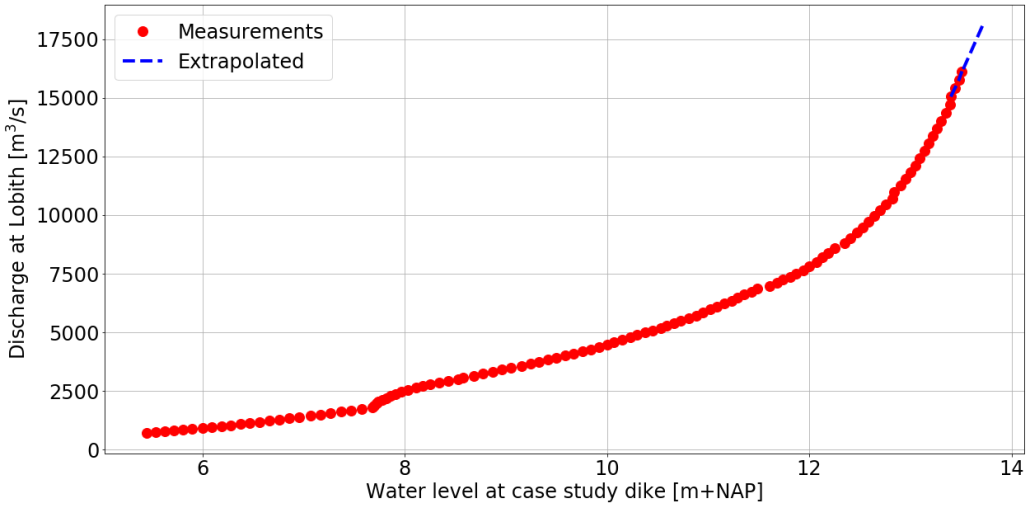

Figure D.1: Stage-relation curve for the discharge at Lobith and the water level at the case study dike, situated at 'dijkpaal 883' (after (Rijkswaterstaat, 2018))

With the stage-relation curve, the height of the water levels where determined with linear interpolation between the points for discharges with varying return period. The discharges according to GRADE and their 95% CI and the calculated water levels are included in table D.1 (Chbab, 2017).

Table D.1: Return periods of the discharges in the Rhine at Lobith and their 95% confidence interval (after (Chbab, 2017)) together with the translation to the water level in the river at the case study dike, based on the empirical stage discharge relation.

Return period [yr]	**Discharge Lobith [m^3/s]**	**95% CI Discharge [m^3/s]**	**Water level at Lathumsedijk [m+NAP]**	**95% CI water level [m+NAP]**
2	5,940	5,280 - 6,600	11.0	(10.59 - 11.36)
10	9,130	8,160 - 10,100	12.44	(12.12 - 12.67)
100	12,770	11,400 - 14,150	13.15	(12.92 - 13.32)
1,250	14,970	13,720 - 16,230	13.40	(13.26 - 13.52)
3,000	15,520	14,060 - 16,980	13.45	(13.31 - 13.60)
10,000	16,270	14,450 - 18,100	13.53	(13.36 - 13.71)

E The influence of the clay type on the height of the phreatic surface: Hydrostatic conditions

An analysis was done to observe the influence of the chosen soil properties of the clay core on the development of the phreatic surface for a situation with a hydrostatic initial condition. The motivation for this analysis were the results presented in chapter 3.4, where the progression of the water table initially seemed to be faster for soil with a lower saturated hydraulic conductivity. In the mentioned analyses, an initial surface flux of 0.1mm/day was used for the steady state calculation of the initial condition. The properties of the clay types that were used in the analysis are included in table E.1.

Table E.1: Parameter ranges in the Staring series (Heinen et al., 2020)

Staringseries number	θ_r **[-]**	θ_s **[-]**	α **[1/cm]**	**n [-]**	K_s **[cm/day]**
Clay layer					
B10	0.01	0.448	0.0128	1.135	3.83
B10·0.1	0.01	0.448	0.0128	1.135	0.383
B10·10	0.01	0.448	0.0128	1.135	38.3
B11	0.01	0.591	0.0216	1.107	6.31
B12	0.01	0.530	0.0166	1.091	2.25

A hydrostatic initial condition is present when there is no rain or evaporation present and the pressure head along a vertical section will be linear. The other soil characteristics, initial- and boundary conditions used in the calculation were as follows:

- The cracked layer has properties of a Staring series B07 soil.
- The sandy clay layer at approximately 7.00 meter NAP has properties of a Staring series O08 soil.
- The sand layer has properties of a O01 soil.
- The initial water level is 7.00 m+NAP.
- After t=0 the water level is heightened in one step to 13.96m+NAP and the polder level is at 9.50m+NAP.

The rise of the water table along sections S1-S4 were plotted over time and included in figure E.1.

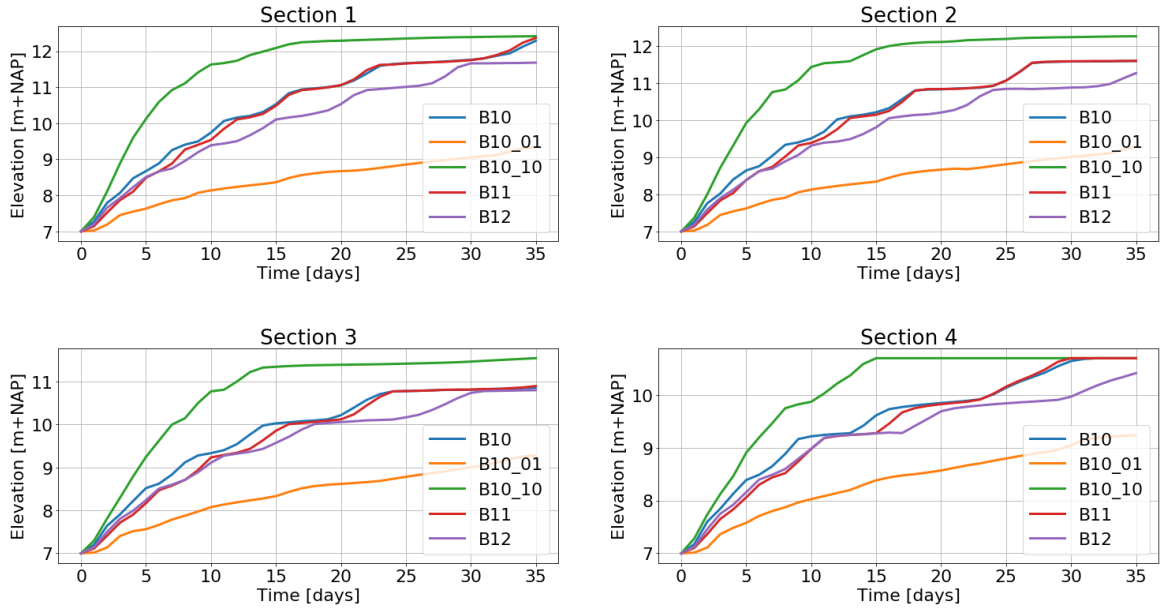

Figure E.1: The rise of the water table over time along sections S1-S4 for a situation with an initial condition without infiltration.

The figure shows that for this situation with a hydrostatic initial condition, the water table progresses fastest for the soils with a higher hydraulic conductivity. This shows that the results included in section 3.4, indeed are the result of the non-zero surface flux. This flux ensures a different steady state condition for each soil type, which is dependent not only on K_s, but also on the parameters that describe the water retention curve. The steady state situation for clay with properties B12, is a situation with a much higher water content, which results in a hydraulic conductivity that is initially higher than a situation with a soil with a higher hydraulic conductivity.

F Results 36 year analysis

This appendix includes the results and observations of the analysis of a 1D soil column that is subjected to real weather data from meteorological weather station De Bilt over the years of 1980 - 2016. The objective of the analysis was to find what (combinations of) events lead to full saturation of a 1D soil column with water tables 7 and 4 meters below ground surface (GS) respectively. The first situation is representative for a vertical section through the crest of the dike, when there are daily conditions at the case study dike. The second situation is representative for a vertical section through the crest during a high water that occurs approximately once per year. The analysis showed that there were 8 moments over the duration of the analysis when complete saturation occurred at a depth of -2m. From those 8 events, 5 resulted in complete saturation of the entire soil column when the water table is 4 meters below GS and 2 events resulted in complete saturation of the soil column with the water table 7 meters below GS. The 8 events are summarized in table F.1. Events 5 and 6 are only 4 days apart, but are included as separate events in this part so no information about the time influence of rain is lost. Before event 5, the initial pressure head in the top of the soil column is already high, although deeper in the soil column the pressure head is not very high. Due to the precipitation that leads to event 5 and the initial pressure head that is high at the top of the soil column, the pressure head is already greater than 0 when event 6 starts, resulting in a very large increase in the pressure head over the entire soil column. Moreover, although events 1, 2 and 3 do not result in complete saturation at the bottom of the profile, the pressure head is very close to one and the strength increase due to suction will be negligible. For every event, a plot is included of the pressure heads (-7 - 14 days relative to the event) and the precipitation that occurred a week before the event in figure F.1.

Table F.1: Summary of the events that led to complete saturation of the soil at a depth of -2m+GS.

Event number	**First day of saturation**	**Season**	**Saturation of entire soil column WT = -4m**	**Saturation of entire soil column WT=-7m**
1	1981-03-13	Winter	Yes	No
2	1994-01-01	Winter	Yes	No
3	1994-12-30	Winter	Yes	No
4	1998-03-09	Winter	No	No
5	1998-10-30	Autumn	Yes	Yes
6	1998-11-03	Autumn	Yes	Yes
7	2003-01-04	Winter	No	No
8	2004-01-21	Winter	No	No

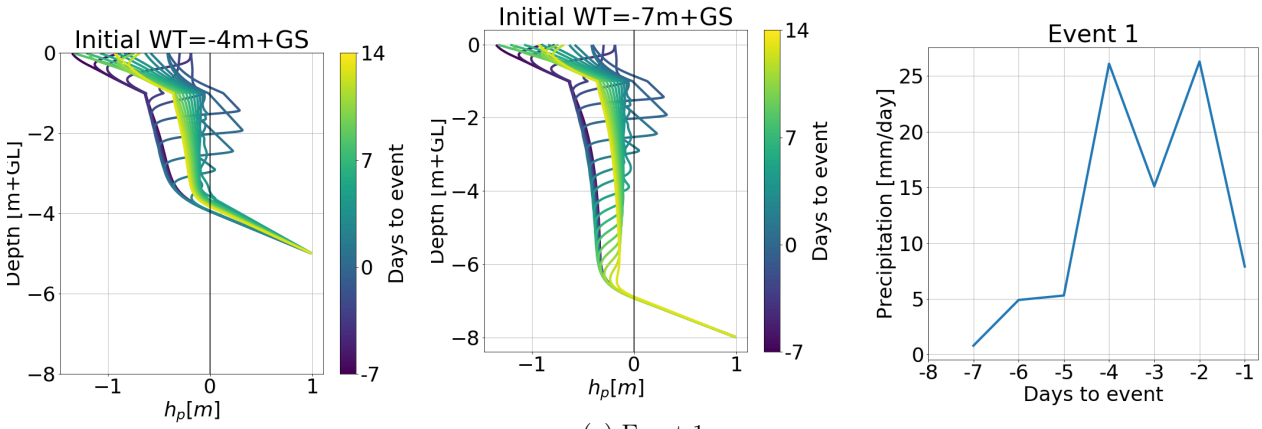

(a) Event 1

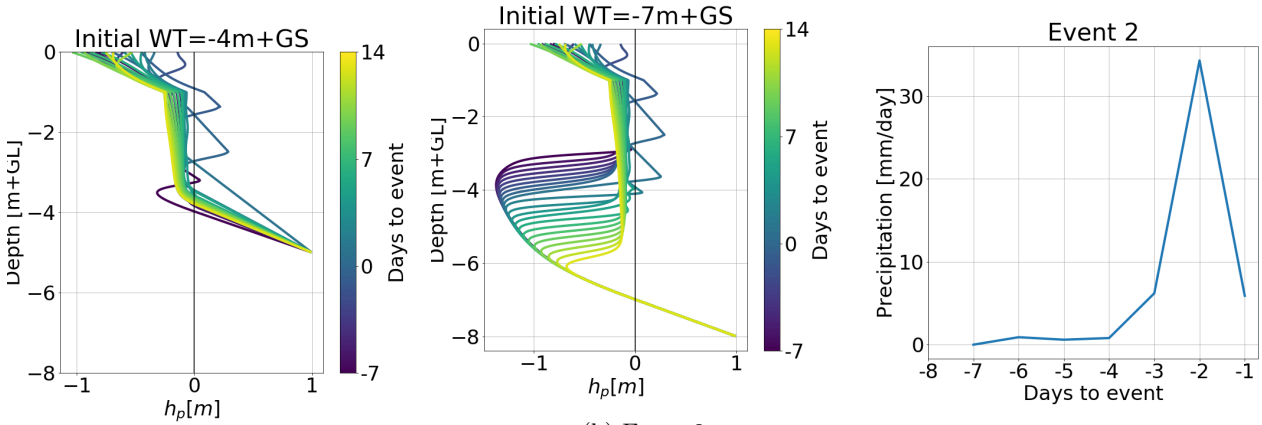

(b) Event 2

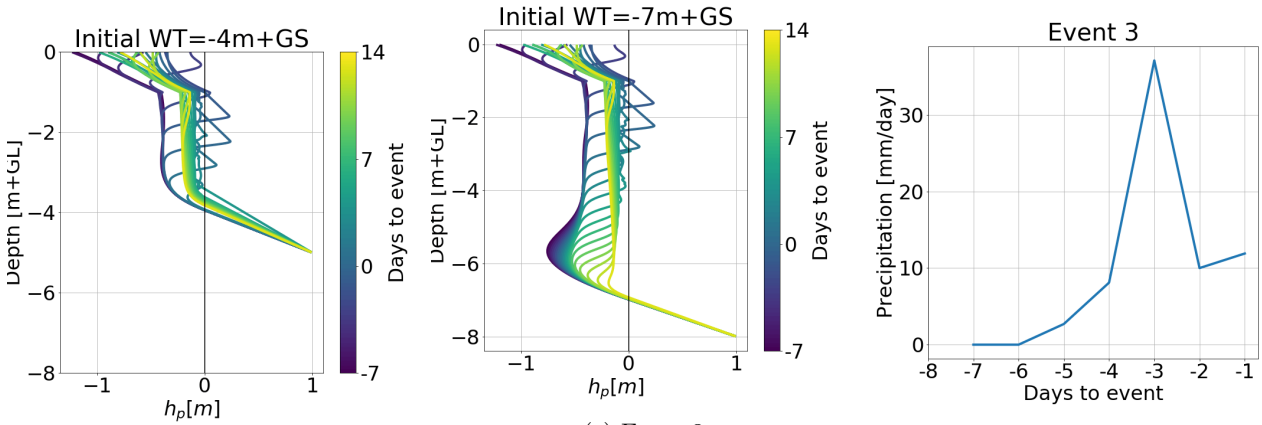

(c) Event 3

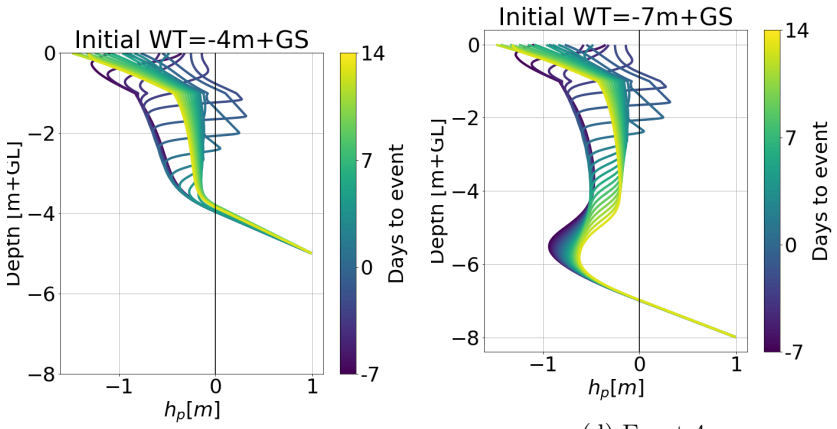

(d) Event 4

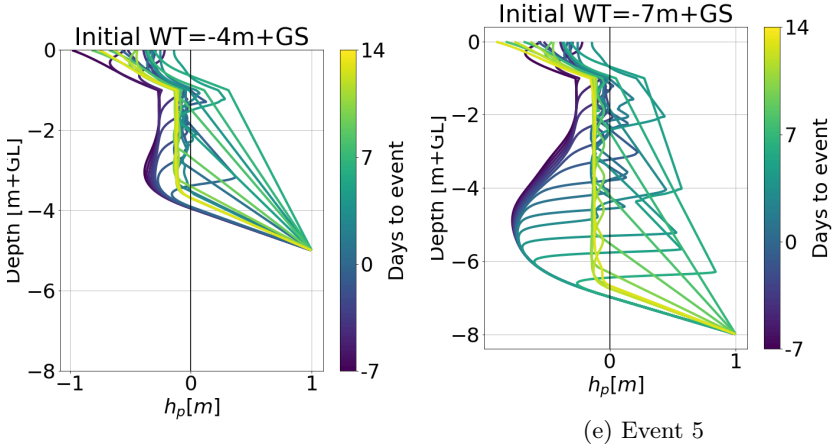

(e) Event 5

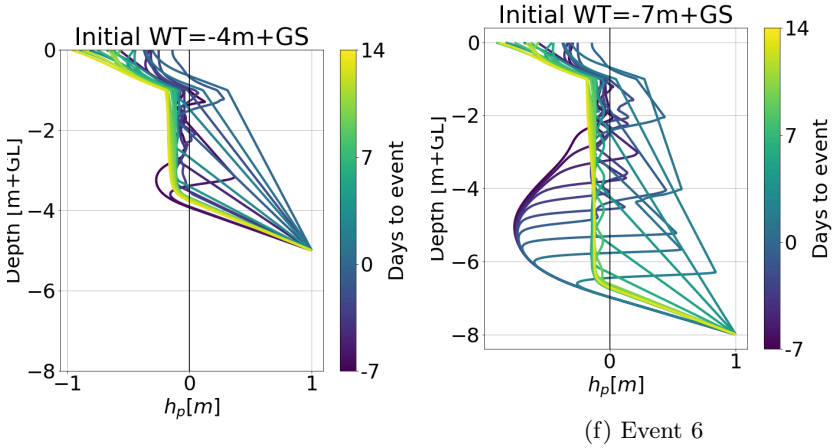

(f) Event 6

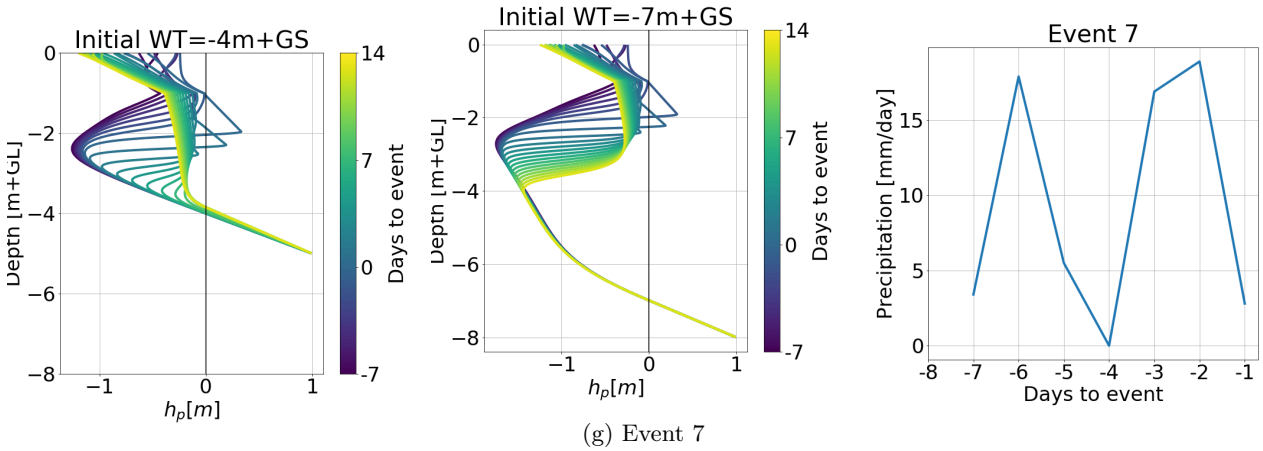

(g) Event 7

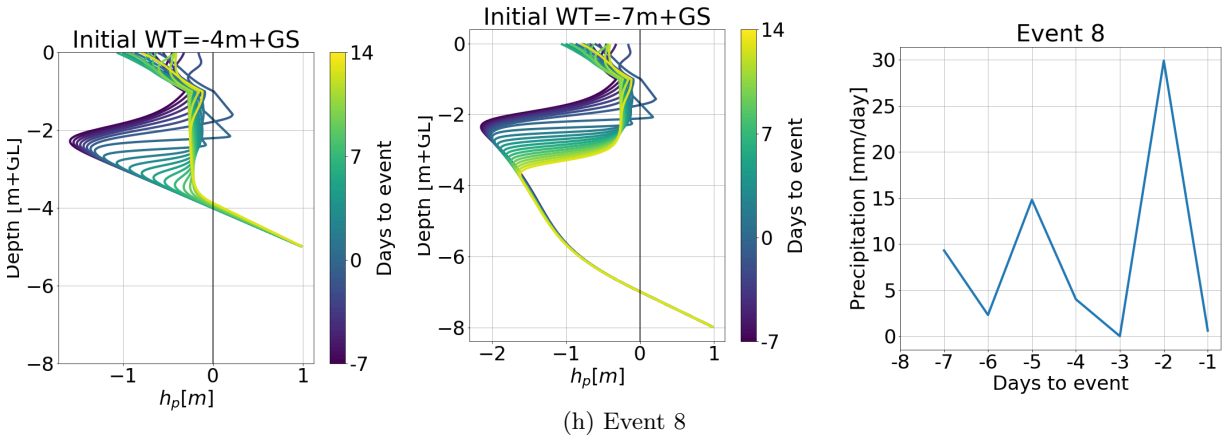

(h) Event 8

Figure F.1: Pressure heads over the depth of a 1D soil column 7 days before and 14 days after the 8 events (a to h) of saturation at a height of -2 m+GS for an initial water table 4m and 7m below ground surface (left and middle) and the daily precipitation 7 days before the events of saturation (right).

The figures show that three of the events leading to saturation are after a peak of precipitation with an intensity $\geq$ 35 mm/day (events 2, 3, 4). Before those events took place, the pressure head in the top of the soil column was already high, resulting in the saturation of that part of the soil column after the rainy day. Events 1, 5, 6, 7 and 8 have in common that there were multiple rainy days that followed each other and that they all contain an event with an intensity $\geq$ 20mm/day. However, it is not the case that every peak $\geq$ 20 mm/day (or 35 mm/day for that matter) results in an event where the soil column is saturated. In figure F.2, all daily precipitation events with an intensity larger than 20 are included and the 8 events that lead to saturation at a depth of -2m are marked. The figure shows that there are many events with a high intensity that did not result in saturation of the soil column. The figure also shows that while many of those high intensity events take place during summer, none of the events have resulted in saturation. Naturally this is a result of the higher evapotranspiration from the surface during summer.

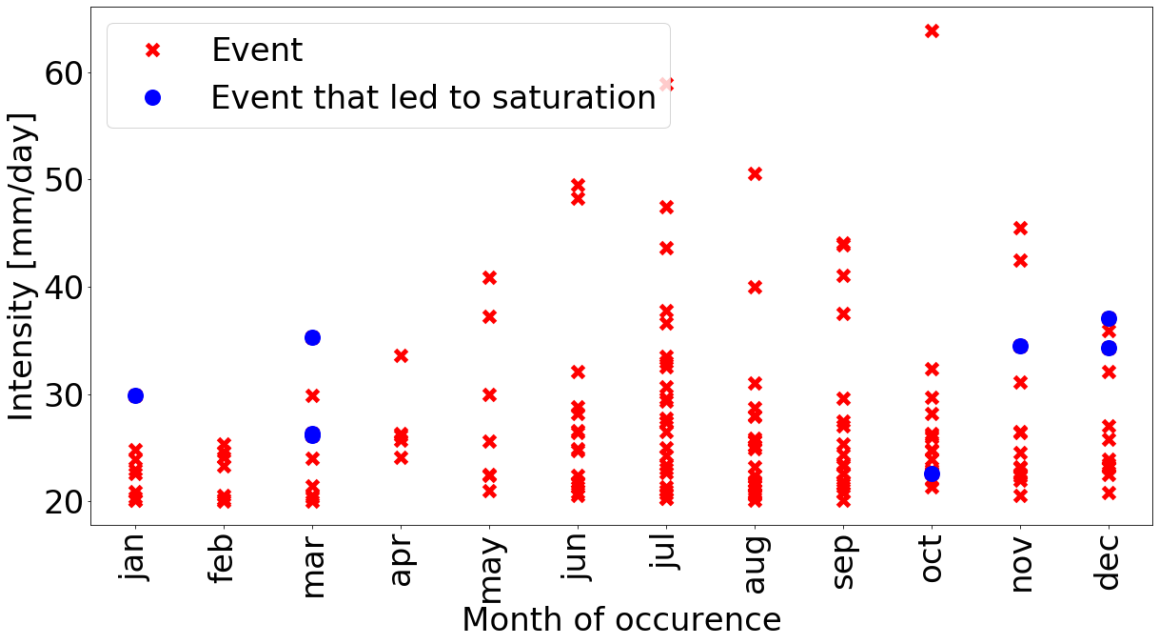

Figure F.2: Daily precipitation events $\geq$ 20mm/day recorded at meteorological station De Bilt from 1980-2016 sorted by the month of occurrence and whether or not it resulted in saturation at a depth 2 meter below the ground surface.

G IDF curves: comparing empirical and fitted distributions

To create IDF curves, a Generalized Extreme Value (GEV) distribution was fitted to the yearly maxima of the summed data. To validate this process, the histogram of the empirical distribution can be compared to the probability density function of the theoretical distribution. To quantify the goodness of fit, a Kolmogorov–Smirnov test was performed, of which the p-value is included in the title of the graph. A p-value of above 0.05 means that we can be 95% sure that the data comes from the presented GEV distribution.

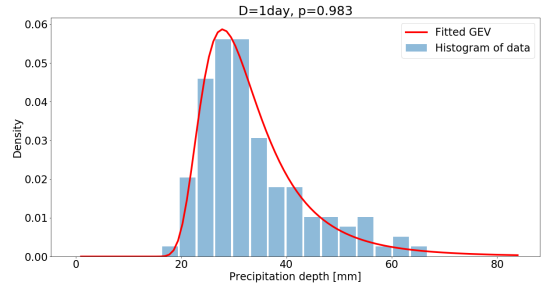

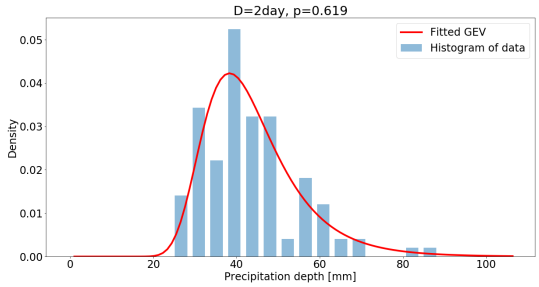

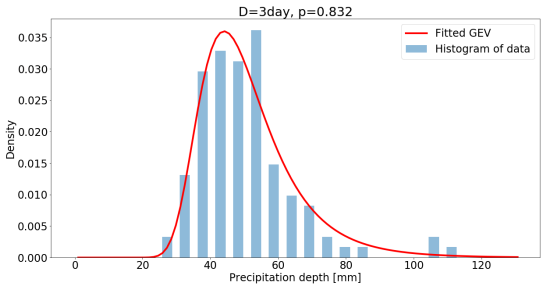

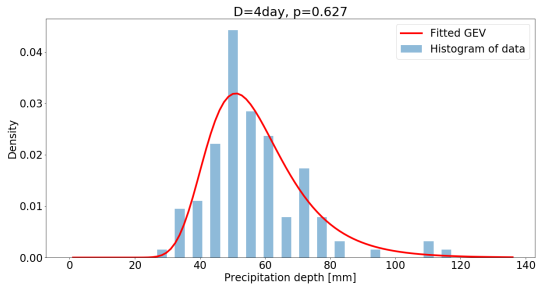

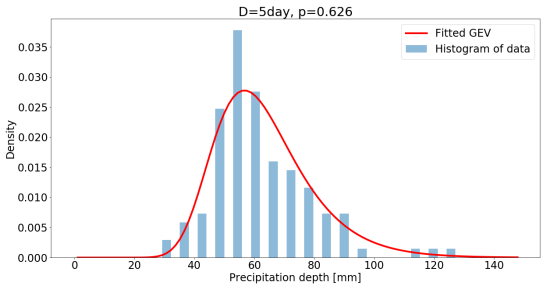

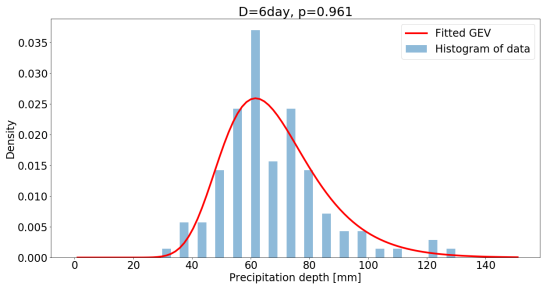

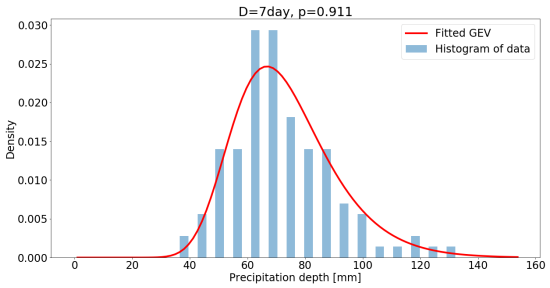

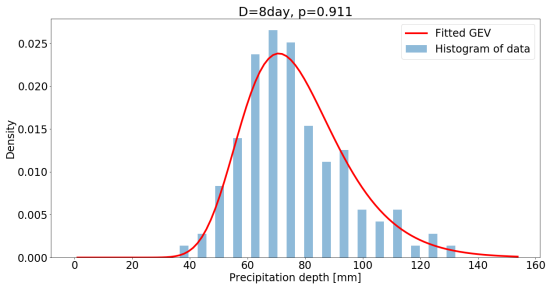

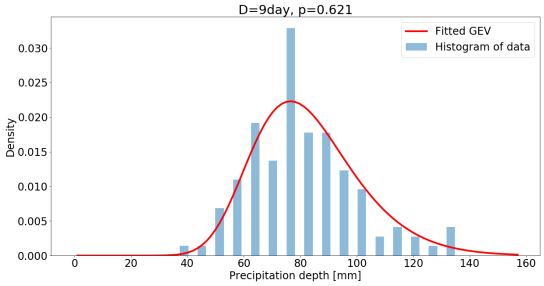
D=9day, p=0.621
Fitted GEV
Histogram of data
Density
Precipitation depth [mm]

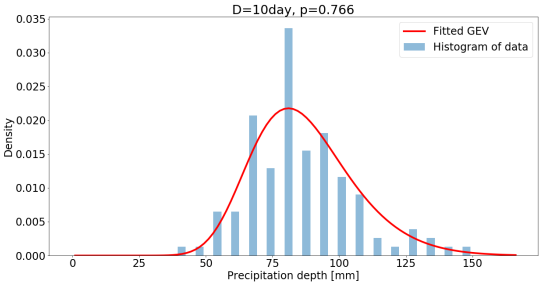
D=10day, p=0.766
Fitted GEV
Histogram of data
Density
Precipitation depth [mm]

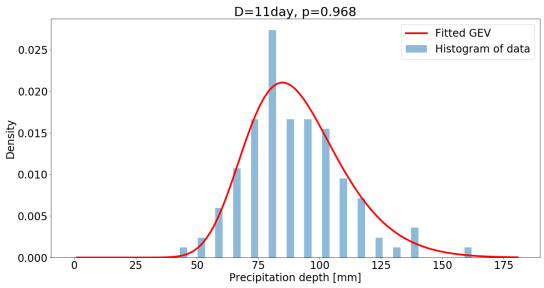
D=11day, p=0.968
Fitted GEV
Histogram of data
Density
Precipitation depth [mm]

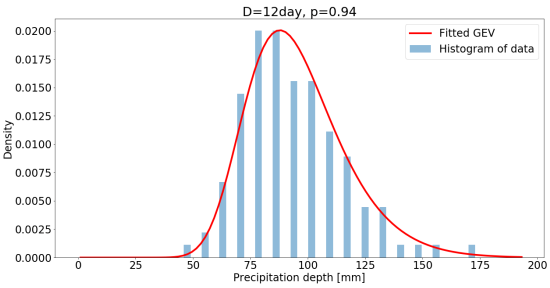
D=12day, p=0.94
Fitted GEV
Histogram of data
Density
Precipitation depth [mm]

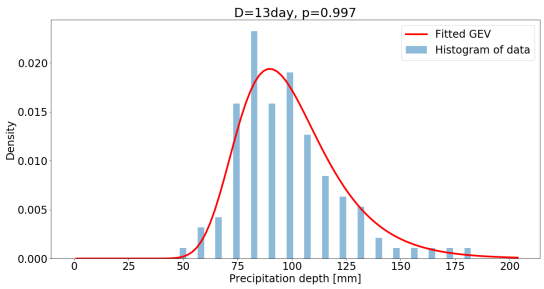
D=13day, p=0.997
Fitted GEV
Histogram of data
Density
Precipitation depth [mm]

H Results of the scenario analysis

This appendix includes the results of the four scenarios in the scenario analysis, where the effect of suction during a high water event is observed is researched. The four scenarios were first calculated in a 2D seepage analysis, from which the maximum height of the water table was determined and the area where suction remains present during the high water. This area, indicated in the figures (b) and (c) below, was included in the stability analysis with as a soil layer with drained characteristics and an apparent cohesion varying between 0 and 10 kPa. The slip plane, included in figures (d) below, is the slip plane for a situation where the apparent cohesion is 0 kPa. The safety factor for this slip plane was determined for the situations with a varying apparent cohesion.

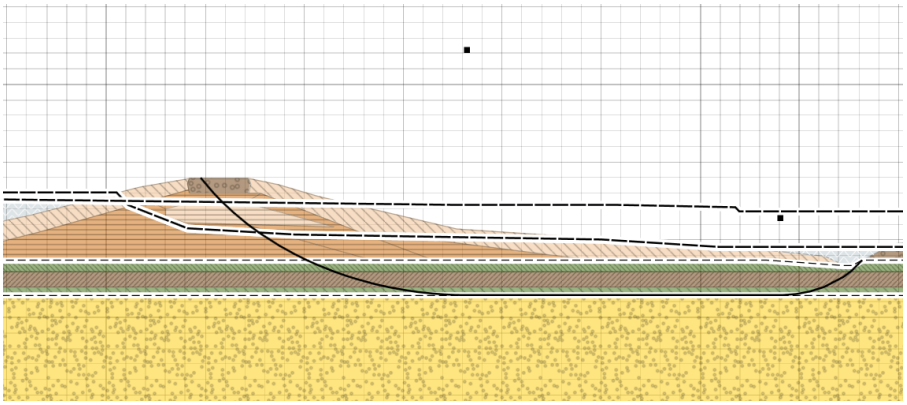

Figure H.1: Governing slip plane for the scnenario in January with soil properties B10

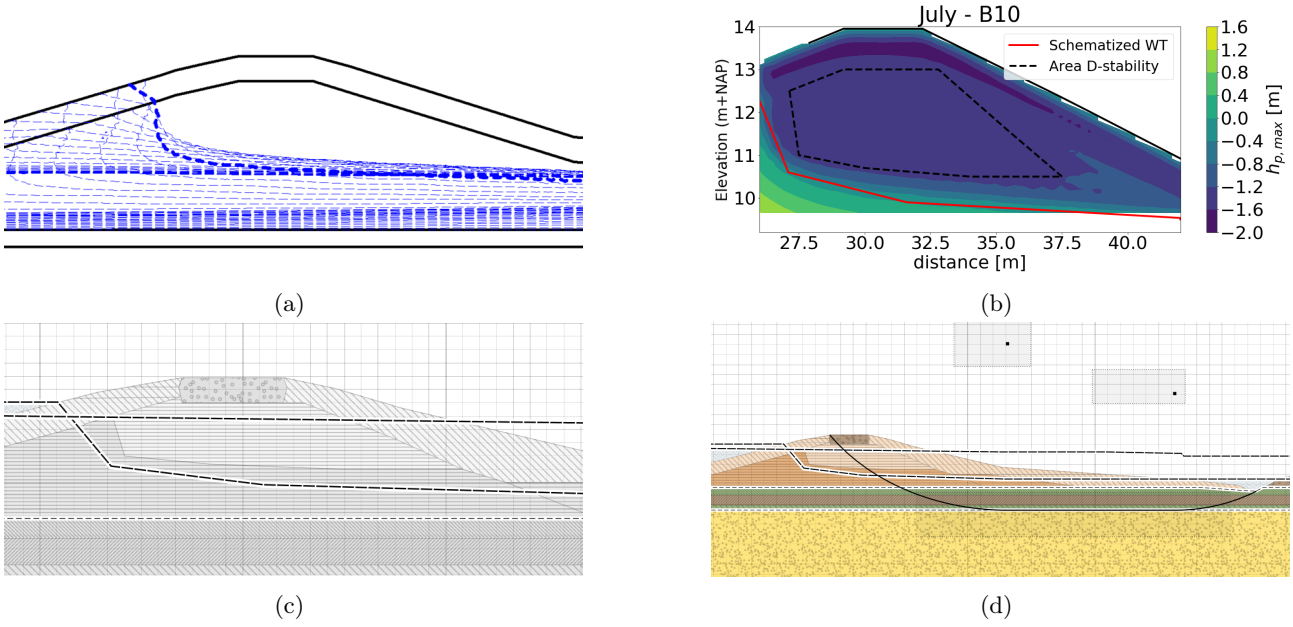

Figure H.2: The results of analysis in July with soil properties B10. The water table in the dike (a), the maximum pressure head and the area that where suction remains present (b), the schematized layer in D-Stability (c) and the governing slip plane for the situation with 0 kPa apparent cohesion (d).

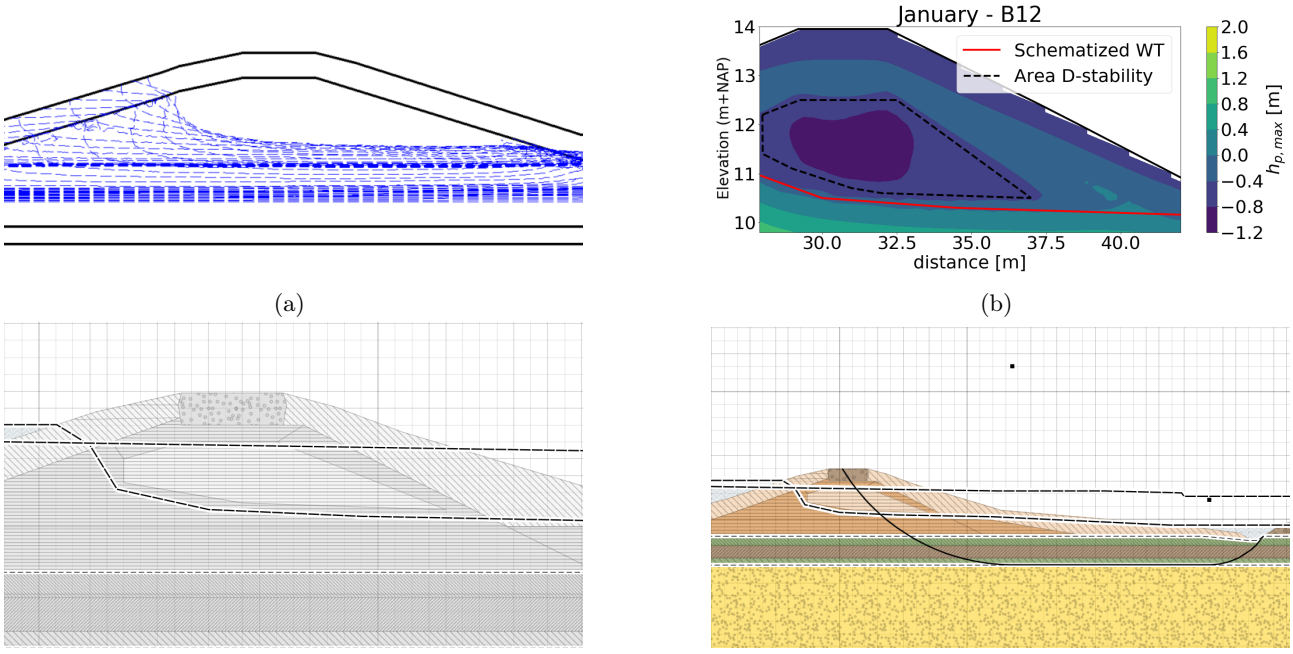

Figure H.3: The results of analysis in January with soil properties B12. The water table in the dike (a), the maximum pressure head and the area that where suction remains present (b), the schematized layer in D-Stability (c) and the governing slip plane for the situation with 0 kPa apparent cohesion (d).

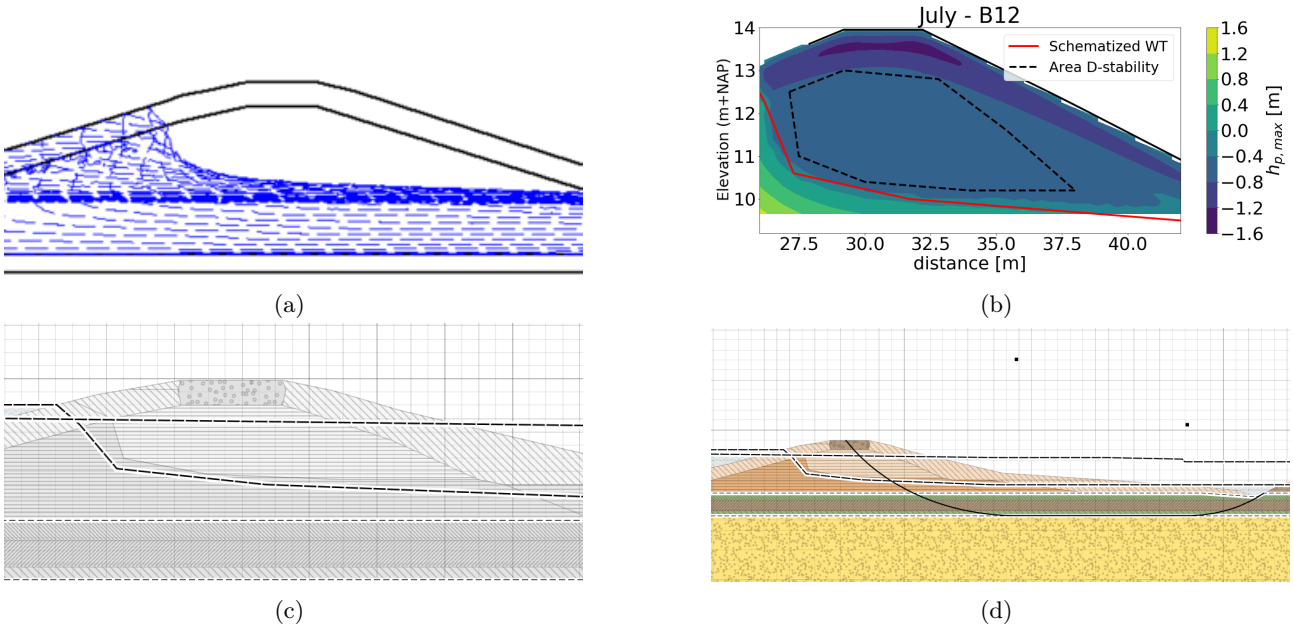

Figure H.4: The results of analysis in July with soil properties B12. The water table in the dike (a), the maximum pressure head and the area that where suction remains present (b), the schematized layer in D-Stability (c) and the governing slip plane for the situation with 0 kPa apparent cohesion (d).

I Results of the Monte Carlo analysis to the variation of the Safety Factor

This appendix includes the results of the Monte Carlo analysis to the variation of the safety factor, given a river stage. For four river stages, first the height of the water table was estimated, and the area that remains unsaturated was schematized. These areas are indicated in the figures (a) below. For the schematized area, the average daily suction (in kPa) was calculated during the months January, February and March from the 36 years quasi 2D analysis. A histogram of the results is included in the figures (b) below. With this empirical distribution, a Monte Carlo analysis was performed to calculate the variation in the apparent cohesion and the relative safety factor (compared to the safety factor for a situation with 0 kPa apparent cohesion). A histogram of these resutls is included in the figures (c) below.

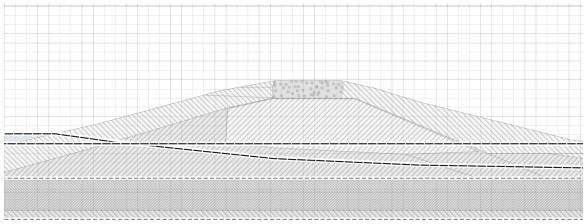

(a)

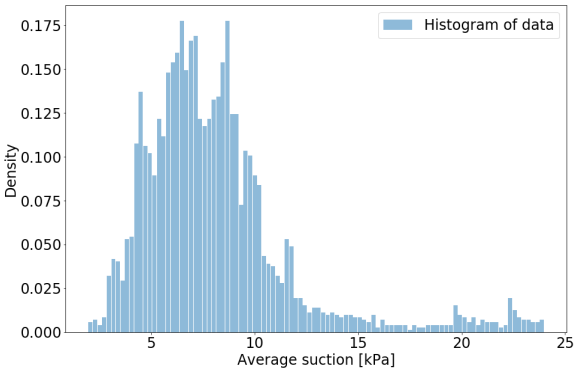

(b)

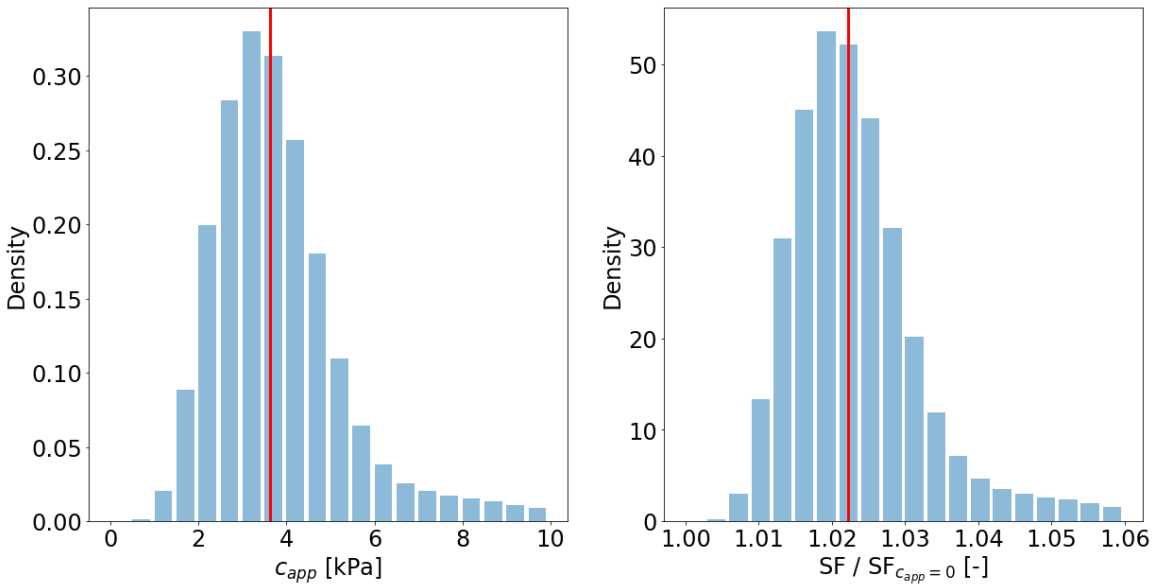

(c)

Figure I.1: Results of the Monte Carlo analysis for a river stage of 11m+NAP. The schematized water table and unsaturated area (a), the histogram of the average daily suction in the area during January, February and March (b) and the variation in apparent cohesion and the relative safety factor (c).

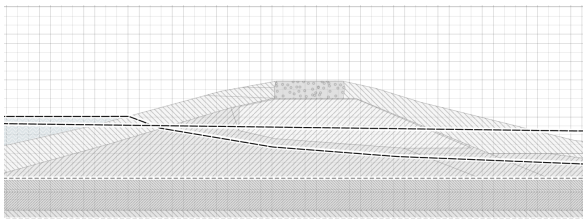

(a)

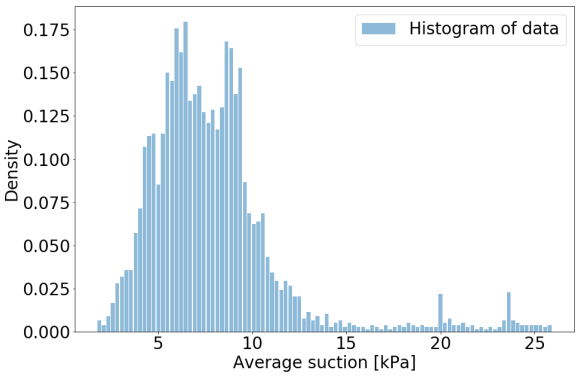

(b)

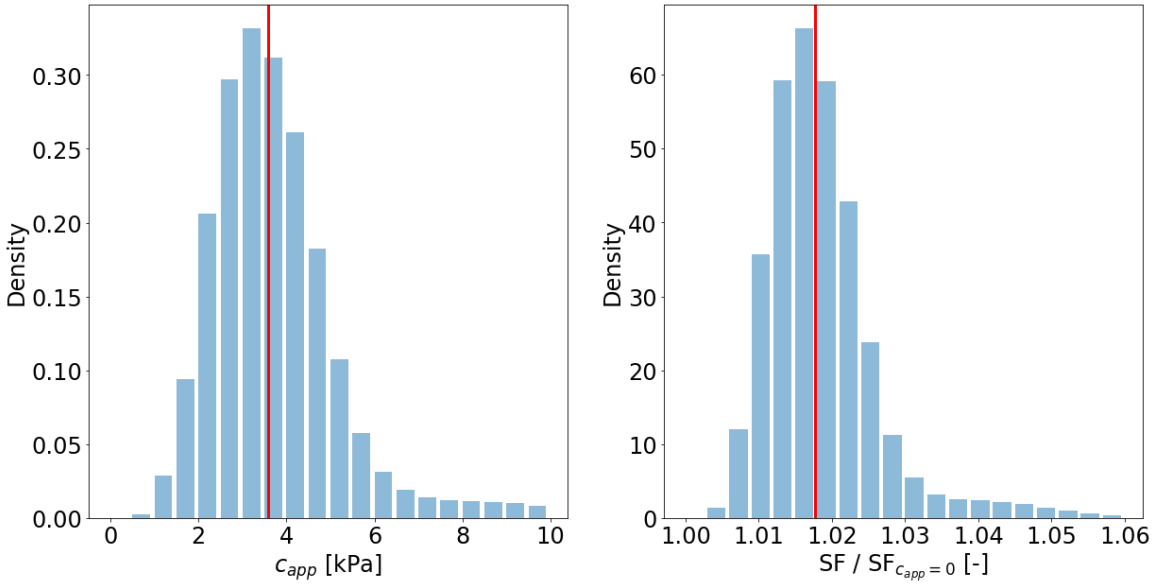

(c)

Figure I.2: Results of the Monte Carlo analysis for a river stage of 12m+NAP. The schematized water table and unsaturated area (a), the histogram of the average daily suction in the area during January, February and March (b) and the variation in apparent cohesion and the relative safety factor (c).

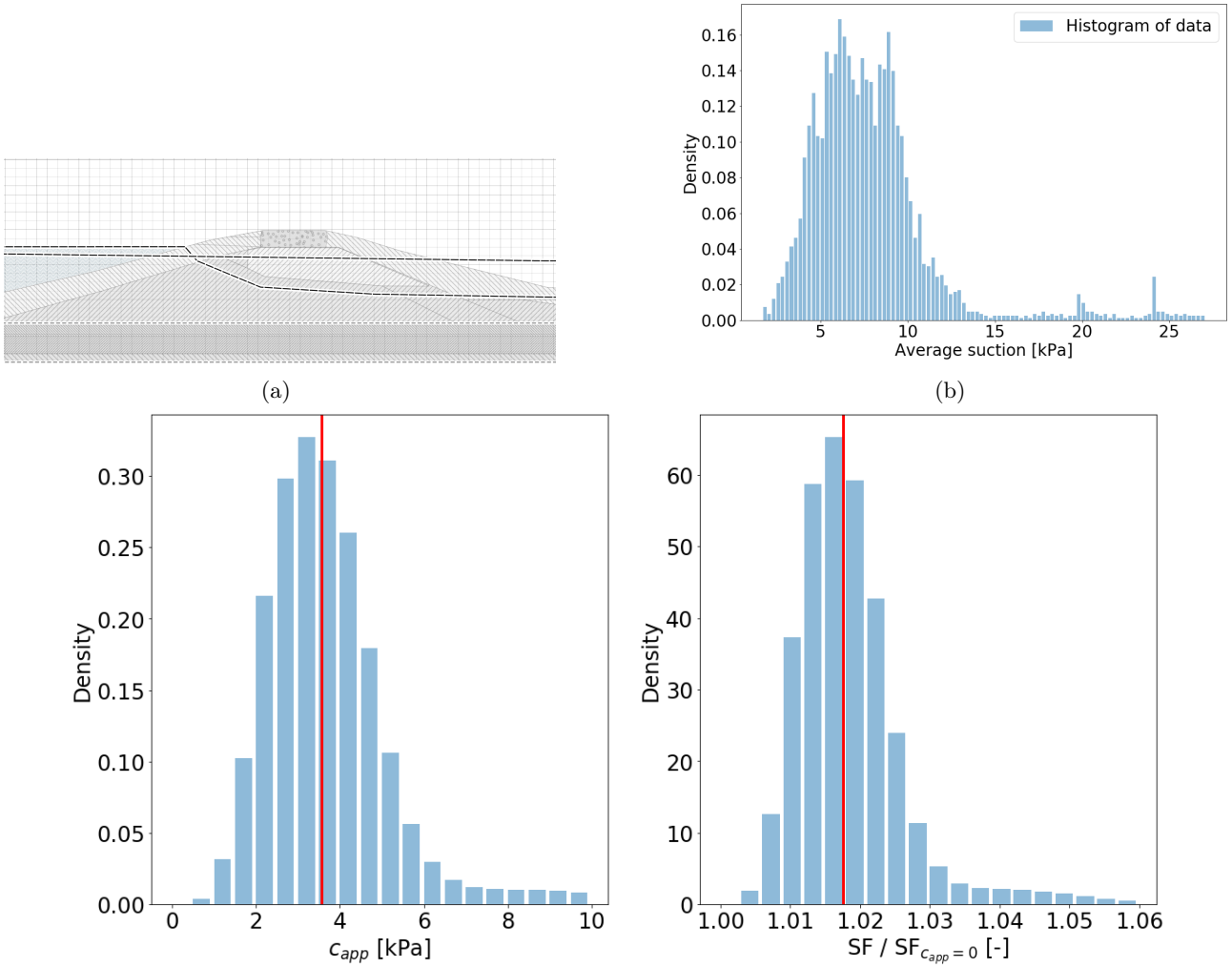

(a) (b) (c)

Figure I.3: Results of the Monte Carlo analysis for a river stage of 13m+NAP. The schematized water table and unsaturated area (a), the histogram of the average daily suction in the area during January, February and March (b) and the variation in apparent cohesion and the relative safety factor (c).

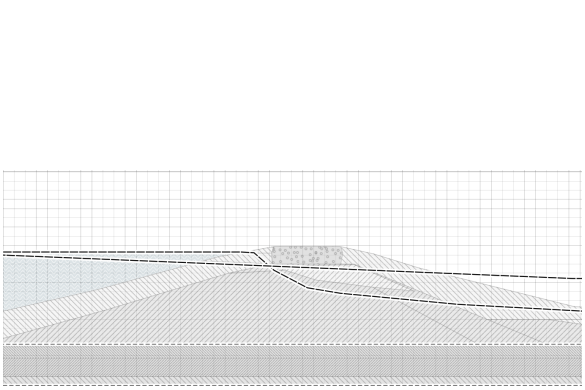

(a)

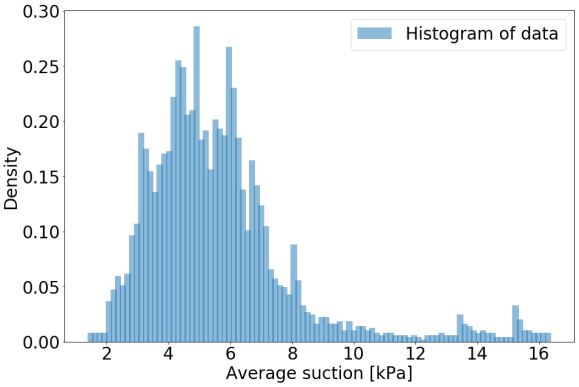

(b)

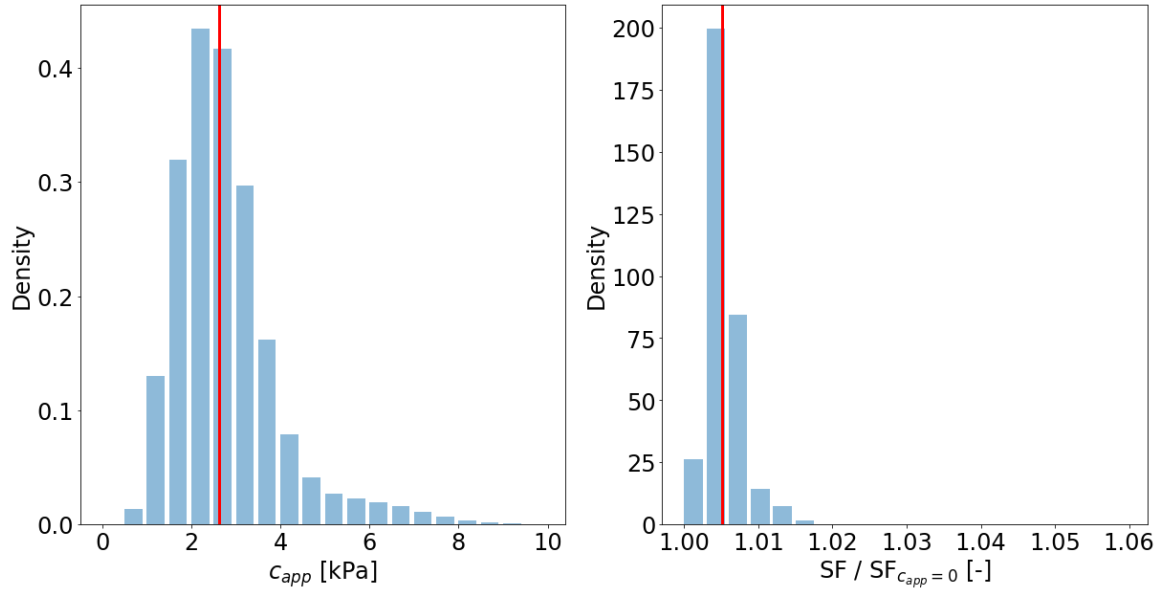

(c)

Figure I.4: Results of the Monte Carlo analysis for a river stage of 13.64m+NAP. The schematized water table and unsaturated area (a), the histogram of the average daily suction in the area during January, February and March (b) and the variation in apparent cohesion and the relative safety factor (c).